Evaluation and Comparison of Linear Quadratic Control Techniques

Exploring Stability and Robustness in Loop Transfer Recovery Approaches

Graduation Report

Janki Kaushal

Delft University of Technology, Faculty of Aerospace Engineering, Department Control & Operations, Section Control & Simulation

TU Delft

Evaluation and Comparison of Linear Quadratic Control Techniques

Exploring Stability and Robustness in Loop Transfer Recovery Approaches

by

Janki Kaushal

to obtain the degree of
Master of Science in Aerospace Engineering at Delft University of Technology,
to be defended publicly on Thursday February 15, 2024 at 12:00 PM.

Student number	5537916
Thesis Committee:	Dr. Eng. S. Theodoulis
	Dr. Ir. C.C. de Visser
	Dr. X. Wang
Date of submission:	February 2024

The work in this thesis was conducted in the:

Section Control & Simulation
Department Control & Operations
Faculty of Aerospace Engineering
Delft University of Technology

Cover: Picture of the Cessna Citation PH-LAB in flight (Nason, 2013) (Modified)

TU Delft

Preface

This document represents the culmination of my Master's thesis, which focuses on assessing various linear quadratic control techniques with particular attention to loop transfer recovery methods. This research aims to highlight the importance of evaluating these methods to ensure safety and prevent failures in flight. As one of the first members of the AEROCON group in the Control & Simulation section, I had the privilege of learning about flight dynamics and control among a group of talented individuals. This experience has been invaluable in understanding the nuances of designing flight controllers. I am optimistic that future researchers will introduce more innovative and robust control methods, and I hope we can collectively enhance safety in the aviation industry through the development of efficient and failure-resistant controllers.

I extend my heartfelt gratitude to the Faculty of Aerospace Engineering at TU Delft for offering abundant opportunities for learning and growth, which have greatly benefited my personal and professional development. I am deeply thankful to my supervisors, Spilios, for his guidance and mentorship throughout my thesis, and to Coen for his support and insights during this journey. I am eternally grateful to my family – my parents and brother, who are the three pillars of my life. It is through their love, support and sacrifices that I have been able to achieve so much, as I would not have reached this point without them. Lastly, I want to express my gratitude to my friends who provided a sense of home away from home. The past two and a half years have been the most thrilling and challenging years of my life. Meeting people from diverse backgrounds has broadened my perspective and contributed significantly to my personal growth. My time at TU Delft was a transformative journey, one that pushed the boundaries of my comfort zone and imparted invaluable life lessons. Ultimately, it brings me great joy that this path has led to the realization of my deeply cherished dream: to proudly carry the title of an Aerospace Engineer.

J.Kaushal
Delft, February 2024

Contents

Nomenclature

List of Abbreviations

AHRS	Attitude Heading and Reference System
ARE	Algebraic Riccati Equation
CAS	Control Augmentation System
DADC	Digital Air Data Computer
DASMAT	Delft University Aircraft Simulation Model and Analysis Tool
ECEF	Earth-Centered Earth-Fixed reference frame
FDLTI	First-order Discrete-time Linear Time-Invariant
FTIS	Flight Test Instrumentation System
LHP	Left Half Plane
LQ	Linear Quadratic
LQG	Linear Quadratic Gaussian
LQI	Linear Quadratic Integral
LQR-OF	Linear Quadratic Regulator-Output Feedback
LQR-SF	Linear Quadratic Regulator-State Feedback
LTI	Linear Time-Invariant
LTR	Loop Transfer Recovery
MIMO	Multiple Input Multiple Output
NASA	National Aeronautics and Space Administration
NLR	Netherlands Aerospace Centre
NMP	Nonminimum Phase
PI	Performance Index
RD	Return Difference
RHP	Right Half Plane
SISO	Single Input Single Output
SR	Stability Robustness

List of Symbols

α	Angle of attack
β	Angle of sideslip
Δ	Uncertainty
δ_a	Aileron deflection
δ_e	Elevator deflection
δ_r	Rudder deflection
μ	Structured Singular Value
ϕ	Roll angle
τ_{act}	Actuator Time Constant
θ	Pitch angle
a_n	Normal Acceleration
A_x	Longitudinal Acceleration
A_y	Lateral Acceleration
A_z	Vertical Acceleration
h_e	Altitude
k_m	Multivariable Stability Margin
n_u	Number of inputs
n_x	Number of states
n_y	Number of outputs
q	Pitch Rate
sat_δ	Actuator deflection saturation
$sat_{\dot{\delta}}$	Actuator deflection rate saturation
V_{TAS}	True Airspeed
x_i	Integrator State
y_{acc}	Accelerations and load factors
y_{air}	Outputs of the Airdata, Wind, and Turbulence Models
y_{pp}	Output of the engine model

List of Figures

List of Tables

1 Introduction

1.1. Motivation

As aircraft have become more advanced, they have become more difficult to control manually. This has increased reliance on automation and advanced control systems to ensure safe and efficient flights. Nowadays, considerable attention is given to developing optimal control systems, which aim to minimize unnecessary movements and reduce fuel consumption and emissions by optimizing the aircraft's trajectory leading to greater efficiency and reduced environmental impact. The feedback renaissance of the 1980s brought a rich and diverse style of feedback design in almost every area of control theory (Kokotovic, 1985). Since then, feedback has been used to stabilize and optimize nonlinear and multivariable models to counteract uncertainties and disturbances.

A revolution in control theory took place in the early 1970s when the dominant focus of research shifted from optimality to robustness (Safonov, 2012). This change was in response to unexpected failures of optimal control theory that failed to generate feedback control designs capable of handling uncertainties and variations in real-world scenarios. M. Athans et al., 1977 presented results of a Linear Quadratic Gaussian (LQG)[1] control design study concerning the NASA F-8C aircraft, describing the theoretical weaknesses in the control algorithm, not accounting for model or external uncertainties. LQG was widely used in aerospace applications because it provides a solution to the problem of the unavailability of all aircraft states for feedback in control system design by using a state estimator to estimate all unmeasured states. This eliminates the need for expensive sensors, making LQG a cost-effective solution for aerospace applications. However, some noticeable failures pointed to the lack of robustness properties in LQG-controlled applications. To address this issue, a design process called Loop Transfer Recovery (LTR) was developed to recover the robustness properties of LQG controllers, ensuring that they exhibit the required stability and overall control performance.

This study focuses on implementing and assessing different linear quadratic control methods on a simulation model of the Cessna Citation PH-LAB aircraft[2] shown in Figure 1.1. This aircraft is a research platform operated by the Faculty of Aerospace Engineering and is co-managed with the Netherlands Aerospace Centre. The study involves developing a reference tracker for tracking normal acceleration commands by using state feedback, static output feedback and dynamic output feedback control methods. Each of these methods has distinct advantages and disadvantages in terms of practicality, time-domain characteristics, and frequency-domain characteristics, which are extensively explored in this study. This research focuses on a detailed comparison of these linear quadratic controller design methods, with a particular emphasis on the application and analysis of loop transfer recovery (LTR) techniques. The thesis is driven by the aim to explore whether the LTR approach proposed by Lavretsky, 2012 in their work, can effectively restore the stability that is compromised during the implementation of the LQG controller. Additionally, the study conducts robustness analysis, introducing different types of uncertainties to the plant to validate the results.

[1] When optimal regulator (LQR) is combined with optimal state estimation (Kalman filter), the control design is called the Linear Quadratic Gaussian (LQG).

[2] Cessna Citation PH-LAB: https://cs.lr.tudelft.nl/citation/

Figure 1.1: Cessna Citation PH-LAB in flight

1.2. Research Objective Formulation

Research Objective

"To conduct a comparative analysis of loop transfer recovery design methodologies alongside various linear quadratic control strategies, and assess their robustness and performance, utilizing a linear state-space model of the Cessna Citation PH-LAB"

In order to pursue the research objective, the following research questions were formulated.

1. What are the characteristics and structure of the plant?
    - Is the plant minimum or non-minimum phase?
2. What are the characteristics of LQR controller design?
    - Do the stability margins of the full-state feedback LQR-controlled system align with the theoretically guaranteed stability margins at the input of the plant?
    - How are the stability margins at the output of the plant?
    - What are the differences between state and output feedback LQR controller designs?
    - Can LQR controllers be designed using the `systune` function in `MATLAB`?
3. What are the characteristics of the dynamic output feedback LQG controllers?
    - What is the accuracy of the state estimation obtained from the Kalman filter, which is used to estimate the unmeasured states?
    - How are the robustness properties at the input and output of the plant when using the LQG controller? How do they compare to the LQR state and output feedback controllers?
    - Does the LQG-controlled system exhibit degraded robustness properties at both the input and output compared to the previously designed LQR-controlled system?
4. Is an LTR procedure required for the LQG-controlled system obtained in the previous step?
    - Does the resulting LQG/LTR-controlled system meet the desired stability margins? Are there any shortcomings in the closed-loop system?
    - Does the LTR procedure proposed by Lavretsky, 2012 lead to improved stability compared to the LTR procedure discussed by J. Doyle and Stein, 1981?
5. How does the LTR procedure proposed by Lavretsky, 2012 compare with other linear quadratic controllers developed in the study?

- What types of uncertainties can be introduced in the plant? What are the various robustness tools that can be used to analyse the closed-loop performance in the presence of uncertainties?
- Does the resulting LQG/LTR-controlled system exhibit robustness properties better than other linear quadratic controllers?
- How do the uncertainties within the system impact the time-domain and frequency-domain properties of the closed-loop system?

1.3. Report Structure

The report is structured into three main parts. Part I provides a discussion of the linear state-space model of the Citation aircraft utilized in this study. It details the processes of trimming and linearization that are applied to derive the linearized state-space system from the nonlinear model. This Part also describes the sensor system employed in this study, highlighting the significance of sensor noise covariance as a key parameter for this research.

Part II of the report primarily concentrates on the linear quadratic control techniques explored in this research ranging from state feedback and static output feedback methods to dynamic output feedback approaches. Chapter 3 focuses on the linear quadratic regulator problem, examining its frequency-domain characteristics and the implementation and tuning of these controllers to meet specific design requirements. It further highlights the use of the `systune` function in `MATLAB` for designing state and static output feedback LQR techniques. Chapter 4 addresses the design of the LQG controller using the separation theorem, which allows for the independent design of the LQR state-feedback control law and the Kalman filter for state estimation. Additionally, it notes the degradation of robustness properties in the LQR technique when incorporated into the LQG controller. Chapter 5 explains the classical loop transfer recovery as introduced by J. Doyle and Stein, 1981 and the LTR theory proposed by Lavretsky, 2012. It delves into the differences in the inner workings of both theories and provides detailed descriptions of their implementation procedures.

Part III of the thesis delves into the analysis of the linear quadratic design methods outlined in Part II. This section conducts a comprehensive robustness analysis for all the control techniques, including an examination of the stability margins at both the input and output of the plant. It also elaborates on the key features of the LTR methods, particularly their ability to recover guaranteed stability margins at the plant input which is a characteristic of full-state feedback LQR control technique, within an LQG framework. Furthermore, this part focuses on the robustness properties of the dynamic output feedback controllers, specifically the LQG and LQG/LTR controllers in the presence of different types of uncertainties and also explores how these uncertainties impact the time-domain characteristics of the closed-loop system.

Part I

Modelling

2

Aircraft Model Setup

The Cessna Citation II is a twin-jet business aircraft and has a maximum operating altitude of 13 km and a maximum cruising speed of 710 km/h (Konatala, Kampen, and Looye, 2021). The model of the aircraft is built with MATLAB/Simulink and is called DASMAT (Delft University Aircraft Simulation Model and Analysis Tool) which has became a valuable tool for analyzing and designing new control algorithms within the C&S section (van der Linden, 1998). Currently, DASMAT is composed of eight blocks that are divided as follows: (1) Airdata, Wind, and Turbulence Models, (2) Aerodynamic Model, (3) Engine Model, (4) Gravity Model, (5) Landing Gear Model, (6) Mass Model, (7) Equations of Motion, and (8) Observation Model, as shown in Figure 2.1. The outputs of these models are denoted as y. The output of the engine model is denoted by y_{pp}, which contains the engine state vector that typically includes the rotational rates of the fans and gas turbine.

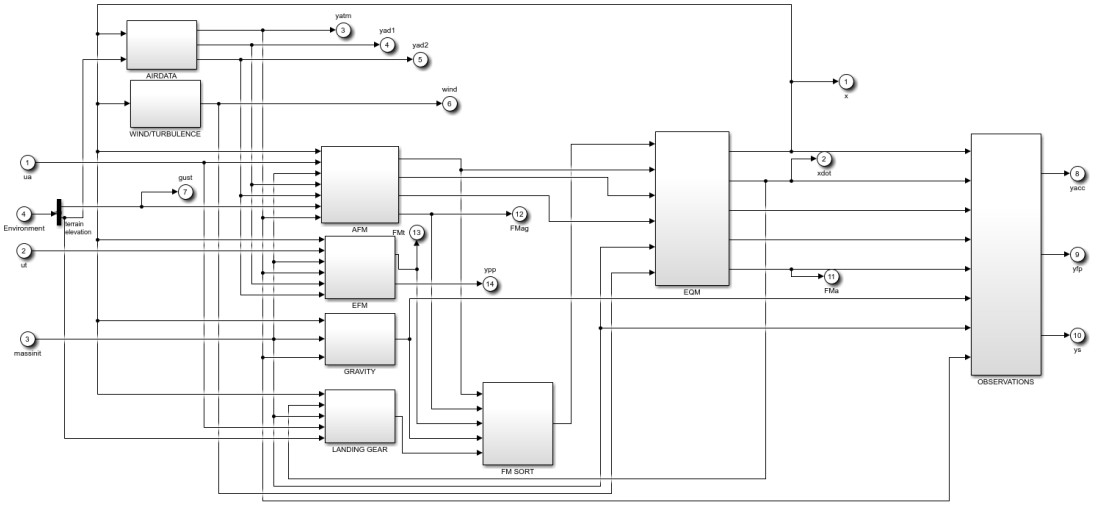

Figure 2.1: Overview of the Citation model simulation framework in the DASMAT package

2.1. Trimming and Linearization

The DASMAT trimming tool is designed to establish a steady-state flight condition for a given aircraft configuration at a specific operating point. This trimmed flight condition is characterized by the stability of all motion variables, meaning they are either constant or zero. In essence, this condition is achieved when both rotational and translational accelerations of the aircraft are zero as given in Equation 2.1. Furthermore, the engine model must also be adjusted to a trimmed state, and requires the engine state derivatives to become zero.

$$\begin{aligned} \dot{p}_b \quad &= \dot{q}_b = \dot{r}_b = 0 \\ \dot{V}_{\text{TAS}} = \dot{\alpha} \ &= \dot{\beta} \ = 0 \end{aligned} \tag{2.1}$$

For trimming the aircraft model, only the primary flight controls and thrust are considered independent variables, and thus they are determined by the trim routine. The other control inputs, such as secondary flight controls including trim-tab adjustments, flap angles, and landing gear positioning, are treated as fixed parameters of the aircraft configuration, predetermined by the user. The aircraft's position and orientation in the horizontal plane do not affect the forces and moments exerted on it within an isentropic atmosphere. Therefore, the state variables x_e, y_e, and ψ are irrelevant for trimming and are set to zero. The geometric altitude, denoted as h_e, is significant due to its influence on air density. Along with the true airspeed, V_{tas}, it is considered a defining factor of the operating point. The other state variables of the aircraft, namely the body axis rates, angle of attack (α), sideslip angle (β), roll angle (ϕ), and pitch angle (θ), are either constrained or considered independent, depending on the chosen flight condition. During the trimming procedure, one can select from six different flight conditions.

1. Straight-and-level trim
2. Pushover-pull up
3. Level turn
4. Thrust-stabilized turn
5. Beta trim
6. Specific power turn

The final trimmed values are determined through a minimization heuristic aimed at minimizing the trim cost function J, given in Equation 2.2. This cost function is of the least square type and incorporates weight factors w_i for the acceleration terms.

$$J = w_1\dot{p}_b^2 + w_2\dot{q}_b^2 + w_3\dot{r}_b^2 + w_4(\dot{V}_{tas} - \dot{V}_{tas_{spec}})^2 + w_5\dot{\alpha}^2 + w_6\dot{\beta}^2 \tag{2.2}$$

The DASMAT linearization tool provides a linearized state-space model of the Citation aircraft at the trim condition and assumes zero wind and no turbulence conditions. The control inputs for this linear model include the primary flight controls and thrust, while the state vector comprises only the relevant state variables associated with the Citation aircraft. The states and input of the linearized Citation model are given in Equation 2.3.

$$\begin{aligned} x &= \begin{bmatrix} p_b & q_b & r_b & V_{TAS} & \alpha & \beta & \phi & \theta & \psi & h_e & x_e & y_e \end{bmatrix} \\ u &= \begin{bmatrix} \delta_e & \delta_a & \delta_r & T_{N1} & T_{N2} \end{bmatrix} \end{aligned} \tag{2.3}$$

The influence of the thrust controls within the input vector u on the state derivatives and the output of the linear system is expected to be minimal. Therefore, while creating the linear state-space system, the input vector can be simplified to include only the elevator (δ_e), aileron (δ_a) and rudder (δ_r) deflections.

2.2. Sensor Model

The system's output signals are determined based on the presence of physical measurement devices installed on the aircraft. For instance, the body angular rates (p, q, r) are typically measured using rate gyroscopes. These same devices can also be configured to provide measurements for the three Euler angles (ϕ, θ, ψ). Additionally, most aircraft are equipped with at least three accelerometers that continuously measure longitudinal, lateral, and vertical loads, represented as A_x, A_y, and A_z. Each accelerometer measures an acceleration component (in units such as feet per second squared or g-forces) along its respective axis at its installation point (Lavretsky and K. Wise, 2013).

The PH-LAB is outfitted with a Flight Test Instrumentation System that comprises an Attitude Heading and Reference System (AHRS), a Digital Air Data Computer (DADC), a Global Positioning System, an air data boom, and control surface synchros used to measure deflection angles of the control surfaces. Additionally, the angle of attack is obtained from a body-mounted vane sensor. The PH-LAB's sensor instrumentation model is established through the analysis of flight test data (Grondman et al., 2018; Veld, Kampen, and Chu, 2018). This modelling process incorporates various practical factors such as bias, noise, delays, resolution, and sampling rate. Sensor noise is characterized as Gaussian white noise with a mean value of zero. Table 2.1 displays the sensor characteristics of the various sensor systems.

Table 2.1: PH-LAB sensor model characteristics (Grondman et al., 2018)

Signal	Noise (σ^2)	Bias	Resolution	Delay (ms)	Sampling rate (Hz)
$p, q, r, \dot{\phi}, \dot{\theta}, \dot{\psi}$ (rad/s)	$4.0 \cdot 10^{-7}$	$3.0 \cdot 10^{-5}$	$6.8 \cdot 10^{-7}$	90	52
θ, ϕ (rad)	$1.0 \cdot 10^{-9}$	$4.0 \cdot 10^{-3}$	$9.6 \cdot 10^{-7}$	90	52
f_x, f_y, f_z (g)	$1.5 \cdot 10^{-5}$	$2.5 \cdot 10^{-3}$	$1.2 \cdot 10^{-4}$	117	52
V_{tas}, V_{cas} (m/s)	$8.5 \cdot 10^{-4}$	2.5	$3.2 \cdot 10^{-2}$	300	16, 8
h (m)	$4.5 \cdot 10^{-3}$	$8.0 \cdot 10^{-3}$	$3.0 \cdot 10^{-1}$	300	16
$\dot{h}$ (m/s)	$5.5 \cdot 10^{-4}$	$4.5 \cdot 10^{-2}$	$8.1 \cdot 10^{-2}$	300	16
M (-)	$1.0 \cdot 10^{-8}$	$7.0 \cdot 10^{-7}$	$6.3 \cdot 10^{-5}$	300	8
$\delta_e, \delta_a, \delta_r$ (rad)	$5.5 \cdot 10^{-7}$	$2.4 \cdot 10^{-3}$	-	~ 0	100
$\alpha_{boom}, \beta_{boom}$ (rad)	$7.5 \cdot 10^{-8}$	$1.8 \cdot 10^{-3}$	$9.6 \cdot 10^{-5}$	100	100
$\delta_{se}, \delta_{sa}, \delta_{sr}$ (rad)	$5.5 \cdot 10^{-7}$	-	-	~ 0	1000
I_{ax}, I_{ae}, I_{ar} (A)	$5.0 \cdot 10^{-4}$	-	-	~ 0	1000

2.3. Actuator Model

The PH-LAB actuator system has been characterized by a first-order model derived from flight data that is documented in (Grondman et al., 2018). This dataset not only accounts for the fundamental first-order lag component but also encompasses other crucial aspects of the system, including actuator deflection and rate limitations, as well as a transport delay represented by λ_{act}.

$$\dot{\delta}(t) = sat_{\dot{\delta}}\{\tau_{act}^{-1}\delta_{cmd}(t - \lambda_{act}) - \tau_{act}^{-1} sat_{\delta}[\delta(t)]\} \tag{2.4}$$

In Equation 2.4, the functions sat_{δ} and $sat_{\dot{\delta}}$ represent saturation limits for actuator deflection and rate, respectively. The actuator time constant τ_{act} is determined by fitting the measured actuator deflection response to the general step input time response of a first-order system. The estimation of τ_{act} is obtained using a nonlinear least-square curve-fitting method. Additionally, for each step input command, the maximum rate of deflection $\dot{\delta}_{max}$ is determined, and the average value is considered as the final estimate. The transport delay is calculated based on the time difference between the FBW input command and the corresponding response of the control surface deflections (Grondman et al., 2018). The specific parameters and values used for the actuator model are listed in Table 2.2.

Table 2.2: PH-LAB actuator model parameters

	$\delta_{\mathbf{max}}(^\circ)$	$\delta_{\mathbf{min}}(^\circ)$	$\tau_{\mathbf{act}}(\mathbf{ms})$
Aileron	37	-37	
Elevator	15	-20	76.9
Rudder	22	-22	

2.4. Linear Plant Model

Following the trimming and linearization, the longitudinal model of the aircraft can be obtained, as described in Equation 2.5 (Lavretsky and K. Wise, 2013). This model can then be decomposed into its short period and phugoid components or modes. In this study, the short period approximation of the aircraft model is used.

$$\begin{pmatrix} \dot{V}_T \\ \dot{\alpha} \\ \dot{q} \\ \dot{\theta} \end{pmatrix} = \begin{pmatrix} X_V & X_\alpha & 0 & -g\cos\gamma_0 \\ \frac{Z_V}{V_0} & \frac{Z_\alpha}{V_0} & 1 + \frac{Z_q}{V_0} & -\frac{g\sin\gamma_0}{V_0} \\ M_V & M_\alpha & M_q & 0 \\ 0 & 0 & 1 & 0 \end{pmatrix} \begin{pmatrix} V_T \\ \alpha \\ q \\ \theta \end{pmatrix} + \begin{pmatrix} X_{\delta_e} \\ \frac{Z_{\delta_e}}{V_0} \\ M_{\delta_e} \\ 0 \end{pmatrix} \delta_e \tag{2.5}$$

In this system, V_0 denotes the airspeed at which the aircraft is trimmed. The angle α_0 refers to the angle of attack for the trimmed condition. The term γ_0, representing the trimmed flight path angle, is defined as the difference between

the trimmed pitch angle θ_0, and the angle of attack α_0. In Equation 2.5, the matrix components represent stability and control derivatives of the aircraft forces and moments, which are constant for fixed flight conditions. Substituting the aircraft-specific values for these derivatives into the model typically results in the open-loop system eigenvalues comprising two pairs: a fast (short period) pair and a slow (phugoid) pair, both often appearing as complex conjugate numbers. The short-period mode is characterized by the dynamics of α and q. Extracting these dynamics from the longitudinal model in Equation 2.5 results in the short period approximation given in Equation 2.6 (Lavretsky and K. Wise, 2013).

$$\begin{pmatrix} \dot{\alpha} \\ \dot{q} \end{pmatrix} = \begin{pmatrix} \frac{Z_\alpha}{V_0} & 1 + \frac{Z_q}{V_0} \\ M_\alpha & M_q \end{pmatrix} \begin{pmatrix} \alpha \\ q \end{pmatrix} + \begin{pmatrix} \frac{Z_{\delta_e}}{V_0} \\ M_{\delta_e} \end{pmatrix} \delta_e \tag{2.6}$$

The research focuses on the design of a Control Augmentation System (CAS) that tracks the normal acceleration command at a flight point specified by an altitude h_e of 10,238 meters and an airspeed V_{tas} of 87.5 meters per second. The chosen outputs for the linear plant model are the normal acceleration, denoted as a_n and measured in units of g-forces (g), and the pitch rate q measured in radians per second (rad/s). The combined short period and actuator model employed in the study is given in Equation 2.7.

$$\begin{aligned} \begin{pmatrix} \dot{\alpha} \\ \dot{q} \\ \dot{\delta}_e \end{pmatrix} &= \begin{pmatrix} 0.66 & 0.99 & -0.01 \\ -15.21 & -0.74 & -4.00 \\ 0 & 0 & -13 \end{pmatrix} \begin{pmatrix} \alpha \\ q \\ \delta_e \end{pmatrix} + \begin{pmatrix} 0 \\ 0 \\ 13 \end{pmatrix} \delta_e \\ \begin{pmatrix} a_n \\ q \end{pmatrix} &= \begin{pmatrix} -11.86 & -0.19 & -1.50 \\ 0 & 1 & 0 \end{pmatrix} \begin{pmatrix} \alpha \\ q \\ \delta_e \end{pmatrix} + \begin{pmatrix} 0 \\ 0 \end{pmatrix} \delta_e \end{aligned} \tag{2.7}$$

In this system, there is a right half plane (non-minimum phase) zero at 4.34 in the transfer funciton of the normal acceleration. The existence of an RHP-zero introduces fundamental limitations on the level of performance that can be realized in the system's output. RHP-zeros are indicative of an inverse response characteristic within the time domain. This means the system's initial reaction to a step input might be in the reverse direction to its eventual steady-state response, which can vary based on the count of non-minimum phase zeros present. Such a response pattern is generally considered unfavorable from the perspective of a human operator due to its counterintuitive nature. The initial undershoot in the system's response becomes more pronounced with a reduction in the settling time (Middleton, 1991). This indicates a trade-off between the performance of the system and the magnitude of the undershoot.

Part II

Linear Quadratic Control

3

Linear Quadratic Regulator

The Linear Quadratic Regulator (LQR) problem is fundamental in numerous control design techniques. LQR is not only a powerful design method itself, but it also forms the basis for many modern, systematic control design approaches. Since its development in the 1960s, the LQR problem has been extensively researched. It essentially represents a solution to a convex least squares optimization problem, that has several appealing features. These include the assurance of stability at the plant input and the simplicity of its implementation. This chapter discusses in detail the fundamental LQR problem and its various useful adaptations.

3.1. The Regulator Problem

The regulator problem plays an important role in the field of control system design, aiming to keep the system's outputs at zero while simultaneously achieving desired time-response characteristics. Consider a linear system where the state $x(t)$ has been perturbed from equilibrium to a non-zero initial condition. The aim of the problem is to regulate the states back to the equilibrium point $x = 0$. When full-state feedback is assumed, the design challenge involves finding a balance between achieving a rapid transient response for $x(t)$ and maintaining control efforts $u(t)$ within reasonable limits. Consequently, the LQR control utilizes a performance index for this purpose over a finite or infinite period of time. This study focuses on the latter. Consider the state-space representation of a linear time-invariant (LTI) system with full state feedback in Equation 3.1

$$\begin{aligned} \dot{x}(t) &= Ax(t) + Bu(t), \quad x_0 = x(0) \\ y(t) &= Cx(t), \quad C = I \end{aligned} \tag{3.1}$$

where $A \in \mathcal{R}^{n_x \times n_x}$ and $B \in \mathcal{R}^{n_x \times n_u}$ are constant matrices. The quadratic performance index over an infinite period of time is considered in Equation 3.2.

$$J = \int_0^\infty (x(t)^T Q x(t) + u(t)^T R u(t)) dt \tag{3.2}$$

Here, $Q = Q^T \geq 0$ and $R = R^T > 0$ with $Q \in \mathcal{R}^{n_x \times n_x}$ and $R \in \mathcal{R}^{n_u \times n_u}$, where n_x and n_u are the number of states and inputs respectively, with the pair (A, B) stabilizable and the pair $(A, \sqrt{Q})$ detectable. If these assumptions hold, the linear quadratic controller is the unique, optimal, full state feedback control law given in Equation 3.3

$$u(t) = -Kx(t) \quad \text{where } K = R^{-1}B^T P \tag{3.3}$$

where $K \in \mathcal{R}^{n_u \times n_x}$ is a constant matrix of the LQR-optimal feedback gains and P is the unique, symmetric, positive semidefinite solution to the algebraic Riccati equation (ARE) given in Equation 3.4.

$$PA + A^T P - PBR^{-1}B^T P + Q = 0 \tag{3.4}$$

Substituting the control law in Equation 3.3 into the system dynamics in Equation 3.1, the following closed-loop system is obtained.

$$\dot{x} = \underbrace{(A - BK)}_{A_{cl}} x \tag{3.5}$$

The LQR approach ensures stability for the closed-loop system characterized by the constant matrix A_{cl}. Consequently, the eigenvalues of A_{cl} are situated in the left half of the complex plane, satisfying $\mathcal{R}(\lambda(A_{cl})) < 0$. Increasing the LQR gains can improve time-domain performance of the closed loop system but high gains could cause saturation of the actuators (Anderson and Moore, 2007).

3.2. Guaranteed Stability Margins

The full-state feedback LQR approach demonstrates guaranteed classical stability margins at the plant's input. This can be validated through an analysis of the input return difference transfer function within the frequency domain (Lavretsky and K. Wise, 2013). The open loop transfer function obtained by breaking the loop at the plant input (u_c) in Figure 3.1 is given in Equation 3.6.

$$L(s) = K(s - I)^{-1}B \tag{3.6}$$

Using the ARE in Equation 3.4 and subtracting sP from both sides results in Equation 3.7.

$$P(sI - A) + (-sI - A^T)P + PBR^{-1}B^TP = Q \tag{3.7}$$

Here, $(sI - A)^{-1}$ is denoted by Φ, following which the equation is manipulated and rearranged to get Equation 3.8.

$$B^TP\Phi B + B^T\Phi^*PB + B^T\Phi^*PBR^{-1}B^TP\Phi B = B^T\Phi^*Q\Phi B \tag{3.8}$$

The term $R > 0$ is added to both sides of Equation 3.8. By substituting the expressions $K = R^{-1}B^TP$ and $L(s) = K(sI - A)^{-1}B = K\Phi B = R^{-1}B^TP\Phi B$ in Equation 3.8 and further simplifying gives Equation 3.9.

$$(I + L(s))^*R(I + L(s)) = R + B^T\Phi^*Q\Phi B \tag{3.9}$$

where $I + L(s)$ is the return difference matrix, computed at the system input break point and the term $B^T\Phi^*Q\Phi B$ is a Hermitian positive semidefinite matrix. Thus, Equation 3.9 can be written as given below.

$$(I + L(s))^*R(I + L(s)) \geq R \tag{3.10}$$

Assuming an equal penalty for each control element, where R is set as $R = \rho I$, with ρ being a positive constant results in Equation 3.11.

$$(I + L(s))^*(I + L(s)) \geq I \tag{3.11}$$

This describes the magnitude characteristics of the input return difference. In systems with a single input, where $n_u = 1$, this condition is analogous to the Nyquist plot not intersecting the unit circle centered at $(-1, j0)$. For systems with multiple inputs, where $n_u > 1$, it implies that the smallest singular value of the return difference matrix, when evaluated across different frequencies, consistently exceeds a magnitude of one. Hence, LQR control guarantees minimum gain margin of $[-6, \infty]$ dB and phase margin of 60° at the plant input.

These features contribute to the popularity of LQR in industrial applications. However, discrepancies in modelling, overlooked dynamics, noise, and various other perturbations can prevent these ideal margins from being achieved in actual systems. Therefore, it is crucial to exercise caution to prevent excessive control gains that lead to designs with high bandwidth, which is particularly important in most physical systems and especially so in the field of aerospace (Lavretsky and K. Wise, 2013; Levine, 2018).

3.3. Asymptotic Properties

In a system designed using LQR, the location of the closed-loop poles is determined by the tunable weight parameters Q and R. The closed-loop poles are computed using the Algebraic Riccati Equation (ARE) and it is possible to anticipate the asymptotic behavior of these poles as the control gains are increased. Consider the performance index in Equation 3.12 where ρ is a scalar design parameter.

$$J = \int_0^\infty (x(t)^TQx(t) + \rho u(t)^TRu(t))dt \tag{3.12}$$

Altering the scalar parameter ρ directly impacts the feedback control gains. It is interesting to note how the performance of the LQR changes as ρ decreases or increases. The control input relevant to this scenario is provided in Equation 3.13.

$$u = -Kx = -\frac{1}{\rho}R^{-1}B^TPx(t) \tag{3.13}$$

As $\rho \to \infty$, the closed-loop poles originate from the stable open-loop poles located in the LHP, and for any unstable open-loop poles, they begin at the corresponding mirror images about the $j\omega$-axis. If any open-loop poles lie exactly on the $j\omega$-axis, the closed-loop poles start from the left of them. Under these conditions, the LQR gains remain small. Conversely, as $\rho \to 0$, the closed-loop poles will converge upon the locations that cancel the plant's open-loop minimum phase zeros. If there are non-minimum phase open loop zeros, the closed loop poles move towards their mirror images, about the $j\omega$-axis. Any remaining poles will diverge towards infinity following stable loci. In this case, the LQR gains remain large (Levine, 2018).

3.4. Implementation

The magnitude of the optimal feedback gains is dependent on the relative sizes of Q and R. Holding R constant, if Q is increased, the system places a higher penalty on the state deviations compared to the control effort, leading to larger feedback gains and a faster closed-loop response. Conversely, reducing Q emphasizes penalization on the control effort over state deviations, which gives smaller gains and consequently, a slower system response. When selecting performance weights for an LQR design, a straightforward approach is to set the matrices R and Q as given in Equation 3.14.

$$\begin{aligned} R &= I \\ Q &= diag(Q_{11}, \ldots, Q_{ii}, \ldots, Q_{n_x n_x}) \end{aligned} \tag{3.14}$$

Here, it is assumed that the control inputs are comparable in magnitude. The individual state weights Q_{ii} should be adjusted to emphasize the states x_i that require regulation, while assigning zero or very small values to the weights of less critical states. Iterative adjustment of Q_{ii} and subsequent evaluation of the closed-loop system's performance can help determine appropriate values, taking into account factors such as settling time, overshoot, undershoot, and the system's stability margins.

This setup of using the LQR method to track a reference, in this case the normal acceleration (a_n) command, is usually referred to as the Linear Quadratic Integral (LQI). For this purpose, the tracking error is augmented with an integrator, hence yielding an additional state and then a full-state feedback LQR controller is designed for the augmented system, see Figure 3.1. Note that this setup includes computation of an integrator gain in addition to the regulator gains. In Figure 3.1, G denotes the linear model of the plant, as defined in Section 2.4. Recall that the

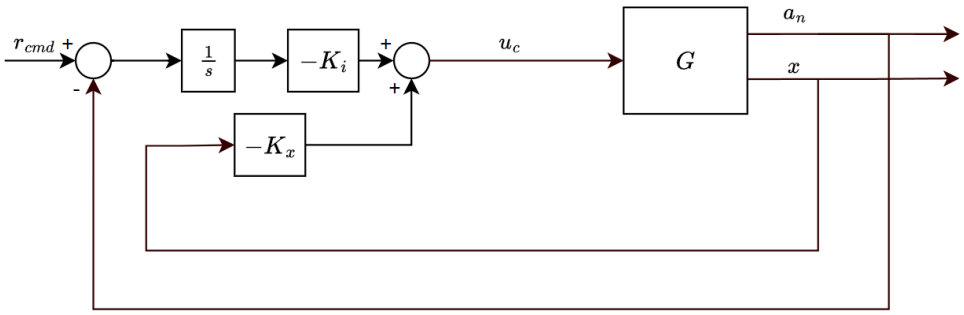

Figure 3.1: Linear Quadratic Integral-controlled closed loop system

state-space representation comprising matrices A, B, C, and D for G is derived by linearizing the Citation model as discussed in Chapter 2. This linearization is performed at an operating point specified by an altitude h_e of 10,238 meters and an airspeed V_{tas} of 87.5 meters per second. This point was selected by conducting a batch trim and linearization of the flight envelope and selecting a flight point with the presence of right half plane zero and less damping, so that the necessity for LTR arises during the stability analysis stage. Consider the open-loop system described in Equation 3.15.

$$\begin{aligned} \dot{x}(t) &= Ax(t) + Bu(t), \quad x_0 = x(0) \\ y(t) &= Cx(t) \end{aligned} \tag{3.15}$$

For tracking a reference signal, the state dynamics are augmented with an integrator state as shown in Figure 3.2. The inputs to the control gains are now the system states and the integrator state. The augmented state dynamics is given in Equation 3.16. Here, C_{yr} is the row in matrix C corresponding to the a_n output. Compared to the regulator problem, in this case, the Q matrix has an extra dimension corresponding to the integral of the tracking error $x_i(t)$

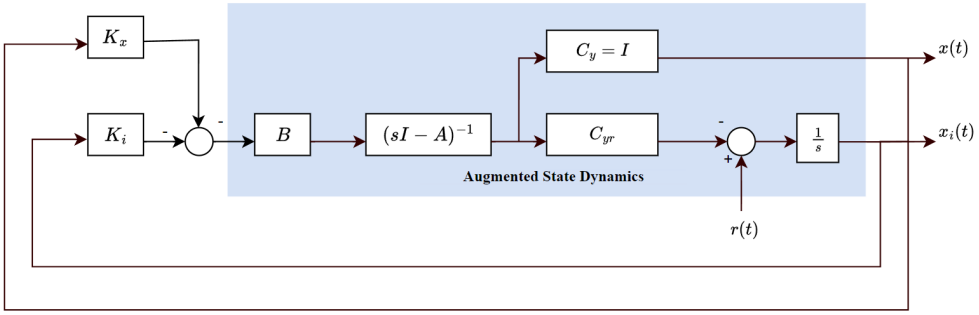

Figure 3.2: Linear Quadratic Integral-controlled closed loop system with augmented state dynamics

state that is to be kept small. The Q matrix is given in Equation 3.16c.

$$\begin{bmatrix} \dot{x}(t) \\ \dot{x}_i(t) \end{bmatrix} = \begin{bmatrix} A & 0 \\ -C_{yr} & 0 \end{bmatrix} \begin{bmatrix} x(t) \\ x_i(t) \end{bmatrix} + \begin{bmatrix} B \\ 0 \end{bmatrix} u(t) \tag{3.16a}$$

$$\dot{x}_{aug}(t) = A_{aug}x_{aug}(t) + B_{aug}u(t), \quad y_{aug}(t) = x_{aug}(t) \tag{3.16b}$$

$$Q = \text{diag}(Q_x, Q_{xi}), \quad Q_x = 0 \text{ and } Q_{xi} \text{ is varied} \tag{3.16c}$$

According to Lhachemi, Saussie, and Zhu, 2014, the settling time for normal acceleration is desired to be less than 3 seconds. Additionally, we aim to keep the step response within 5% tolerance band of the reference value. With this goal, the weight on the x_i state is swept from 1 to 100 and the locus of the closed-loop system poles along with the open loop system's poles and zeros are shown in Figure 3.3. This also includes the non-minimum phase zero at 4.342. Two of the poles, one from the integrator and the actuator pole are approaching the LHP zero of the system at -3.79 and the mirror image of the RHP plane zero at 4.342 along the negative real axis respectively. The remaining short-period poles move out to infinity along the negative real axis. In this analysis, the time-domain performance

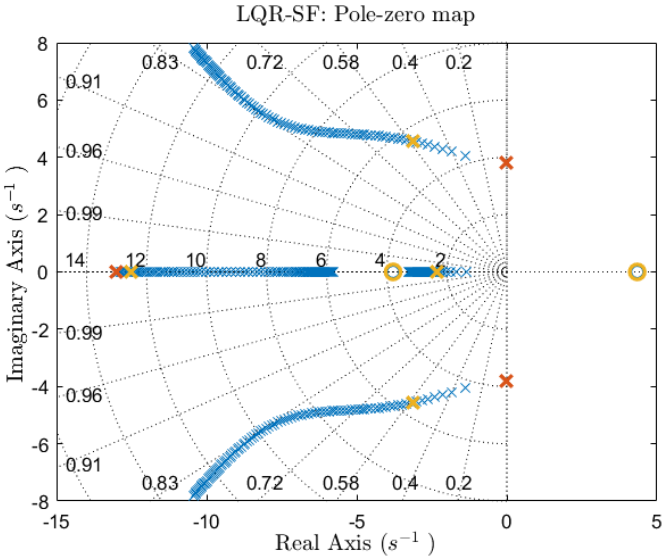

Figure 3.3: Locus of closed-loop poles (blue) for full-state feedback LQR design, with open-loop poles and zeros (red), and the poles and zeros corresponding to the optimal Q_{44} value (yellow)

metrics being focused on are rise time, settling time, percent overshoot, and percent undershoot, with the latter being particularly pertinent due to the system's non-minimum phase nature. For the frequency domain, the attention is on the minimum singular value of the return difference function, denoted as $\underline{\sigma}(I + L)$, and that of the stability robustness function, represented as $\underline{\sigma}(I + L^{-1})$. When plotted against the Q_{44} weighting parameters, these metrics help to

assess how an increase in the system's bandwidth influence its characteristics, thereby guiding the selection of an appropriate Q_{44} value.

As the Q_{44} weighting parameter value becomes larger, the system exhibits a faster response to the step command. This is evident in Figure 3.4a, which illustrates that as Q_{44} value increases (thereby increasing the bandwidth), the rate of improvement in response speed diminishes. The root locus presented in Figure 3.3 further supports this observation. As the system's dominant poles move towards the zero positions, the change in their locations becomes less pronounced with increasing Q_{44} value. While the poles that are moving towards infinity continue to move along the asymptotes, their impact on the system's response diminishes rapidly as the eigenvalues grow large and negative. This suggests that excessively high gains are not necessary to achieve a fast response in the system.

As the Q_{44} weighting parameter value increases, there is a noticeable increase in the percentage undershoot as seen in Figure 3.4c. This undesirable characteristic needs to be minimized and hence, lower gains are preferred. An attractive feature of LQR state-feedback designs, the value of $\underline{\sigma}(I + L)$ remains constant at one across all Q_{44} design values. Conversely, $\underline{\sigma}(I + L^{-1})$, which is essentially the reciprocal of the infinity norm of the complementary sensitivity function, acts as an indicator of the damping within the dominant poles of the closed-loop system. The objective is to maximize $\underline{\sigma}(I + L^{-1})$. Figure 3.4b indicates that this metric tends to be more favorable towards lower gains.

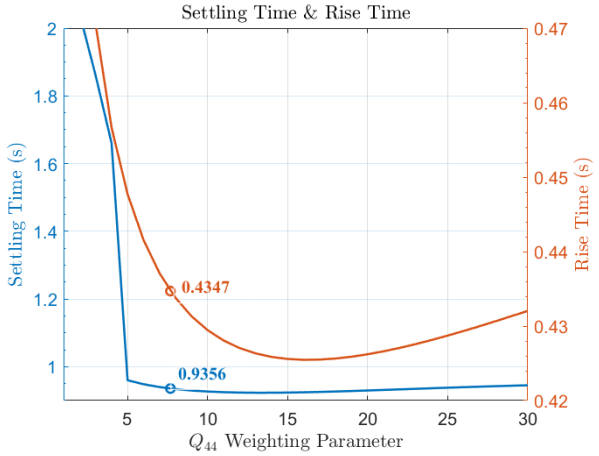

(a) Settling Time (blue) and Rise Time (red)

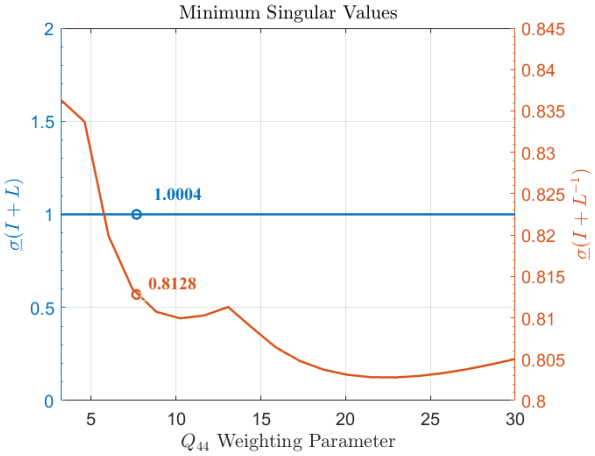

(b) Minimum singular values of return difference (blue) and stability robustness (red) functions

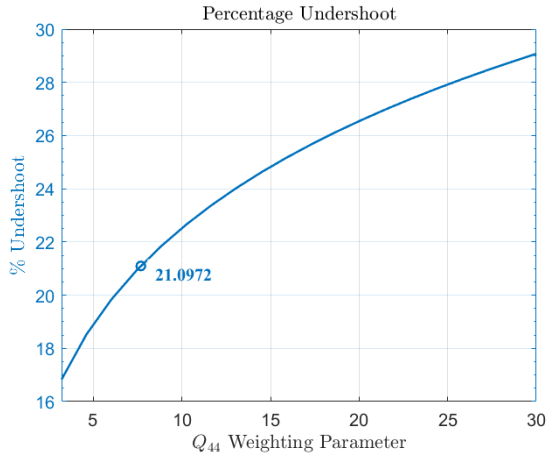

(c) Percentage undershoot

Figure 3.4: Time-domain and frequency-domain performance metrics with increasing Q_{44} weighting parameter for full-state feedback LQR-controlled system

The situation presents a conflict where certain performance indicators favour larger feedback gains, and some prefer smaller gains. Therefore, it is crucial to find a middle ground, carefully balancing the benefits of increased bandwidth from a higher Q_{44} value with the negative aspects that also arise from this increase. Considering the analysis and the requirement of the step response to be in the 5% envelope, the optimal value of Q_{44} is found to be 7.6751 and the corresponding integrator and state feedback gains are given in Equation 3.17.

$$\begin{aligned} K_i &= -2.77 \\ K_x &= [\underbrace{-8.4249}_{K_\alpha} \quad \underbrace{-3.6338}_{K_q} \quad \underbrace{0.6176}_{K_{\delta_e}}] \end{aligned} \tag{3.17}$$

The increase in the magnitude of the gains with increasing Q_{44} weighting parameter can be seen in Figure 3.5. In Figure 3.6, the plots display the behavior of the tracked variable a_n and the state variables of the closed-loop systems with varying Q_{44} weighting parameter. It is observed that the normal acceleration responses exhibits no overshoot. This could be attributed to the system's relatively slow response and limited control authority, a consequence of the presence of RHP zero in the closed-loop system. Given the absence of overshoot in these responses, the percentage overshoot metric was not used in determining the optimal value for the Q_{44} parameter.

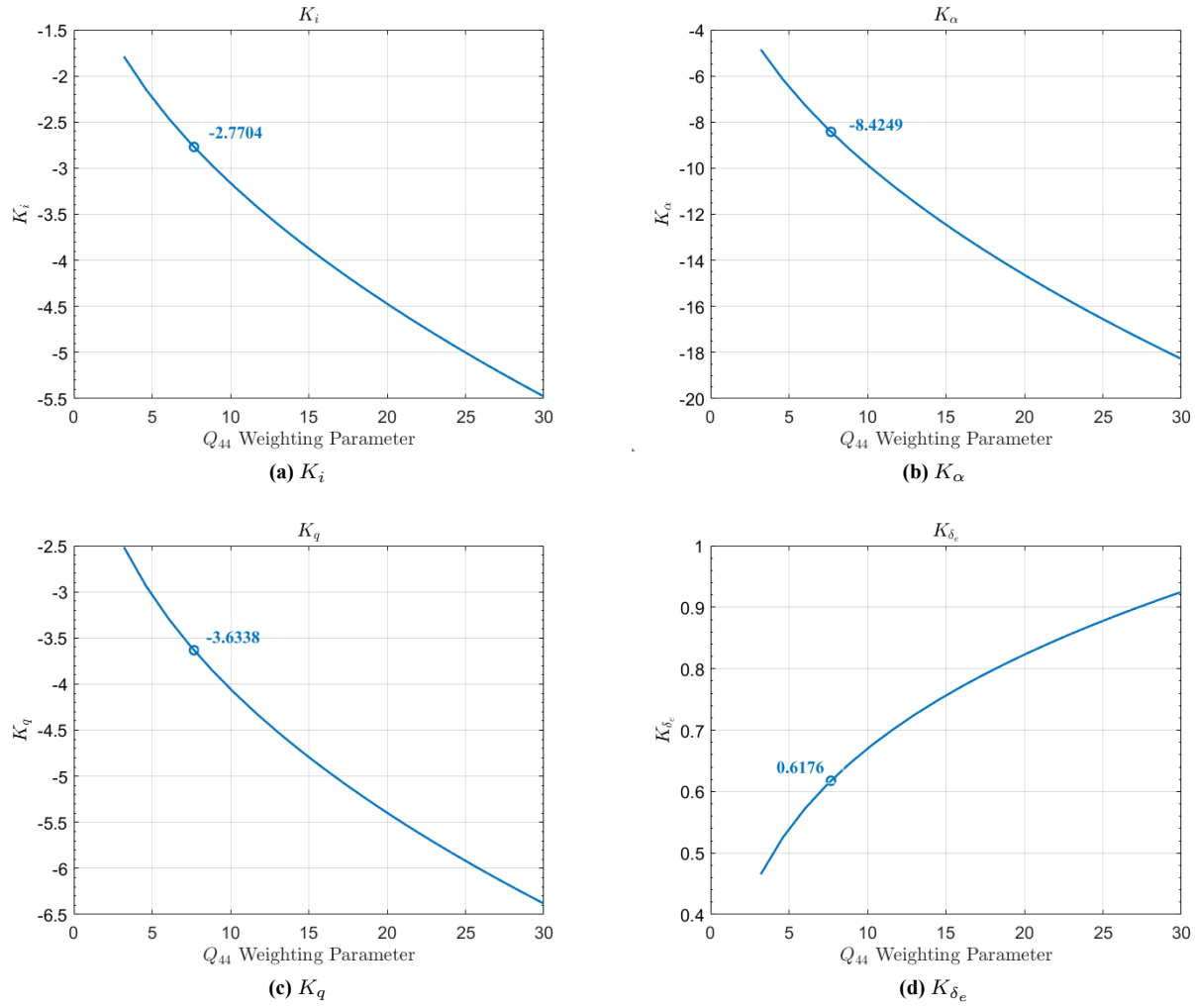

(a) K_i **(b)** K_α **(c)** K_q **(d)** K_{δ_e}

Figure 3.5: Controller state-feedback gains with increasing Q_{44} weighting parameter for full-state feedback LQR-controlled system

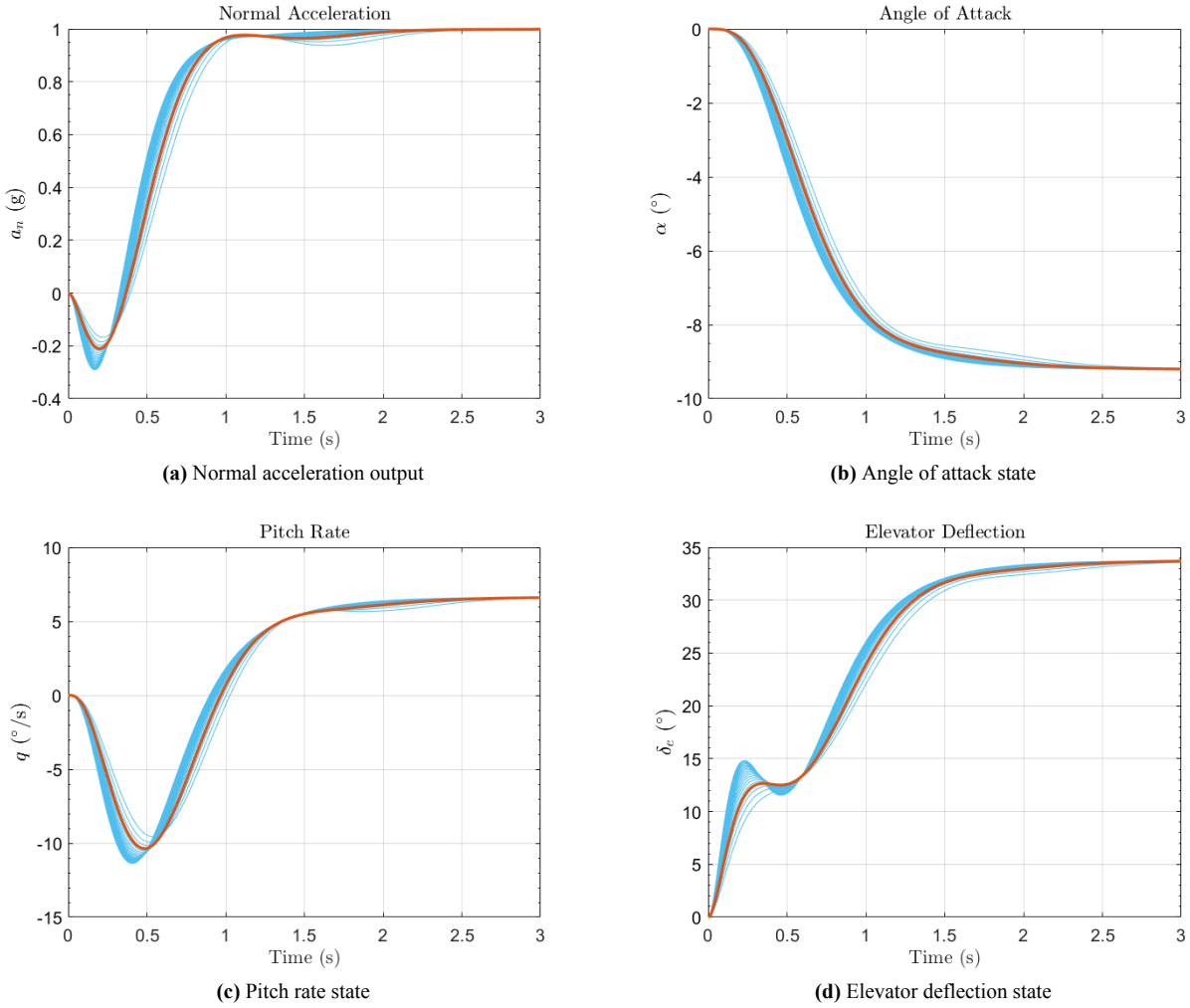

(a) Normal acceleration output

(b) Angle of attack state

(c) Pitch rate state

(d) Elevator deflection state

Figure 3.6: Time responses of system states (α, q, δ_e) and output (a_n, q) to a unit normal acceleration command with varying Q_{44} weighting parameter (blue) and the optimal Q_{44} value (red) for state-feedback LQR design

3.5. Linear Quadratic Regulator with Output Feedback

Full-state feedback LQR controllers assume the availability of all state measurements for feedback, which is not always practical. In such a case, using a dynamic observer to estimate the states based on available output measurements is an alternative, like in LQG-controlled systems. Another option is to use static output feedback methods. This section discusses how LQR design method can be adapted for static output feedback designs as shown in Figure 3.7. Consider a linear system given in Equation 3.18 where the state has been perturbed from equilibrium to a non-zero initial condition. The aim of the problem is to regulate the states back to the equilibrium point $x = 0$.

$$\begin{aligned} \dot{x}(t) &= Ax(t) + Bu(t), \quad x_0 = x(0) \\ y(t) &= Cx(t), \end{aligned} \tag{3.18}$$

Here, $A \in \mathcal{R}^{n_x \times n_x}$ and $B \in \mathcal{R}^{n_x \times n_u}$ are constant matrices. The quadratic performance index over an infinite period of time is considered in Equation 3.19 and the control law along with the gain calculation is given in Equation 3.20.

$$J = \int_0^\infty (x(t)^T Q x(t) + u(t)^T R u(t)) dt \tag{3.19}$$

$$u(t) = -Ky(t) \quad \text{where } K = R^{-1}B^T PSC^T(CSC^T)^{-1} \tag{3.20}$$

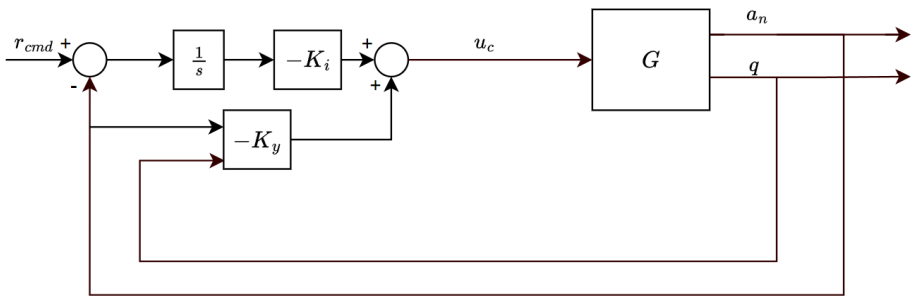

Figure 3.7: Linear Quadratic Integral-controlled closed loop system with static output feedback

Here, $Q = Q^T \geq 0$ and $R = R^T > 0$ with $Q \in \mathcal{R}^{n_x \times n_x}$ and $R \in \mathcal{R}^{n_u \times n_u}$, with the pair (A, B) output stabilizable, the pair $(A, \sqrt{Q})$ detectable and the matrix C has full rank. Here, the matrices P and S are the solutions of two Lyapunov equations. Assuming the closed-loop system achieves asymptotic stability, causing $x(t)$ to diminish over time, the performance index in Equation 3.19 can be expressed as given in Equation 3.21.

$$J = \frac{1}{2} x^T(0) P x(0) \tag{3.21}$$

The challenge in the output feedback LQR problem lies in identifying the feedback gains K within the control input in Equation 3.20 that will minimize the performance index given in Equation 3.19. The matrix K, where $K \in \mathcal{R}^{n_u \times n_y}$ represents a constant matrix of LQR-optimal feedback gains. It has been demonstrated by Stevens, Lewis, and Johnson, 2016 that given any fixed feedback matrix K, if a constant, symmetric, and positive-semidefinite matrix P exists that satisfies Equation 3.22a and the closed-loop system ($A_{cl} = A - BKC$) is stable, the cost J can be defined in terms of P as per Equation 3.21.

$$g = A_{cl}^T P + P A_{cl} + Q + (KC)^T R (KC) = 0 \tag{3.22a}$$

$$A_{cl} S + S A_{cl}^T + X = 0 \tag{3.22b}$$

The matrix X depends on the expected value of the initial state $X = E\{x_0 x_0^T\}$. Hence, in the output feedback scenario, the gain is dependent on the initial state conditions through the Equations 3.20 and 3.22b. The dependence on the initial conditions is an undesirable property of LQR output feedback designs as the initial condition is unknown in many applications. This issue is circumvented by assuming the expected value of a uniformly distributed x_0. Hence, now the expected value of the performance index, given in Equation 3.23, is minimized instead.

$$E\{J\} = \frac{1}{2} E\{x^T(0) P x(0)\} = \frac{1}{2} tr(PX), \quad \text{where} \quad X = E\{x(0) x^T(0)\} \tag{3.23}$$

3.5.1. Establishing the Output Feedback Gain

The optimal output feedback gains are obtained using an iterative algorithm as detailed by (Moerder and Calise, 1985; Stevens, Lewis, and Johnson, 2016). This algorithm operates under several convergence conditions outlined as follows.

1. There exists a gain K such that A_{cl} is stable. When such a gain exists, the system is regarded as output stabilizable.
2. The output matrix C must have full rank.
3. Control weighting matrix (R) needs to be positive definite, indicating that all the control inputs are weighted in the performance index.
4. The matrix (Q) must be positive semidefinite and the pair $(\sqrt{Q}, A)$ must be detectable. This implies that the observability matrix polynomial shown in Equation 3.24 has full rank for all values of the complex variable s that are not on the left half of the complex plane. This condition implies that all unstable systems must be observable in the performance index.

$$O(S) = \begin{bmatrix} sI - A \\ -\sqrt{Q} \end{bmatrix} \tag{3.24}$$

Under these conditions, the algorithm detailed in Algorithm 1 successfully determines an output feedback gain that stabilizes the plant and also minimizes the performance index.

Algorithm 1: LQR static output feedback solution

Step 1: Initialize

Set $k = 0$.

Obtain an initial gain K_0 so that $A - BK_0C$ is asymptotically stable.

Step 2: Iteration

Set $A_k = A - BK_kC$.

Solve for P_k and S_k in the following equations:

$0 = A_k^T P_k + P_k A_k + C^T K_k^T R K_k C + Q$

$0 = A_k S_k + S_k A_k^T + X$

Set $J_k = \frac{1}{2}\text{tr}(P_k X)$.

Evaluate the gain update direction:

$\Delta K = R^{-1}B^T P_k S_k C^T (C S_k C^T)^{-1} - K_k$

Update the gain:

$K_{k+1} = K_k + \alpha \Delta K$

where α is chosen such that $A - BK_{k+1}C$ is asymptotically stable and $J_{k+1} \leq J_k$.

If J_{k+1} and J_k are sufficiently close, proceed to terminate.

Otherwise, increment k by 1 and repeat Step 2.

Step 3: Terminate:

Set $K = K_{k+1}$ and $J = J_{k+1}$.

Terminate the algorithm.

Since the algorithm presented here is iterative in nature, an initial output feedback gain K_0 must be selected that stabilizes the closed loop $A - BK_0C$. In this study, the initial gain is obtained by the method of pole placement. This is done by using the `TuningGoal.Poles` constraint in the `systune`[1] function in `MATLAB` which is used to specify requirements on the location of the closed-loop poles of a control system.

A tuning method similar to the LQR state-feedback design, as detailed in Section 3.4, is employed. Here, the Q_{44} weighting parameter is varied from 1 to 5 in 20 increments, and both time-domain and frequency-domain characteristics are examined to ascertain the optimal Q_{44} value. Similarly, the pole locus of the closed-loop system reveals that two of its poles - one associated with the integrator and the actuator pole - converge towards the open-loop LHP zero at -3.79 and the negative of the RHP zero at -4.342. Post-convergence, these poles begin to diverge. Meanwhile, the remaining two poles, pertaining to the short period mode, trend towards infinity. It is important to note that in the depiction of the closed-loop pole locus in Figure 3.8, more than 20 samples are utilized to illustrate the trajectory of the poles across the complex plane. For the selected optimal Q_{44} values for the state-feedback and output-feedback cases, the time-domain properties are given in Table 3.1.

Table 3.1: Time-domain characteristics of optimal state feedback and static output feedback LQR-controlled systems

Controller	Settling Time (s)	Rise Time (s)	Undershoot (%)
LQR-SF	0.93	0.43	21.10
LQR-OF	1.02	0.45	15.31

In terms of frequency-domain analysis, unlike the LQR full state-feedback case, the output feedback configuration shows that the minimum singular values of the return difference matrix do not remain constant across all frequencies. In fact, a decrease in these values was observed as the Q_{44} weighting parameter increased, as expected for the stability robustness matrix. However, for the optimal Q_{44}, both $\underline{\sigma}(I + L)$ and $\underline{\sigma}(I + L^{-1})$ maintained values exceeding 0.5,

[1] Mathworks Documentation: https://nl.mathworks.com/help/control/ref/dynamicsystem.systune.html

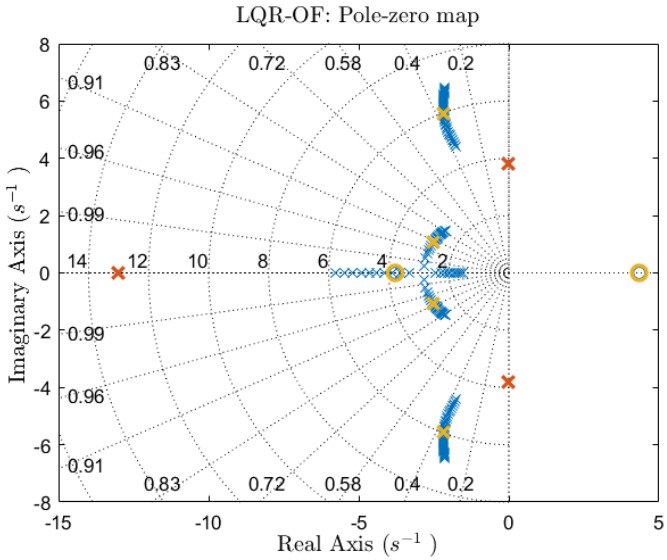

Figure 3.8: Locus of closed-loop poles (blue) for output feedback LQR design, with open-loop poles and zeros (red), and the poles and zeros corresponding to the optimal Q_{44} value (yellow)

specifically 0.50 and 0.60, respectively, as depicted in Figure 3.9. The gains corresponding to the optimal value of the Q_{44} weighting parameter are given in Equation 3.25.

$$\begin{aligned} K_i &= -0.8456 \\ K_x &= [\underbrace{0.1904}_{K_{an}} \quad \underbrace{-1.2358}_{K_q}] \end{aligned} \tag{3.25}$$

The plots depicting the evolution of time-domain characteristics, specifically settling time, rise time, and percentage undershoot, as the Q_{44} weighting parameter increases, can be found in Appendix A.1. Additionally, this section includes time responses of the system's outputs and states to a normal acceleration command signal equivalent to 1 g as seen in Appendix A.3.

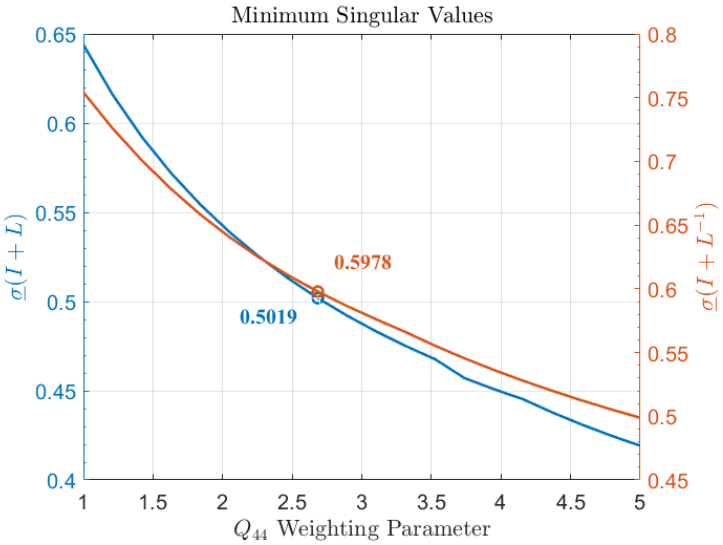

Figure 3.9: Minimum singular values of return difference (blue) and stability robustness (red) functions with increasing Q_{44} weighting parameter for static output-feedback LQR-controlled system

3.6. LQR-OF Implementation Using `systune`

The function `systune` in MATLAB can be used for tuning control systems modelled as `genss` (generalized state-space) models containing tunable blocks. It automatically adjusts the parameters of a control system to achieve specified high-level tuning goals. `systune` differentiates between 'hard' and 'soft' tuning goals, where hard goals are mandatory objectives that must be met, and soft goals are more flexible targets. The command aims to satisfy hard goals by keeping their associated cost functions below a threshold value of 1, and simultaneously tries to fulfill soft goals within this constraint.

This study uses `TuningGoal.LQG` (or the LQR/LQG Goal) to set a tuning objective that quantifies control performance as an LQG cost as given in Equation 3.26. This tuning goal is flexible and can be applied to a wide range of control structures, beyond just the typical observer setup used in standard LQG control.

$$J = E(z(t)^T Q z(t)) = \lim_{T\to\infty} E\left(\frac{1}{T}\int_0^T z(t)^T Q z(t) dt\right) \tag{3.26}$$

Here, $z(t)$ is the system response to a white noise input vector $w(t)$. The covariance of $w(t)$ is given in Equation 3.27.

$$E(w(t)w(t)^T) = QW \tag{3.27}$$

The vector $w(t)$ includes external inputs such as noise and disturbances, whereas $z(t)$ contains performance-related system variables, including control signals and states. The matrices QZ and QW are performance and covariance matrices, respectively, contributing to the LQG cost as specified in Equation 3.26. In case of tuning LQR-controllers, the covariance matrix is essentially an identity matrix while the performance matrix is a combination of the block diagonal matrix Q and R.

When the LQG requirement is used as a hard goal, the software tries to drive the cost function $J < 1$. When it is used as a soft goal, the cost function J is minimized subject to any hard goals and its value is contributed to the overall objective function. The steps involved in constructing LQR controllers through `systune` are mentioned below.

1. The first step is to create a generalized state-space system of the plant. In this study, the auxiliary system as shown in Figure 3.10 and Equation 3.28 (Levine, 2018) is used for this purpose where the closed-loop system is taken to be the function from the disturbance signals $w(t)$ to the performance output $z(t)$.

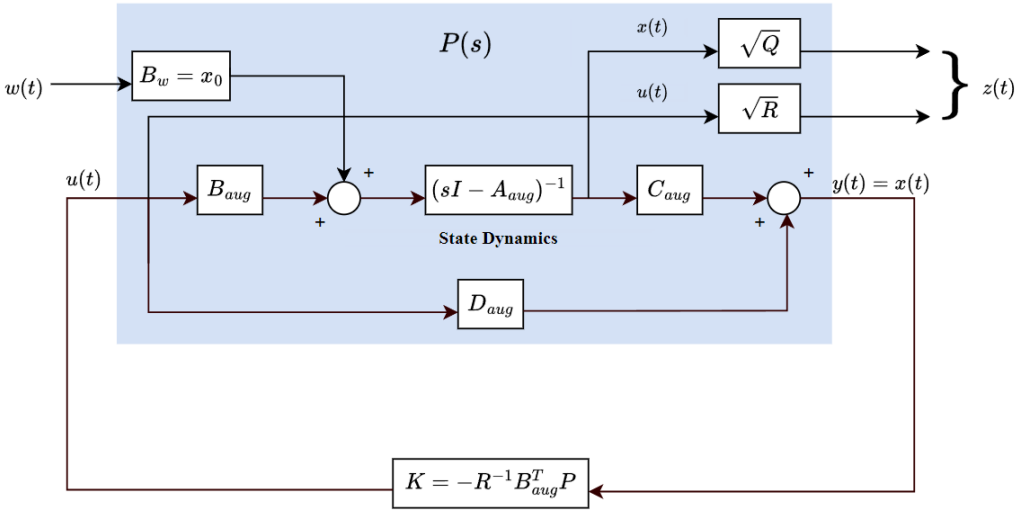

Figure 3.10: LQR-controlled closed-loop system in standard form with full-state feedback

$$\begin{aligned}
\dot{x}(t) &= Ax(t) + B_w w(t) + B_u u(t) \\
z(t) &= C_z x(t) + D_{zw} w(t) + D_{zu} u(t) \\
y(t) &= C_y x(t) + D_{yw} w(t) + D_{yu} u(t)
\end{aligned} \tag{3.28}$$

In the context where $B_w = x_0$ represents the initial state condition and the disturbance $w(t) = \delta(t)$ is modelled as an impulse input, the performance matrices are as specified in Equation 3.29. With the state feedback $C_y = I$, $D_{yu} = 0$, and with the matrices D_{zw}, D_{yw} set to zero, substituting $u = Kx$ (positive feedback in this case), yields the closed-loop transfer functions $T_{wz}(s)$ as given in Equation 3.30b.

$$C_z = \begin{bmatrix} \sqrt{Q} \\ 0 \end{bmatrix}, \quad D_{zu} = \begin{bmatrix} 0 \\ \sqrt{R} \end{bmatrix} \tag{3.29}$$

$$\begin{aligned} \dot{x}(t) &= (A + B_u K)x(t) + x_0\delta(t) \\ z(t) &= (C_z + D_{zu}K)x(t) \end{aligned} \tag{3.30a}$$

$$T_{wz}(s) = (C_z + D_{zu}K)(sI - (A + B_u K))^{-1}x_0 \tag{3.30b}$$

It is shown in (Levine, 2018) that the performance index used in LQ control, given in Equation 3.2, is equivalent to the square of the $\mathcal{H}_2$ norm of the closed loop system ($||T_{wz}||_2^2$). To design the LQR gains, a theorem exists which stipulates that a state feedback control in the form $u(t) = Kx(t)$ can ensure $J(x, u) < \gamma$ for a positive γ if, and only if, there exist matrices X in $\mathcal{R}^{n_x \times n_x}$, Y in $\mathcal{R}^{n_u \times n_u}$, and W in $\mathcal{R}^{n_u \times n_x}$, all of which must satisfy the constraints given in Equation 3.31 to minimize the performance index.

$$\begin{aligned} (AX + B_u W) + (AX + B_u W)^T + x_0 x_0^T &< 0 \\ \text{tr}(\sqrt{Q}X\sqrt{Q^T}) + \text{tr}(Y) &< \gamma \\ \begin{bmatrix} -Y & \sqrt{R}W \\ (\sqrt{R}W)^T & -X \end{bmatrix} &< 0 \end{aligned} \tag{3.31}$$

The state feedback gain is consequently defined as $K = -WX^{-1}$. It becomes clear that to minimize the quadratic performance index $J(x, u)$ one must minimize γ while adhering to the constraints in Equation 3.31. The optimal gain K is then derived form the smallest value of γ, denoted as γ_{min} ensuring that $J = \|T_{wz}(s)\|_2^2 < \gamma_{\text{min}}$.

2. The second step involves defining the tunable gain matrices and building the tunable closed-loop system. Tunable gain matrices consist of static gains, either for full-state feedback or output-feedback scenarios.
3. Next, the design objectives are outlined and the tunable parameters are adjusted accordingly. In this context, the LQG tuning goal is applied, where the noise covariance matrix is set as an identity matrix and the performance weights matrix is a block diagonal combination of the Q and R matrices. The LQG goal is considered a soft constraint, and the `systune` function is utilized for parameter tuning. The MATLAB code relevant to this design method is given in Appendix A.2.

4

Linear Quadratic Gaussian

During the 1960s, the optimal control field matured significantly with the advent of linear quadratic Gaussian (LQG) control, built upon Wiener's work on optimal filtering from the 1940s. The name LQG arises from using a linear model, an integral quadratic cost function and Gaussian white noise processes to model disturbance signals and noise. This development was closely linked to substantial research programs and funding in the United States and the former Soviet Union, focusing on space-related challenges. Problems such as minimizing fuel consumption during rocket manoeuvres were well-defined and suited for optimization methods, making LQG control a valuable tool for addressing them (Skogestad and Postlethwaite, 2005). However, LQG designs sometimes lacked the robustness required for application, even outside the aerospace industry. The special issue on LQG problems, see (M. Athans, 1971), sheds light on the state of the art of this problem in various aspects, offering clear and instructive accounts. Despite the relative maturity of LQG control in the 1960s, additional research was necessary to address unresolved issues.

4.1. Linear Quadratic Gaussian

The challenge of designing flight control systems without access to all state measurements has driven the innovation of dynamic output feedback controllers. In LQG, the control mechanism employed is the linear, optimal full-state feedback controller (LQR) as described in Section 3.1. On the other hand, the estimator is a linear, optimal state estimator, often referred to as the Kalman-Bucy filter (Kalman, 1964) or observer, which is tailored to minimize the state estimation error covariance in the presence of input/output disturbances. This is referred to as the Linear Quadratic Estimator (LQE). In the LQG problem, the plant dynamics are assumed to be linear, given in Equation 4.1.

$$\begin{aligned} \dot{x}(t) &= Ax(t) + Bu(t) + w(t) \\ y(t) &= Cx(t) + Du(t) + v(t) \end{aligned} \tag{4.1}$$

Here, $w(t)$ represents the disturbance or process noise, and $v(t)$ signifies the measurement noise. Both are typically assumed to be uncorrelated zero-mean Gaussian stochastic processes with power spectral density matrices, denoted by W for the disturbance and V for the measurement noise as given in Equation 4.2.

$$\begin{aligned} E\{w(t)w(\tau)^T\} &= W\delta(t-\tau) \\ E\{v(t)v(\tau)^T\} &= V\delta(t-\tau) \end{aligned} \tag{4.2a}$$

$$E\{w(t)v(\tau)^T\} = 0, \quad E\{v(t)w(\tau)^T\} = 0 \tag{4.2b}$$

Here, E is the expectation operator and $\delta(t-\tau)$ is a delta function. The stochastic assumptions made in the plant model in Equation 4.1 may not always reflect real-world conditions. The disturbances impacting the system inputs and the disturbances at the output, including sensor noise, are not necessarily white, unbiased with zero mean, and normally distributed.

4.2. Separation Theorem

The LQG problem is elegantly resolved through what is termed the separation theorem. This approach begins by establishing the optimal control solution for the LQR problem, specifically, the LQG problem without $w(t)$ and $v(t)$.

The solution emerges as a straightforward state feedback law, described in Equation 4.3a. Here, P is the unique, symmetric positive semidefinite solution to the algebraic Riccati equation given in Equation 4.3b and K is a constant gain matrix.

$$u(t) = -Kx(t) \quad \text{where } K = R^{-1}B^T P \tag{4.3a}$$

$$PA + A^T P - PBR^{-1}B^T P + Q = 0 \tag{4.3b}$$

Optimal state estimate, $\hat{x}$, is deduced so that the state estimation error covariance $E\{[x - \hat{x}][x - \hat{x}]^T\}$ is minimized by using the Kalman filter state estimator dynamics given in Equation 4.4 which is independent of the Q and R matrices. The Kalman filter gain K_f is given in Equation 4.5a where P_f is the solution to the dual algebraic Riccati equation given in Equation 4.5b. Consequently, the solution to the LQG problem is solved by substituting x by $\hat{x}$, resulting in $u(t) = -K\hat{x}(t)$. Therefore, the development of an LQG controller can be divided into two separate processes as depicted in Figure 4.1.

$$\dot{\hat{x}}(t) = A\hat{x}(t) + Bu(t) + K_f(y(t) - C\hat{x}(t)) \tag{4.4}$$

$$K_f = P_f C^T V^{-1} \tag{4.5a}$$

$$AP_f + P_f A^T - P_f C^T V^{-1} C P_f + W = 0 \tag{4.5b}$$

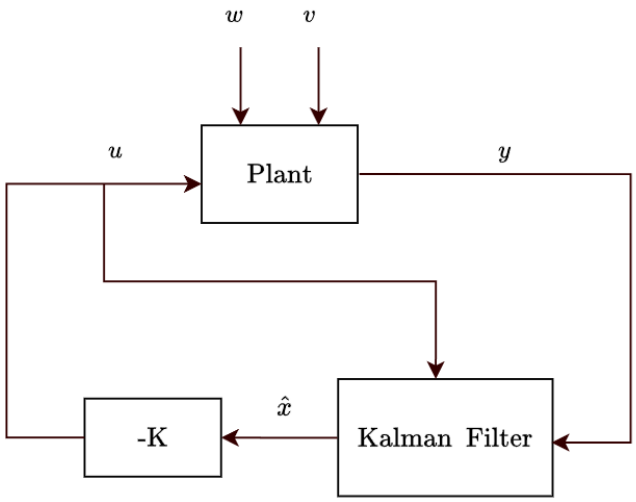

Figure 4.1: Independent design of state-feedback LQR gains and Kalman filter state estimator by the separation theorem

As shown in Figure 4.1, the LQG dynamic controller, with its structure given in Equation 4.6, processes the output from the plant to produce the corresponding input for the plant. Substituting the control law from Equation 4.3a in the estimator dynamics given in Equation 4.4 results in the LQG controller system, given in Equation 4.7a.

$$\begin{aligned} \dot{x}_K(t) &= A_K x_K(t) + B_K y(t) \\ u(t) &= C_K x_K(t) + D_K y(t) \end{aligned} \tag{4.6}$$

$$K_{LQG} = \begin{bmatrix} A_k & B_k \\ C_k & D_k \end{bmatrix} = \begin{bmatrix} A - BK - K_f C & K_f \\ -K & 0_{n_u \times n_y} \end{bmatrix} \tag{4.7a}$$

or equivalently,

$$K_{LQG}(s) = -K[sI_{n_x} - (A - BK - K_f C)]^{-1} K_f = -K\Phi_K(s)K_f \tag{4.7b}$$

where $\Phi_K(s) = [sI - (A - BK - K_f C)]^{-1}$ is the so-called LQG resolvent matrix. Note that the negative feedback in the LQR problem is already included in these controller matrices (note the term $-K$) hence, LQG controllers given here are designed with assumed positive feedback. As shown in Figure 4.2, the closed-loop dynamics can be arranged to show its dependency on the estimation error, as given in Equation 4.8a. Coupled with the estimation

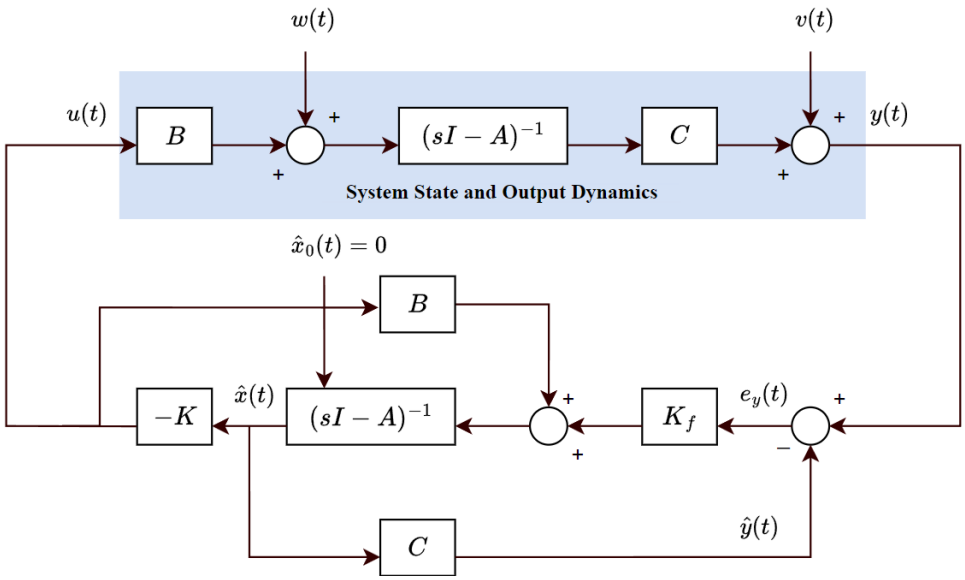

Figure 4.2: LQG-controlled closed-loop system with Kalman filter dynamics

error dynamics, see Equation 4.8b, the separation theorem can be revealed in Equation 4.8c. This demonstrates that the closed-loop poles of the LQG controller are the union of the poles of the regulator (eigenvalues of $A - BK$) and those of the Kalman filter (eigenvalues of $A - K_f C$).

$$\dot{x} = (A - BK)x + BKe + w \tag{4.8a}$$

$$\dot{e} = \dot{x} - \dot{\hat{x}} = (A - K_f C)e + w - K_f v \tag{4.8b}$$

$$\begin{bmatrix} \dot{x} \\ \dot{e} \end{bmatrix} = \begin{bmatrix} A - BK & BK \\ 0_{n_x \times n_u} & A - K_f C \end{bmatrix} \begin{bmatrix} x \\ e \end{bmatrix} + \begin{bmatrix} I_{n_x} & 0_{n_x \times n_y} \\ I_{n_x} & -K_f \end{bmatrix} \begin{bmatrix} w \\ v \end{bmatrix} \tag{4.8c}$$

4.3. Implementation

In this study, the focus is on a normal acceleration reference tracker hence, the LQG regulator controller matrices given in Equation 4.7a require certain changes to incorporate the integrator gain associated with the tracker. One way to do this is to augment the plant as done in Section 3.4 with an additional state that corresponds to the integral of the error and consequently, estimate all the four system states (α, q, δ_e and x_i) with the Kalman filter. In this case, the gains corresponding to the three states of the plant will be the same as that in the regulator problem. This is a straightforward way but it presents redundancy as the additional estimated state will not be used. A way to avoid this redundancy is to estimate only the three primary states of the plant. The revised controller matrices for the tracker case is given in Equation 4.9.

$$K_{LQG} = \begin{bmatrix} A_k & B_k \\ C_k & D_k \end{bmatrix} = \left[\begin{bmatrix} 0_{nu} & 0_{nu \times nx} \\ -BK_i & A - BK - K_f C \end{bmatrix} \quad \begin{bmatrix} 1 & 0_{1 \times (ny-1)} \\ & -K_f \end{bmatrix} \right] \\ \begin{bmatrix} -K_i & -K \end{bmatrix} \quad \begin{bmatrix} 0_{nu \times ny} \end{bmatrix} \tag{4.9}$$

Here, it should be noted that the controller takes as input the normal acceleration a_n and the pitch rate measurement q. Since, the system being developed is a reference tracker, the first input to the controller is the error between the normal acceleration and the second input would be the pitch rate in negative feedback. In this case, the reference change is directly sent to the Kalman filter which can result in a derivative or proportional "kick", typically characterized by a sudden and often large movement in the output.

By structuring the LQG controller to separate the error signal from the control law, the system can avoid this abrupt response, leading to a more gradual and controlled step response. This is seen in Figure 4.3 where the reference

change is separated form the output measurements being fed back to the controller. In this case, the controller matrices, B_k and D_k in Equation 4.9 are altered and are given in Equation 4.10.

$$B = \begin{bmatrix} 1 & 0 & 0 \\ 0_{n_x \times 1} & & -K_f \end{bmatrix} \qquad D = \begin{bmatrix} 0_{n_u \times (n_y+1)} \end{bmatrix} \tag{4.10}$$

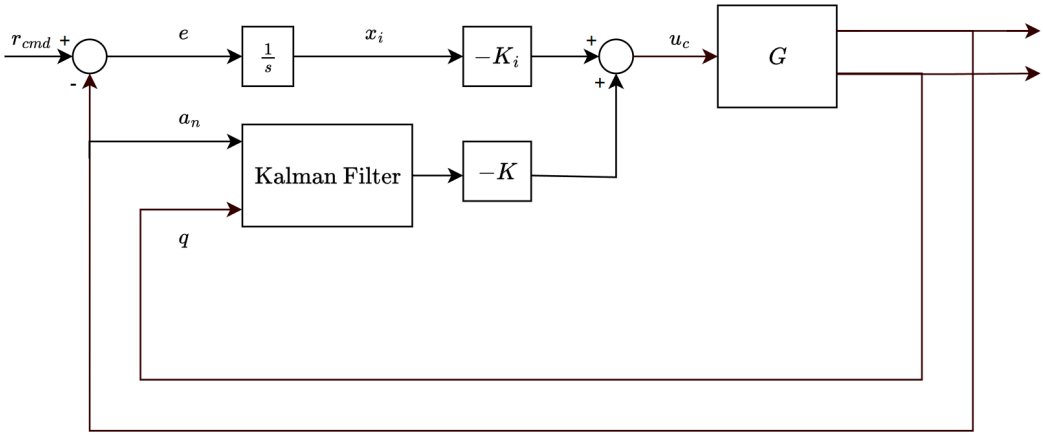

Figure 4.3: LQG-controlled closed-loop system with dynamic output feedback

The step responses of the two configurations are shown in Figure 4.4. It is evident that when the error signal is integrated into the control law, the controller exhibits a more aggressive response, as indicated by the significant undershoot-nearly twice that observed with the controller where the error signal is processed independently. The state-space representation of the resulting LQG controller, which handles the error signal separately, is presented in Equation 4.11.

$$A_k = \begin{bmatrix} 0 & 0 & 0 & 0 \\ 0 & -579.3 & -4.381 & -73.44 \\ 0 & -0.2388 & -7.871 & -2.112 \\ 36.02 & 109.5 & 47.24 & -21.03 \end{bmatrix}, \qquad B_k = \begin{bmatrix} 1 & 0 & 0 \\ 0 & 48.9 & 4.112 \\ 0 & -1.262 & -7.385 \\ 0 & 0 & 0 \end{bmatrix}$$
$$C_k = \begin{bmatrix} 2.77 & 8.425 & 3.634 & -0.6176 \end{bmatrix}, \qquad D_k = \begin{bmatrix} 0 & 0 & 0 \end{bmatrix} \tag{4.11}$$

An important point to note here is that the robustness properties of both structures of the LQG controllers would be the same as robustness is given by the feedback loop which is the same in both structures (Skogestad and Postlethwaite, 2005).

Tuning the LQG Controller

The tuning objective for the LQG controller was to match its normal acceleration time-response with that of the previously developed LQR state-feedback controller. The adopted approach in this study does this by computing the differences between the settling times, rise times, and percentage undershoots of both responses and minimizing the sum of these squared errors.

For tuning the full-state feedback LQR controller, which has been detailed earlier in Section 3.4, the elements Q_{11}, Q_{22} and Q_{33} were set to zero, while the element Q_{44} was varied across a range of values. The optimal value of Q_{44} was determined to be 7.6751. Following this optimization, the integral gain and state-feedback gains were calculated and are given in Equation 3.17.

For tuning the Kalman filter, the primary parameters were the power spectral density matrices, W for the process disturbance and V for the measurement noise. In this scenario, the measurement noise spectral density V for the outputs is constant, as determined from Table 2.1. Therefore, the main tuning focus shifted to the W matrix, structured as given in Equation 4.12.

$$W = diag(W_{11}, W_{22}, W_{33}), \quad \text{where } W_{22}, W_{33} = 0 \text{ and } W_{11} \text{ is varied} \tag{4.12}$$

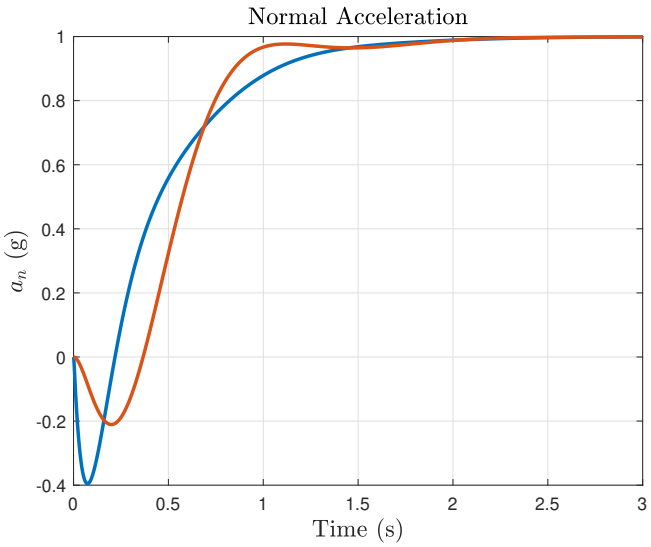

Figure 4.4: LQG-controlled closed-loop system responses for the cases where the error signal is included in the control law (blue) and where the error signal is separated from the control law (red)

Here, the emphasis was on varying W_{11}, which represents the disturbance on the angle of attack (α) state, as normal acceleration is primarily influenced by α. After sweeping the W_{11} parameter, the optimal value for minimizing total error was found to be $W_{11} = 3.58 \cdot 10^{-2}$. The estimated outputs from the noisy measurements are depicted in Figure 4.5. It can be seen that the normal acceleration response does not exhibit a typical step response. This is because the disturbance on α was used to model a system where the Kalman filter remains robust to disturbances of such magnitude on the angle of attack state. It is important to note that in output feedback systems, states are typically not directly accessible. However, during the modelling phase, the accuracy of the estimated states can still be compared with the actual system states, as demonstrated in Figure 4.6. Figures 4.5 and 4.6 illustrate that the Kalman filter is capable of accurately estimating both the outputs and the states of the system.

When tuning the Kalman filters, increasing the elements of the process noise covariance matrix W (or increasing the ratio of the W and V magnitude) generally leads to a Kalman gain K_f that places more trust in the measurements relative to the model, because it assumes more uncertainty in the model. This can result in faster poles of the estimator, as the system is more responsive to changes in measurements. Conversely, increasing the elements of the measurement noise covariance matrix V (or decreasing the ratio between W and V magnitudes) results in a Kalman gain that trusts the measurements less, because it assumes the measurements are noisier. This typically leads to slower poles of the estimator, as the system is less responsive to changes in measurements.

According to the separation theorem, the poles of the closed-loop system should be the union of the eigenvalues of the LQR and LQE closed-loop dynamics, $A - BK$ and $A - K_f C$ respectively. The LQR gains and the Kalman filter gains used for the optimal LQG-controlled system are given in Table 4.1 and the pole-zero map of the LQG-controlled closed-loop system is given in Appendix B.1.

Table 4.1: LQR and LQE closed-loop poles and gain matrices

LQR Poles	State-Feedback LQR Gains	LQE Poles	Kalman Filter Gains
$-12.5100 + 0.0000i$		-579.2992	
$-3.1297 \pm 4.5610i$	$K_{lqr} = \begin{bmatrix} -8.4249 & -3.6338 & 0.6176 \end{bmatrix}$	-7.8691	$\begin{bmatrix} -48.8957 & -4.1115 \\ 1.2623 & 7.3849 \\ -0.0000 & 0.0000 \end{bmatrix}$
$-2.3246 + 0.0000i$	$K_i = -2.7704$	-13.0000	

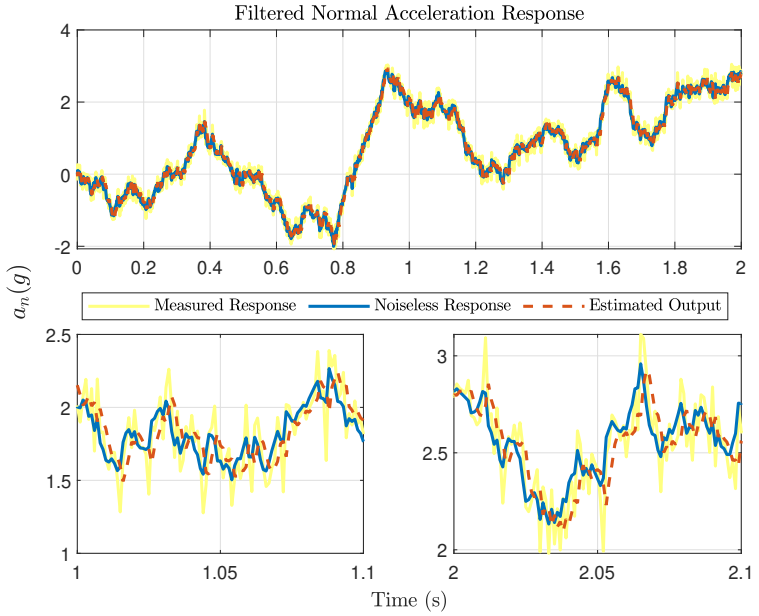

(a) Kalman filter estimate of normal acceleration output

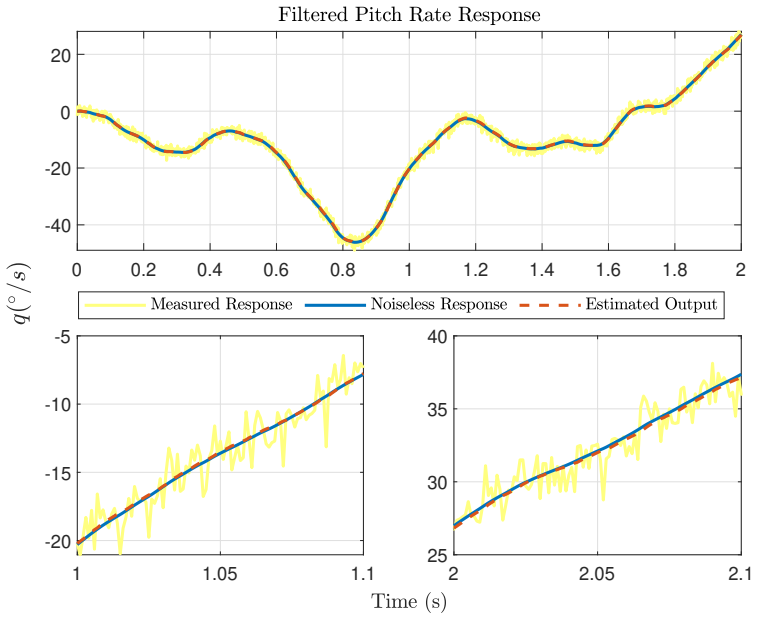

(b) Kalman filter estimate of pitch rate output

Figure 4.5: Kalman filter estimates (red- -) from measured responses (yellow) compared with noiseless responses (blue) to a unit normal acceleration command in the presence of white measurement noise and a disturbance on the angle of attack

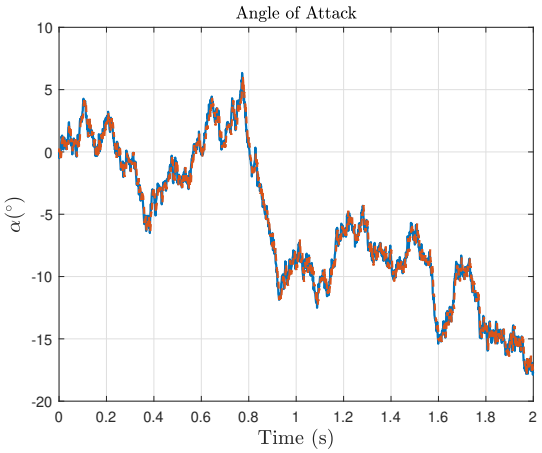

(a) Estimated angle of attack

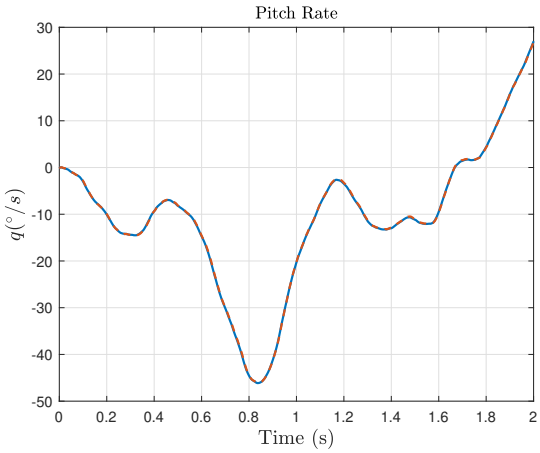

(b) Estimated pitch rate

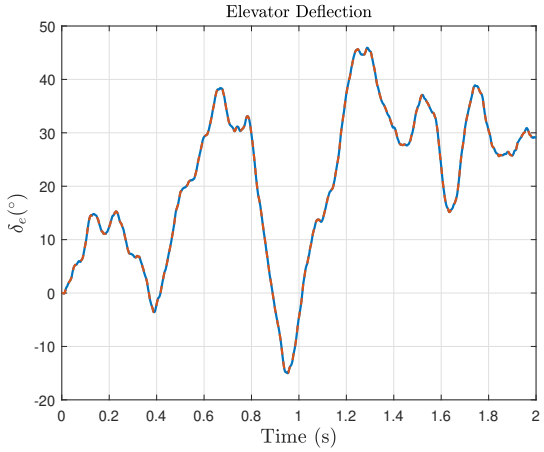

(c) Estimated elevator deflection

Figure 4.6: Kalman filter estimates of system states (red- -) compared with actual system states responses (blue) to a unit normal acceleration command in the presence of white measurement noise on the outputs and a disturbance on the angle of attack

4.4. Robustness Properties of LQG Controlled Systems

Multivariable linear-quadratic optimal regulators are known to have guaranteed stability margins, including guaranteed classical gain margins of - 6 dB to + ∞ dB and phase margins of 60° in each input control channel (Kalman, 1964; Safonov and Michael Athans, 1977). This means the system can tolerate complex diagonal perturbations at the plant inputs without causing instability. The result is only valid, however, for the full-state feedback case. If observers or Kalman filters are used in the implementation, no guaranteed robustness properties hold. Hence, the LQG-controlled system, which combines a Kalman filter and LQR control law, does not have guaranteed stability margins. This was demonstrated by J. Doyle, 1978, who showed that there exist LQG combinations with arbitrarily small stability margins.

Because of the dual nature of the algebraic Riccati equations involved in the development of the LQR and Kalman filter, at the input to the Kalman gain matrix, there will be infinite gain margin, a gain reduction margin equal to 0.5, and a minimum phase margin of 60° provided the power spectral density matrix of the measurement noise is chosen to be diagonal. In Equation 4.13, the transfer functions at various break points (BP) in the LQG controlled system in Figure 4.7 are given.

$$L_1(s) = K_{LQG}(s)G(s) \tag{4.13a}$$

$$L_2(s) = G(s)K_{LQG}(s) \tag{4.13b}$$

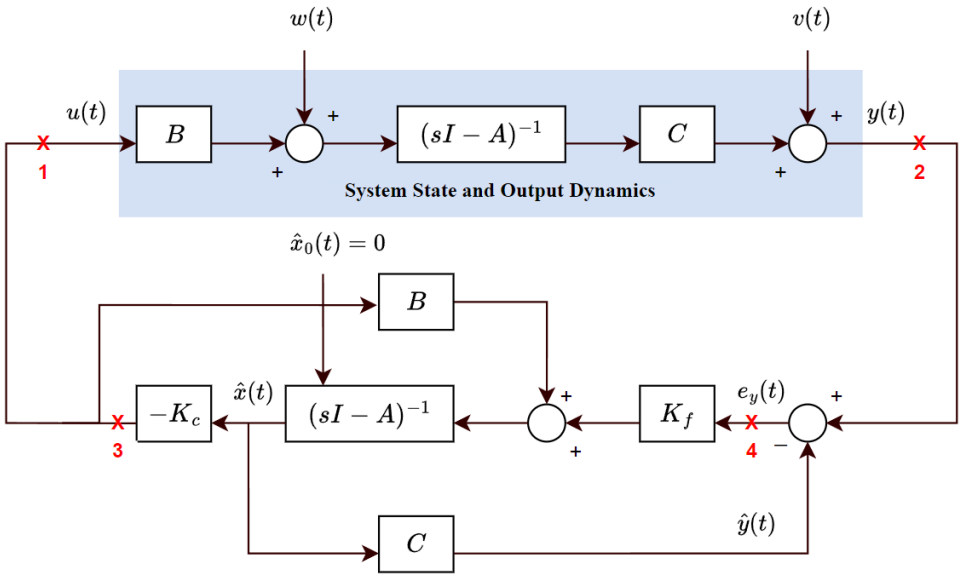

Figure 4.7: LQG-controlled closed loop system with break points at which the robustness of the system is discussed

$$L_3(s) = K(sI - A)^{-1}B \tag{4.13c}$$

$$L_4(s) = C(sI - A)^{-1}K_f \tag{4.13d}$$

At the actual input (BP 1) and output (BP 2) of the plant, where designers are most interested in achieving good stability margins, there are complex transfer functions which, in general, give no guarantees of satisfactory robustness properties (Skogestad and Postlethwaite, 2005). In light of these observations, the robustness properties of control systems with filters or observers must be evaluated separately for each design.

4.5. LQG Implementation Using `systune`

The implementation of the LQG-controlled system is more or less the same as explained in the case of the LQR-controlled system in Section 3.6. As is already known from Chapter 3, the LQG problem is equivalent to minimizing the quadratic performance index given in Equation 3.26. This QPI is equivalent to the square of the $\mathcal{H}_2$ norm, $||T_{wz}||_2^2$, of the closed loop system from the disturbance $w(t)$ to the performance output $z(t)$ of the system $\mathcal{P}(s)$ in feedback with the controller $K(s)$ as shown in Figure 4.8.

To establish the generalized state-space model for the plant, the dynamics specified in Equation 3.28 are employed. For the system under LQG control, the relevant performance matrices are defined in Equation 4.14. Here, the term K_c denotes the LQR state feedback gains, K_i denotes the gain for the state resulting from the integration of the error between the normal acceleration output measurement and the reference command, and the term K_f denotes the Kalman filter gains. Additionally, the matrices D_{zw} and D_{yu} are assigned zero values.

The control law applied in the LQG scenario is represented as $u(t) = K_{LQG}y(t)$. It is important to note that the auxiliary system $P(s)$ in the LQG context differs from that in the LQR setup. Unlike the LQR, where system dynamics can be easily expanded with an additional state for the error integral, the LQG approach does not directly utilize the augmented system shown in Figure 3.10. This is because the Kalman filter does not estimate the extra integrator state due to its redundancy, a design decision justified in Section 4.3. The auxiliary system used in implementing the LQG controller is shown in Figure 4.8, in which the error between the normal acceleration output and the reference signal is separately integrated and fed back to the LQG controller. The `MATLAB` script for developing the LQG controller using `systune` can be found in Appendix B.2 for further reference.

$$A = A_{aug}, \quad B_u = B_{aug}, \quad C_y = \begin{bmatrix} 0 & 1 \\ C_{aug} & 0 \end{bmatrix} \tag{4.14a}$$

$$B_w = \begin{bmatrix} \sqrt{W} & 0 & 0 \\ 0 & -1 & 0 \end{bmatrix}, \quad D_{yw} = \begin{bmatrix} 0 & 0 \\ 0 & \sqrt{V} \end{bmatrix} \tag{4.14b}$$

$$C_z = \begin{bmatrix} \sqrt{Q} \\ 0 \end{bmatrix}, \quad D_{zu} = \begin{bmatrix} 0 \\ \sqrt{R} \end{bmatrix} \tag{4.14c}$$

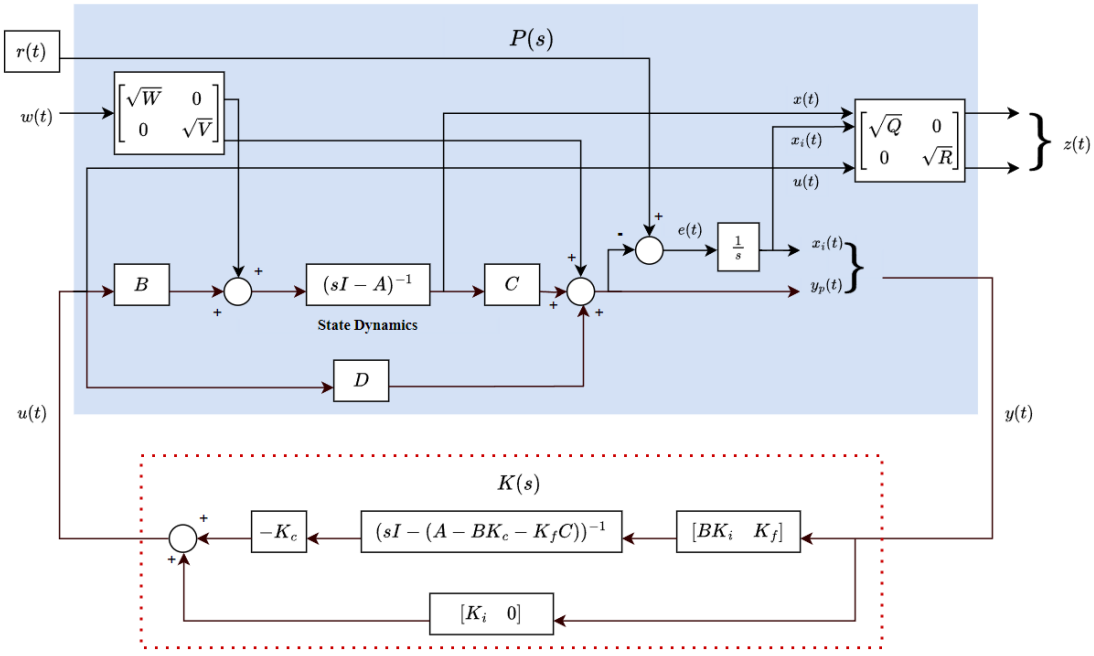

Figure 4.8: LQG-controlled closed-loop system in standard form with dynamic output feedback

5

Linear Quadratic Gaussian/ Loop Transfer Recovery

While the Kalman filter is optimal in minimizing the error covariance, it may not necessarily yield the best overall control properties when used in dynamic output-feedback controllers. To address this, a tuning technique known as Loop Transfer Recovery (LTR) is employed that aims to asymptotically restore the frequency domain properties associated with state-feedback, thereby enhancing the overall control design. The origin of the LTR concept is usually credited to a paper by Kwakernaak, 1969, who provided a method for selecting the weights in the quadratic performance index so that full-state sensitivity properties are achieved asymptotically as the control weight goes to zero. Ten years later, the LQG/LTR design technique was explicitly formulated for full-order observers in two papers by (J. Doyle and Stein, 1979; J. Doyle and Stein, 1981).

This chapter delves into two significant advancements in LTR research. The first is the traditional LTR method, as outlined by J. Doyle and Stein, 1981. This approach, while foundational, has its limitations, primarily because it was formulated for minimum phase systems. The second, a more recent development presented by Lavretsky, 2012, offers greater flexibility and is applicable to non-minimum phase systems as well. In the following sections, both these methodologies will be explored in depth and their effectiveness and applicability will be thoroughly analyzed in the context of this study.

5.1. *input*-Loop Transfer Recovery

J. Doyle and Stein, 1981 proposed a method to recover the stability margins associated with full-state LQR by introducing a scalar parameter in the LQG framework which can be tuned to balance stability margins at the plant input and output. This approach aligns with the perspective of Niemann and Stoustrup, 1995, who described LTR methods as "heuristic tools invented to introduce robustness into the LQG design framework." The LQG control architecture, given in Figure 4.3, combines the LQR state-feedback control law with the Kalman filter state estimator. Hence, the frequency-domain properties of the LQG at the plant input as given in Equation 5.1b do not equal those of the LQR given in Equation 5.1a, as was discussed in Section 4.4.

$$L_{LQR}(s) = K_c(sI - A)^{-1}B \tag{5.1a}$$

$$L_{LQG}(s) = K_c(sI - (A - BK_c - K_fC))^{-1}K_fC(sI - A)^{-1}B \tag{5.1b}$$

LTR can be implemented by two ways, depending on if the recovery is needed at the plant input or output. The first method involves adjusting the dynamics of the Kalman filter to align with the dynamics of the full-state feedback open-loop function at plant input, effectively making the transfer function in Equation 5.1b to approach Equation 5.1a. The second method modifies the LQR controller so that the transfer function in Equation 4.13b approaches the dynamics of the Kalman filter, represented by $C(sI - A)^{-1}K_f$. In this study, the first approach, henceforth referred to as "iLTR," is employed. In iLTR, the plant process disturbance covariance matrix W is parameterized using a scalar ρ, as shown in Equation 5.2 where, W_0 is the nominal plant process disturbance covariance tuned while designing the LQG controller, B is the control input matrix, and ρ serves as the adjustment parameter for the iLTR method.

$$W_{iLTR} = W_0 + \rho BB^T \tag{5.2}$$

Here, W_{iLTR} is utilized to calculate the steady-state covariance matrix P_f and subsequently, the Kalman filter gain matrix K_f. The parameter ρ is varied to identify the value at which the frequency-domain characteristics meet the specified requirements.

5.2. Asymptotic Properties of the Observer's Eigenstructure

The tuning parameters in the Kalman filter, namely the process and the noise covariance matrices W and V, determine the eigenstructure of the Kalman filter dynamics shown in Figure 5.1. These dynamics greatly influence the system's robustness characteristics, making it important to understand how the magnitude of these tuning weights affect the Kalman filter characteristics. Here, the LTI system in Equation 5.3 is considered.

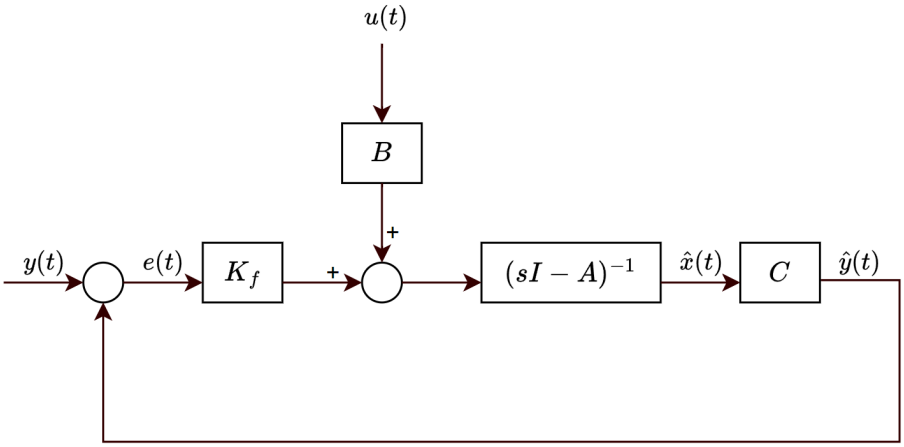

Figure 5.1: Kalman filter dynamics for state estimation

$$\begin{aligned} \dot{x} &= Ax + Bu, \quad x \in R^{n_x} \quad u \in R^{n_u} \\ y &= Cx, \quad y \in R^{n_y} \end{aligned} \tag{5.3}$$

Here, $W_0 = W_0^T \geq 0$, $V_0 = V_0^T \geq 0$, and $P \in R^{n_x}$. The Hamiltonian matrix associated with the algebraic Riccati equation (Equation 5.4), is given in Equation 5.5.

$$AP + PA^T - PC^T V_0^{-1} CP + W_0 = 0 \tag{5.4}$$

$$H = \begin{bmatrix} A & W_0 \\ C^T V_0^{-1} C & -A^T \end{bmatrix} \tag{5.5}$$

The Kalman filter gains K_f are derived by $K_f = PC^T V_0^{-1} C$ using the matrix P in Equation 5.4. In the study by K. A. Wise and Lavretsky, 2013, the dependency of observer dynamics on the Hamiltonian matrix is derived,

$$\begin{aligned} det[sI - H] &= \phi_{ol}(s)\phi_{ol}(-s) det\big[I - W_1^T (sI + A^T)^{-1} C^T \underbrace{C(sI - A)^{-1} W_1}_{H_1(s)}\big] \\ &= \phi_{ol}(s)\phi_{ol}(-s) det\big[I + H_1^T(-s) H_1(s)\big] \\ &= \phi_{KF}(s)\phi_{KF}(-s) \end{aligned} \tag{5.6}$$

In this context, ϕ_{ol} represents $det(sI - A)$, which defines the open-loop characteristic polynomial, and ϕ_{KF} represents $det(sI - A + K_f C)$, describing the characteristic polynomial of the Kalman filter in closed-loop. The ϕ_{KF} polynomial is affected by the choices of W_0 and V_0, respectively. When implementing the iLTR method, W_0 is adjusted to include a tuning parameter ρ as given in Equation 5.2. As ρ is increased towards infinity, the expression for the Kalman filter's characteristic equation becomes increasingly influenced by $det[H_1(s)]$, which incorporates the input matrix B. Consequently, the Kalman filter's eigenvalues begin to align with the transmission zeros of the plant, effectively neutralizing the influence of the Kalman filter on the closed-loop system dynamics (Kazerooni and Houpt, 1986; Lavretsky and K. Wise, 2013).

The trajectory of the Kalman filter poles is illustrated in Figure 5.2 as the recovery parameter ρ is swept from $\rho = 0$, where it is equivalent to the optimal Kalman filter dynamics as in the standard LQG setup, to $\rho = 7.5 \cdot 10^{-4}$. The two low frequency poles of the Kalman filter for the LQG case as given in Table 4.1, initially move towards each other along the real axis before shifting towards infinity and forming a complex conjugate pair. Meanwhile, the single high-frequency pole shifts towards infinity along the real axis. This high-frequency pole's trajectory is not depicted in the pole-zero map presented in Figure 5.2.

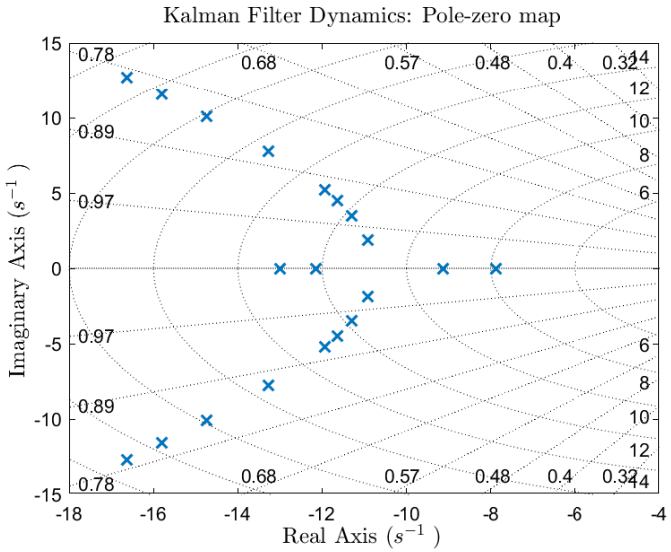

Figure 5.2: Locus of the poles of the Kalman filter dynamics with increasing value of the recovery parameter ρ in iLTR-controlled system

As ρ increases, certain elements of the error covariance matrix P_f in Equation 5.4 become large which in turn makes some elements of the Kalman filter gains larger. Consider the LQG controller transfer function matrix that relates the measurement y to the control u given in Equation 5.7.

$$\begin{aligned} u &= -K_c\phi_K K_f y, \quad \text{where } \phi_K = (sI - A + BK_c + K_f C)^{-1} \\ &= -K_c\phi_K K_f (Cx + v) \\ &= -K_c\phi_K K_f Cx - K_c\phi_K K_f C(K_f C)^{-1} K_f v \end{aligned} \tag{5.7}$$

As the recovery parameter ρ increases towards infinity, in the iLTR case, $\phi_K K_f C$ approaches the identity matrix I, leading to $u = -K_c x - K_c(K_f C)^{-1} K_f v$. Consequently, the term $(K_f C)^{-1} K_f$ may result in the amplification of noise.

Although iLTR can be applied to non-minimum phase systems, caution is required to avoid compromising the stability of the LQG controller, which consequently restricts the extent to which recovery can be achieved. This section is a key component for grasping the inner workings of the iLTR methodology, particularly the evolution of the Kalman filter dynamics when the recovery parameter tends toward infinity. Further demonstrating that the open-loop system at the input, represented by $K_{LQG}(s)G_p(s)$, becomes equivalent to $K_c(sI - A)^{-1}B$ as ρ approaches infinity is thoroughly detailed in (J. Doyle and Stein, 1981).

5.3. Loop Transfer Recovery-*input / output*

Lavretsky, 2012 introduced an alternative approach to the classical LTR called the LTR method of Lavretsky, which in this study, will be referred to as the "LTRio" method[1]. It applies to systems with controllable and observable nominal linearized dynamics and assumes that the number of sensors is greater than the number of actuators. The method implements observer-based loop transfer recovery, asymptotically achieving positive real system behavior at certain loop break points during recovery. To handle non-minimum phase, the system is "squared-up" by augmenting it with pseudo-control signals which is achieved by adding "fictitious" columns to the input transfer function matrix.

5.3.1. System Squaring-Up

An LTI system is given in Equation 5.3 with the assumption that the pair (A, B) is controllable, the matrix B has a full column rank of n_u and the rank of the product CB is equal to n_u. The transmission zeros of the system are identified as a collection of complex numbers, denoted by λ_i, that fulfill the inequality specified in Equation 5.8, as

[1] In this study, it is known to balance the stability margins at both plant input and output, fulfilling the design requirements

given in (K. A. Wise and Lavretsky, 2013).

$$rank \begin{bmatrix} (A - \lambda I) & B \\ C & 0 \end{bmatrix} < n_x + \min(n_u, n_y) \tag{5.8}$$

The objective is to expand the system by introducing pseudo-controls, thereby ensuring that the number of controls equal the number of measurements, and hence, "square up" the system. This is achieved by forming $\bar{B}_{n_x \times n_y} = [B \;\; X]$, where $rank(C\bar{B})$ equals n_y. The addition of the columns $X \in \mathcal{R}^{n_x \times (n_y - n_u)}$ as part of the squaring-up process allows for the placement of transmission zeros in the left half of the complex plane and ensure that the augmented system is minimum phase.

5.3.2. Positive Real Systems

Among linear-time-invariant systems, a notable subset comprises dynamics classified as positive real (PR) and strictly positive real (SPR), as discussed in (Zhou, John Doyle, and Glover, 1996; Khalil, 2002). These specific types of systems exhibit interesting characteristics that facilitate the design of robust output feedback control.

Positive Real

A proper rational transfer function matrix $G(s)$ with dimensions $(p \times p)$ of the complex variable $s = \sigma + j\omega$, assuming the pair (A, B) is controllable and (A, C) is observable is defined as positive real under the following conditions:

1. All poles of the elements in $G(s)$ are located in the left half of the complex plane.
2. For every real value of ω where $j\omega$ does not correspond to a pole in $G(s)$, the matrix $G(j\omega) + G^*(j\omega)$ is positive semi-definite.
3. If an element of $G(s)$ has a pole at a purely imaginary number $j\omega$, it must be a simple pole, and the resulting residue matrix, defined as $\lim_{s \to j\omega}(s - j\omega)G(s)$ should be a positive semi-definite Hermitian matrix.

Strictly Positive Real

The transfer function $G(s)$ is termed *strictly positive real* when $G(s - \epsilon)$ satisfies the criteria for being positive real, given that ϵ is a positive number greater than zero. In scalar systems, where $p = 1$, the Nyquist frequency response of Positive Real (PR) and Strictly Positive Real (SPR) dynamics is confined to the right half of the complex plane. Consequently, it avoids encircling the point $(-1, j0)$ on the complex plane. Therefore, such systems maintain stability across a broad range of uncertainties, a trait that is highly desirable for any system. The association between PR, SPR transfer function matrices, and the presence of a Lyapunov function for analyzing stability is clarified through two key lemmas (Khalil, 2002).

1. **Positive Real Lemma**
   The transfer function $G(s) = C^T(sI - A)^{-1}B + D$ is defined as Positive Real if there exist matrices P, L, and W, where P is symmetric and positive definite ($P = P^T > 0$), satisfy the following conditions.
   $$PA + A^T P = -L^T L \tag{5.9}$$
   $$PB = C^T - L^T W \tag{5.10}$$
   $$W^T W = D + D^T \tag{5.11}$$
2. **Kalman-Yakubovich-Popov (KYP) Lemma**
   The transfer function $G(s) = C^T(sI - A)^{-1}B + D$ is Strictly Positive Real if matrices $P = P^T > 0$, L, W exist, along with a positive constant ε, fulfilling the following criteria.
   $$PA + A^T P = -L^T L - \varepsilon P \tag{5.12}$$
   $$PB = C^T - L^T W \tag{5.13}$$
   $$W^T W = D + D^T \tag{5.14}$$
   In this case, if $\varepsilon = 0$ and $D = 0$ then the SPR conditions can be given in the following form.
   $$PA + A^T P = -L^T L \tag{5.15}$$
   $$PB = C^T \tag{5.16}$$

Equation 5.15 represents the algebraic Lyapunov equation and Equation 5.16 facilitates the design of output feedback control, as discussed in the subsequent section.

5.3.3. Asymptotic Properties of the Algebraic Riccati Equation

The design of observers in the Loop Transfer Recovery input-output (LTRio) approach involves algebraic Riccati equations (ARE) that depend on the recovery parameter ν, as given in Equation 5.17.

$$P_\nu A + A^T P_\nu - P_\nu \bar{B} R_\nu^{-1} \bar{B}^T P_\nu + Q_\nu = 0 \tag{5.17}$$

Here, ν is a positive scalar, and the pairs $(A, \bar{B})$ and (A, C) represent controllable and observable system, respectively, within the dimensions $A \in \mathcal{R}^{n\times n}$, $\bar{B} \in \mathcal{R}^{n\times m}$, $C \in \mathcal{R}^{m\times n}$, and $m \leq n$ where n is the number of system states and m is the number of inputs. The weight matrices for the ARE are expressed in Equation 5.18.

$$Q_\nu = Q_0 + \left(\frac{\nu+1}{\nu}\right)\bar{B}^T\bar{B}, \quad R_\nu = R_0\left(\frac{\nu}{\nu+1}\right) \tag{5.18}$$

Here, $Q_0 \in \mathcal{R}^{n\times n}$ and $R_0 \in \mathcal{R}^{m\times m}$ being symmetric and strictly positive definite matrices. Incorporating the weight matrices from Equation 5.18 into Equation 5.17 gives the following equation.

$$P_\nu A + A^T P_\nu - \left(1+\frac{1}{\nu}\right) P_\nu \bar{B} R_0^{-1} C P_\nu + Q_0 + \left(1+\frac{1}{\nu}\right)\bar{B}\bar{B}^T = 0 \tag{5.19}$$

equivalently,

$$P_\nu A + A^T P_\nu - P_\nu C^T R_0^{-1} C P_\nu + Q_0 + \bar{B}\bar{B}^T + \frac{1}{\nu}\left[\bar{B}\bar{B}^T - P_\nu C^T R_0^{-1} C P_\nu\right] = 0 \tag{5.20}$$

The analysis of the ARE solution P_ν as the parameter ν tends towards zero involves expressing P_ν as an asymptotic expansion relative to ν, as represented in Equation 5.21.

$$P_\nu = P_0 + P_1\nu + O(\nu^2), \text{ as } \nu \to 0 \tag{5.21}$$

The notation $O(\nu^2)$ represents the "Big O" notation, which is used in mathematics to describe the upper bound of the rate at which a function (or, in this case, matrix terms) grows or shrinks as its argument (here, ν) approaches a specific value, commonly zero or infinity. As ν approaches zero, the solution P_ν is approximated by the matrix P_0, which is the leading term in the expansion, plus a correction term that is linear in ν, represented by $P_1\nu$, and additional higher-order terms that are at most proportional to ν^2 (represented by $O(\nu^2)$) and become negligible as ν becomes very small. In the context of the ARE, the Big O notation $O(\nu^2)$ used in Equation 5.21 signifies a matrix that is dependent on the parameter ν and is of size $n \times n$. The notation indicates that as ν tends towards zero, the norm of the matrix decreases at a rate proportional to ν^2 or slower. Mathematically, this is expressed in Equation 5.22.

$$\lim_{\nu\to 0} \|P_\nu - P_0 - P_1\nu\| = \lim_{\nu\to 0} \|O(\nu^2)\| = 0 \tag{5.22}$$

For matrices which satisfy the asymptotic expansion in Equation 5.21, the following can be claimed.

$$P_0 = \lim_{\nu\to 0} P_\nu \tag{5.23}$$

For the ARE solution P_ν, as the parameter ν trends towards zero, the solution converges to the matrix P_0. This is distinctly different from the scenario observed with the iLTR parameter ρ. In the latter case, as $\frac{1}{\rho}$ approaches 0, the maximum and minimum singular values of the matrix P_f approach infinity and 0 respectively, hence making the matrix P_f singular. The asymptotic expansion of the matrix P_ν in Equation 5.21 is substituted into the ARE, given in Equation 5.20 to yield Equation 5.24. Collecting the zero-order terms in ν from Equation 5.24 results in Equation 5.25, and isolating the first-order terms in ν gives Equation 5.26.

$$\begin{aligned}\nu\left[(P_0 + P_1\nu + O(\nu^2))A + A^T(P_0 + P_1\nu + O(\nu^2))\right] \\ - \nu\left[(P_0 + P_1\nu + O(\nu^2))C^T R_0^{-1} C(P_0 + P_1\nu + O(\nu^2))\right] + Q_0 + \bar{B}\bar{B}^T \\ + \bar{B}\bar{B}^T - (P_0 + P_1\nu + O(\nu^2))C^T R_0^{-1} C(P_0 + P_1\nu + O(\nu^2)) = 0\end{aligned} \tag{5.24}$$

$$\bar{B}\bar{B}^T - P_0 C^T R_0^{-1} C P_0 = 0 \tag{5.25}$$

$$P_0(A - C^T R_0^{-1} C P_1)^T + \underbrace{(A - C^T R_0^{-1} C P_1)}_{\tilde{A}} P_0 + \underbrace{(Q_0 + \bar{B}\bar{B}^T)}_{\tilde{Q}} = 0 \tag{5.26}$$

Given that the controllability of the pair (A, B) remains unaffected by a feedback loop, the modified system represented by $(\tilde{A}, \bar{B})$ maintains controllability. Furthermore, with $\tilde{Q}$ being symmetric and positive definite $\tilde{Q} = \tilde{Q}^T > 0$, the ARE in Equation 5.26 guarantees a unique, symmetric, and positive-definite solution $P_0 = P_0^T > 0$.

Choosing a unit vector x from the n-dimensional real space $\mathcal{R}^n$, it is observed that as ν approaches zero, the product $x^T P_\nu x$ tends towards the product $x^T P_0 x$. This is expressed in Equation 5.27.

$$\lim_{\nu \to 0} x^T P_\nu x = \lim_{\nu \to 0} x^T [P_0 + P_1 \nu + O(\nu^2)] x = x^T P_0 x \geq \lambda_{\min}(P_0) > 0 \tag{5.27}$$

Given that the solution to the ARE, P_ν, retains its invertibility for any positive value of ν, based on Equation 5.27, it can be inferred that as ν reduces to an infinitesimal value, the eigenvalues of P_ν remain above zero. Consequently, the matrix P_ν is globally invertible for all non-negative values of ν. Thus, the ARE in Equation 5.17 with weight matrices Q_ν and R_ν as defined in Equation 5.18, possesses a unique positive-definite solution P_ν. This solution can be expressed via the asymptotic expansion given in Equation 5.21, and the following assertions are valid.

1. Both P_0 and P_1 are symmetric.
2. P_0 uniquely solves the algebraic Lyapunov equation below, derived from Equations 5.25 and 5.26, and is symmetric and strictly positive definite.

$$P_0(A - C^T R_0^{-1} C P_1)^T + (A - C^T R_0^{-1} C P_1) P_0 + \tilde{Q} = 0 \tag{5.28}$$

3. A unitary matrix W of size $m \times m$ exists, satisfying the equation given below, which is concluded from Equations 5.24 and 5.25.

$$P_0 C^T = B W^T \sqrt{R_0} \tag{5.29}$$

4. The unitary matrix W in Equation 5.29 can be chosen according to the following formulation.

$$W = (UV)^T \tag{5.30}$$

   Here, U and V are unitary matrices identified through the singular value decomposition:

$$B^T C^T R_0^{-\frac{1}{2}} = U \Sigma V \tag{5.31}$$

   and Σ is a diagonal matrix containing the singular values.

5. The solution P_ν is invertible for any non-negative ν, and

$$\lim_{\nu \to 0} x^T P_\nu x \geq \lambda_{\min}(P_0) > 0 \tag{5.32}$$

   Here, $\lambda_{\min}(P_0)$ signifies the smallest eigenvalue of P_0.

In the case of non-minimum phase systems, specifically those with the modified matrix $\bar{B}$, the Strictly Positive Real property is implied by Equations 5.28 and 5.29. The LTRio design approach aims to manipulate the transmission zeros of the state estimator by "squaring up the system." The adjustment of transmission zeros ensures that the augmented original system asymptotically satisfies the SPR condition as the parameter ν diminishes towards zero.

5.4. Implementation of LTR Designs

The implementation approach for LTR controllers closely resembles that of LQG controllers, with the primary distinction lying in the choice of covariance matrices W and V. It is important to note that in implementing the LTRio controller, the initial measurement noise covariance V_0 taken from the sensor specifications of the Citation aircraft, may require significant scaling to enhance the numerical balance between W_{LTRio} and V_{LTRio}. Implementing LTR designs with `systune` is relatively straightforward and follows the methodology outlined for LQG controllers in Section 4.5, with the modification being the use of adjusted covariance matrices for the LTR setup. The design process in theoretical terms is explained in Algorithm 2.

Algorithm 2: Loop Transfer Recovery-*input/output* Methodology

System Dynamics:

$$\dot{x} = Ax + Bu + w$$
$$y = Cx + v$$
$$E\{ww^T\} = W_0\delta(\tau), \quad E\{vv^T\} = V_0\delta(\tau)$$

Step 1: Design the LQR controller

Create augmented system

$$\begin{bmatrix}\dot{x}(t)\\ \dot{x_i}(t)\end{bmatrix} = \begin{bmatrix}A & 0\\ -C_{yr} & 0\end{bmatrix}\begin{bmatrix}x(t)\\ x_i(t)\end{bmatrix} + \begin{bmatrix}B\\ 0\end{bmatrix}u(t)$$

Performance Index

$$J = \int_0^\infty (x^TQx + u^TRu)dt$$

Design LQR gains using algebraic Riccati equation

$$P\tilde{A} + \tilde{A}^TP + Q - PBR^{-1}B^TP = 0$$
$$u = -R^{-1}B^TPx = -K_cx$$

Step 2: Design the Kalman Filter State Estimator

Kalman filter dynamics

$$\dot{\hat{x}}(t) = \tilde{A}\hat{x}(t) + Bu(t) + K_f\left(y(t) - C\hat{x}(t)\right)$$
$$y(t) = \hat{x}(t)$$

Kalman filter gains

$$K_f = P_fC^TV_0^{-1}$$
$$\tilde{A}P_f + P_f\tilde{A}^T + W_0 - P_fC^TV_0^{-1}CP_f = 0$$

Step 3: Re-design the Kalman filter State Estimator

iLTR

Revised process noise covariance matrix

$$W = W_0 + \rho BB^T$$
$$\tilde{A}P_f + P_f\tilde{A}^T + W - P_fC^TV_0^{-1}CP_f$$

iLTR Kalman filter gains

$$K_f = P_fC^TV_0^{-1}$$

LTRio

Square-up the system $\bar{B} = [B\ X]$

Revised process and measurement noise covariance matrices

$$W = W_0 + \tfrac{\nu+1}{\nu}\bar{B}\bar{B}^T, \quad V = \tfrac{\nu}{\nu+1}V_0$$
$$\tilde{A}P_\nu + P_\nu\tilde{A}^T - (1+\tfrac{1}{\nu})P_\nu C^TV_0^{-1}CP_\nu + W_0 + (1+\tfrac{1}{\nu})\bar{B}\bar{B}^T = 0$$

LTRio Kalman filter gains

$$K_f = P_\nu C^TV_\nu^{-1}$$

Part III

Analysis

6

Robustness Analysis

In the mid-1970s, the lack of attention to robustness was identified as a significant cause of failures in aircraft control designs, primarily due to the inability of such designs to tolerate significant modelling uncertainties. M. Athans, 1971 had raised concerns about the urgent need to address the issue of modelling inaccuracies in an editorial on the issues with LQG. Similarly, Rosenbrock and McMorran, 1971 noted that although LQG theory was optimal, it failed to meet the crucial requirement that the system must possess sufficient stability margins when loop gains are altered in various combinations. Being a prominent advocate of multiloop LQG feedback, Michael Athans recognized the significance of addressing the LQG robustness problems leading to significant progress in this area. As a result, robust control theory began to take root and expand (Safonov, 2012).

6.1. Uncertainties

Different representations of uncertainty in control systems can be characterized by the amount of structure they possess. For instance, a highly structured representation of uncertainty might involve a set membership statement for the parameters of a known linear time-invariant model. This approach provides a highly structured representation of uncertainty because it defines it in a specific and quantifiable way. 'Structured uncertainties', as termed by J. Doyle and Stein, 1981, are usually the low-frequency error components in the model. In some cases, uncertainty is not necessarily tied to specific variations in model parameters but rather reflects a general lack of knowledge or understanding of the system dynamics. One way to represent this type of uncertainty is through a set membership statement for the transfer function matrix, which defines a range of possible transfer functions that could describe the system. This approach is less structured than the previous example because it does not rely on a specific model structure and can account for a broader range of uncertainties thus termed as 'unstructured uncertainties' by J. Doyle and Stein, 1981.

A detailed overview of the many ways to define uncertainty is provided in (Weinmann, 1991). For recent literature on modelling uncertain systems, robust stability analysis for systems with unstructured or structured uncertainty, and robust control system designs, one can refer to (Petersen and Tempo, 2014). In this research, the analysis of the closed loop system will primarily address parametric uncertainties and certain types of dynamic (frequency-dependent) uncertainties. Unstructured uncertainties can be of six forms with three feedforward forms: additive uncertainty, multiplicative input uncertainty and multiplicative output uncertainty and three feedback or inverse forms: inverse additive uncertainty, inverse multiplicative input uncertainty and inverse multiplicative output uncertainty as given in Equation 6.1 and Figure 6.1 (Skogestad and Postlethwaite, 2005).

$$\begin{array}{llll} G_p = G + E_A, & E_A = w_A\Delta_A & G_p = G(I - E_AG)^{-1}, & E_A = w_A\Delta_A \\ G_p = G(I + E_I), & E_I = w_I\Delta_I & G_p = G(I - E_I)^{-1}, & E_I = w_I\Delta_I \\ G_p = (I + E_O)G, & E_O = w_O\Delta_O & G_p = (I - E_O)^{-1}G, & E_O = w_O\Delta_O \end{array} \tag{6.1}$$

6.2. Robustness Analysis Tools

Models for stability analysis of multivariable systems are developed to examine various aspects such as gain and phase uncertainties, neglected or inaccurately modelled dynamics, uncertainties in real parameters, and their combinations. In these models, uncertainties within the system are typically separated from the system models. Petersen and Tempo,

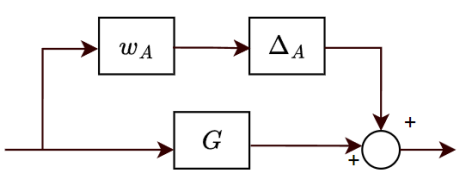

(a) Additive uncertainty

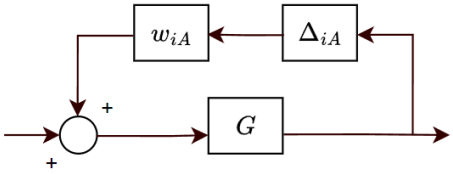

(b) Inverse additive uncertainty

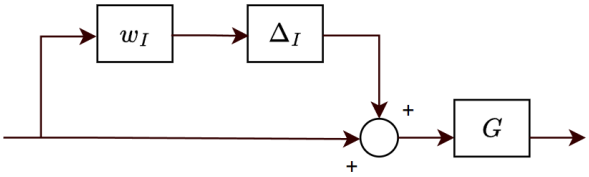

(c) Multiplicative input uncertainty

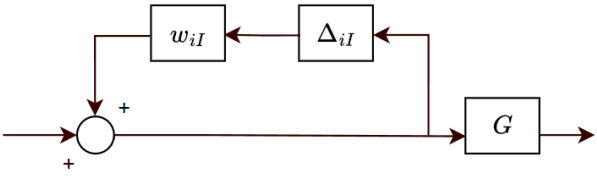

(d) Inverse multiplicative input uncertainty

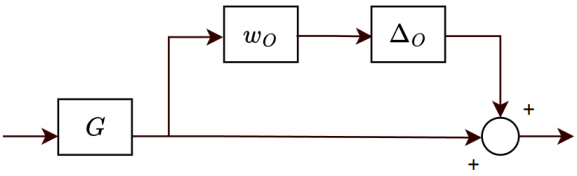

(e) Multiplicative output uncertainty

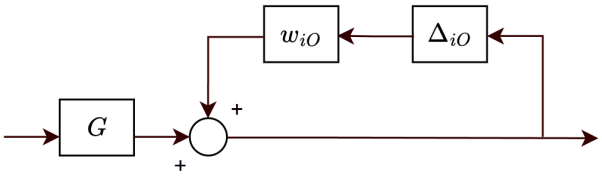

(f) Inverse multiplicative output uncertainty

Figure 6.1: Common forms of unstructured uncertainties, where (a), (c) and (e) are feedforward forms and (b), (d) and (f) are feedback or inverse forms

2014 mentioned the $M - \Delta$ model, which is commonly used in modern control theory and H_∞ control design as a general model to capture the different types of uncertainties that could impact a dynamic system. This feedback structure, depicted in Figure 6.2, comprises two components: the known system, $M(s)$, which is the combination of the plant and the controller, and the uncertain part, $\Delta(s)$. In a control system where there is no uncertainty,

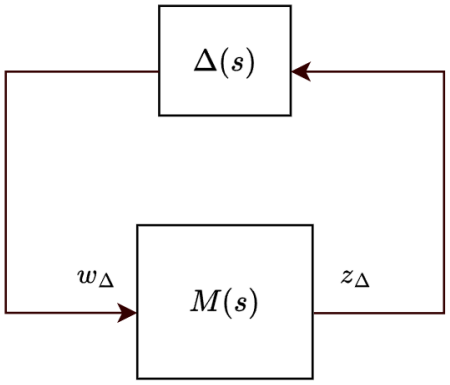

Figure 6.2: $M - \Delta$ configuration for robust stability

the controller ensures the stability of the plant, and the return difference matrix remains non-singular across all frequencies.

$$\det(I + L(s)) \neq 0 \quad \forall s \in \mathcal{D}_r. \tag{6.2}$$

Using the $M - \Delta$ analysis model, Equation 6.2 is equivalent to Equation 6.3.

$$\det(I - \Delta M(s)) \neq 0 \quad \forall s \in \mathcal{D}_r. \tag{6.3}$$

A controller can be designed to stabilize the plant in the absence of uncertainties. The critical question for analysis is to assess the maximum level of uncertainty that the closed-loop system can withstand before it becomes unstable.

6.2.1. Structured Singular Value

According to Lavretsky and K. Wise, 2013, the interconnection shown in Figure 6.2 is said to have robust stability if the matrix $(I - M\Delta(s))$ is not singular, i.e., $det((I - M\Delta(s)) \neq 0 \; \forall \, \omega$, and $\forall \; \Delta$ provided $\bar{\sigma}(\Delta(s)) \leq 1$. However, the condition is of little applicability as a robustness indicator because the $det(I - M\Delta(s))$ does not indicate the near singularity of $(I - M\Delta(s))$ but only determines the absolute stability. To obtain a better estimate of the uncertainty the system can tolerate without being destabilized, it is required to calculate the smallest k_m with which the uncertainty can be scaled that makes the matrix, $(I - k_m M\Delta(s))$ singular. Hence, for a given complex matrix M, a set of complex matrices denoted by $\Delta = diag\{\Delta_i\}$ with $\bar{\sigma}(\Delta) \leq 1$ and with a given block structure, the real non-negative function $\mu(M)$ is defined as the following.

$$\mu(M) \triangleq \frac{1}{\min\{k_m | det(I - k_m M\Delta) = 0 \text{ for structured } \Delta, \bar{\sigma}(\Delta) \leq 1\}} \tag{6.4}$$

The structured singular value (μ) was developed by J. Doyle, 1982 and around the same time (in the same issue of the journal), Safonov, 1981 introduced the Multivariable Stability Margin (k_m) for a diagonally perturbed system, as the inverse of μ.

Structured singular value analysis is a powerful tool that provides a quantitative measure of the sensitivity of the closed-loop transfer function to perturbations in the input or output signals and can be used to design an LQG controller to minimize the impact of noise and disturbances on the system performance. A similar approach toward robust stability analysis of LQG-controlled active suspension systems in the presence of assumed parameter variations is presented in (Kashani and Kiriczi, 1992). The design provides a good example of how practical the structured singular value is as a stability robustness test when compared to the more conservative maximum singular value. For a more comprehensive understanding of the role of SSV in the trade-off between performance and uncertainty that occurs in feedback systems, see (J. Doyle, 1985; Packard, J. Doyle, and G. J. Balas, 1993).

The structured singular value can be readily employed using the Robust Control Toolbox in `MATLAB` to analyse robust stability margins. The multivariable robustness margin k_m (the inverse of μ) could offer a more intuitive representation of robust stability margins as for any uncertain system, the value k_m reflects how much uncertainty the system can handle, relative to the normalized uncertainty modelled in the system, before it reaches the point of instability.

6.3. Stability at Plant Input and Output

This section includes a study of the stability margins for the different control approaches, namely LQR state and output feedback, iLTR, LTRio, and LQG methods. Additionally, the section observes the reduction in stability margins in LQG systems relative to the guaranteed margins in the LQR state-feedback configuration. It further shows the stability variation with respect to changes in the recovery parameters for both the LTR methods discussed in this study.

6.3.1. LQR State and Output Feedback Control

In this section, the tuning process for the LQR involves adjustments to the design matrix Q by modifying the Q_{44} weighting parameter within this matrix. It is examined how this variation affects the LQR state and output feedback system's stability margins. With respect to the LQR state-feedback configuration, it is observed in Figure 6.3 that for all values of Q_{44}, the stability margins at the plant input and output surpass the target of $6dB$ gain and 45° phase margins. Although this control method does not intrinsically guarantee output stability margins, the Bode and Nyquist plots indicate that the margins at the plant's output are not only adequate but also show relative consistency despite the increasing values of Q_{44}. In Section 3.2, it is established that the minimum singular value of the return difference, represented as $\underline{\sigma}(I + L_i)$, where L_i is the open-loop transfer function at the plant input, does not drop below 1 in the context of LQR state-feedback. The return difference for the optimal LQR-SF case, as shown in Figure 6.4, consistently stays beyond the bounds of the unit circle centered at the origin. Similarly, the open-loop transfer function L_i is also observed to maintain its position outside the unit circle that is centered at $(-1, 0j)$.

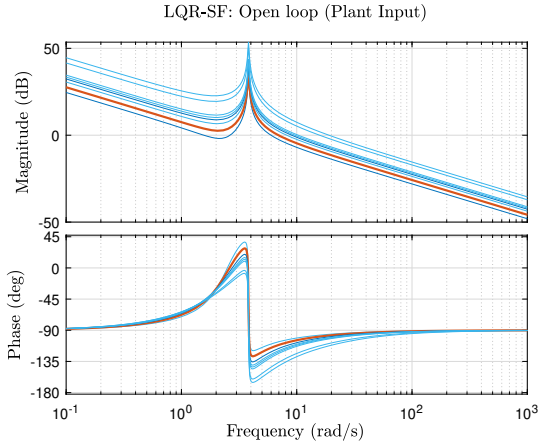

(a) Bode diagrams of the open-loop transfer function at the plant input

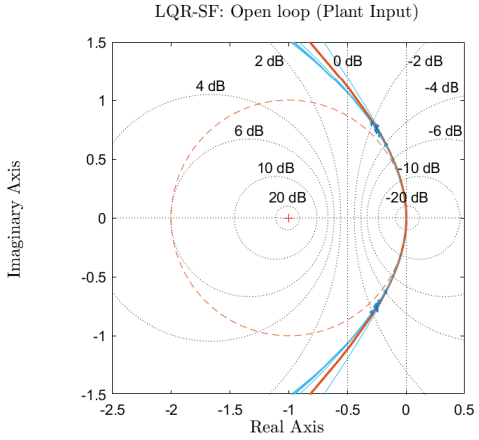

(b) Nyquist diagrams of the open-loop transfer function at the plant input

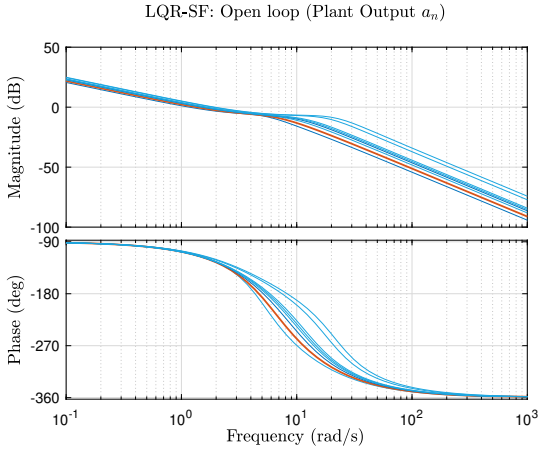

(c) Bode diagrams of the open-loop transfer function at the plant output

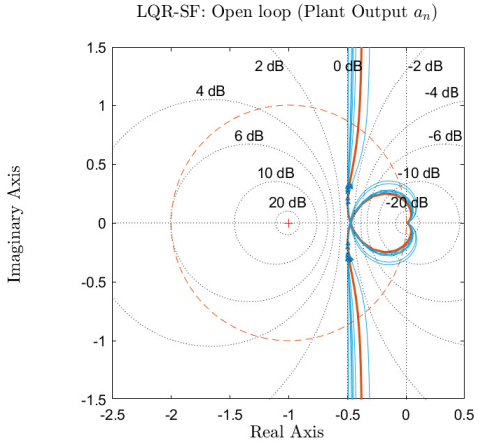

(d) Nyquist diagram of the open-loop transfer function at the plant output

Figure 6.3: Bode and Nyquist plots illustrating the impact of increasing Q_{44} weighting parameter on the open-loop transfer function at the plant input and output for the LQR-SF case with the optimal Q_{44} plots indicated in red

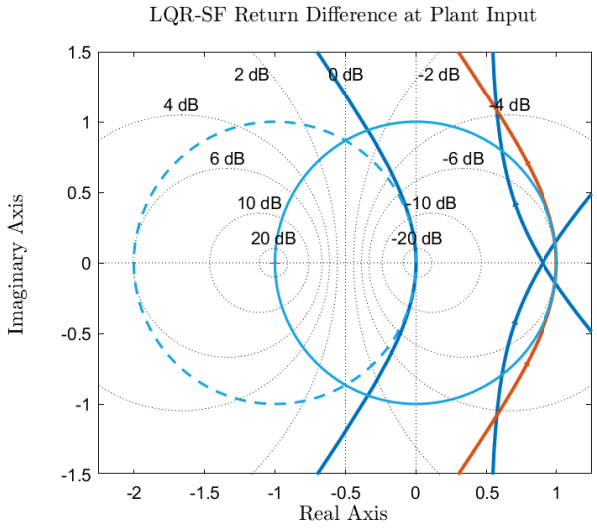

Figure 6.4: Nyquist diagrams of the return difference (red) and the open-loop transfer function (blue) at the optimal value of Q_{44} for the LQR-SF case

In the case of output-feedback LQR, as illustrated in Figure 6.5, there are no definitive stability margins that can be assured. Observing the Bode and Nyquist plots reveals that when the weighting parameter Q_{44} is increased, there is a noticeable rapid decline in the stability margins. However, this rate of decline in the margins tends to slow down beyond a certain threshold. This can be observed in the stem plots in Figure 6.6 depicting the variation of the margins with increasing Q_{44} parameter, swept from 1 to 100. It should be noted that the infinite gain margins typical of the LQR-SF case are not practically representable in the stem plots. Therefore, a representative value of $10dB$ has been selected as a substitute for these infinite gain margins. The step responses for both control methods can be found in Figure 6.7, and key characteristics of each are detailed in Table 6.1.

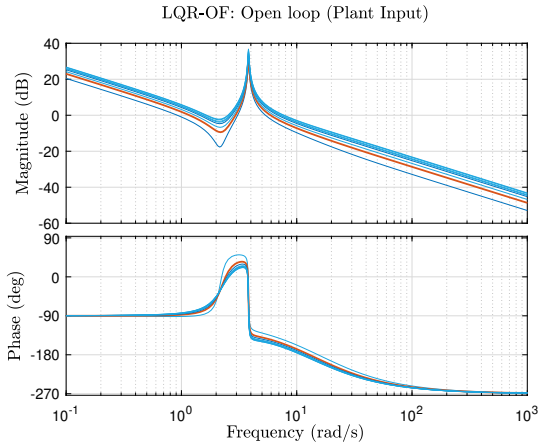

(a) Bode diagrams of the open-loop transfer function at the plant input

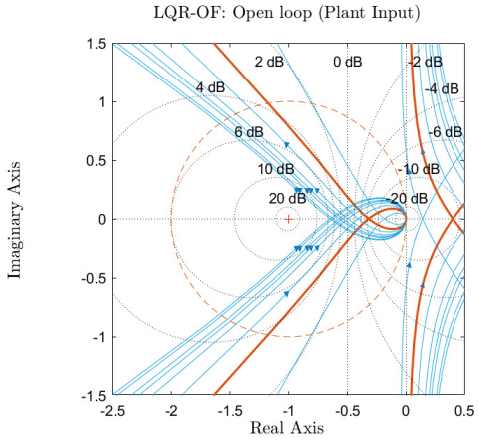

(b) Nyquist diagrams of the open-loop transfer function at the plant input

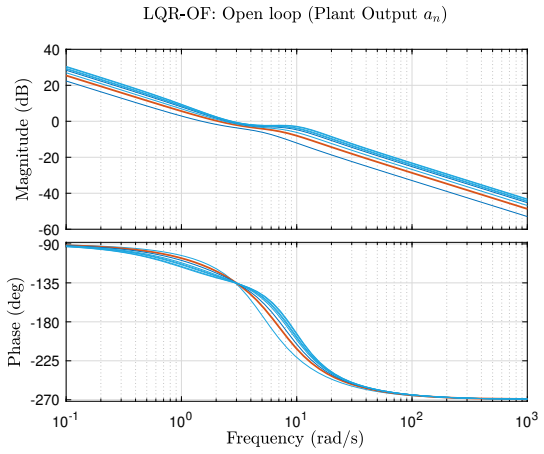

(c) Bode diagrams of the open-loop transfer function at the plant output

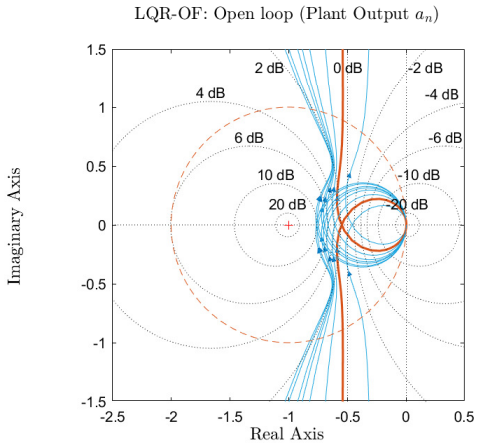

(d) Nyquist diagrams of the open-loop transfer function at the plant output

Figure 6.5: Bode and Nyquist plots illustrating the impact of increasing Q_{44} weighting parameter on the open-loop transfer function at the plant input and output for the LQR-OF case with the optimal Q_{44} plots indicated in red

Recall that in the LQR state-feedback design, the feedback gains are applied on the states: α (angle of attack), q (pitch rate), and δ_e (elevator deflection). However, for the LQR static output feedback scenario, the feedback is applied on the plant outputs: a_n (normal acceleration) and q. Additionally, the feedback gains in the state-feedback setup are of a higher magnitude compared to those in the output-feedback approach. Thus, it can be inferred that the LQR-OF framework is somewhat simpler in its structure compared to the LQR-SF framework. While LQR-SF offers excellent stability at both the input and output of the plant, it has a significant drawback: the necessity to measure all states. In contrast, the LQR-OF approach is more practical in this regard but demonstrates inferior stability margins compared to LQR-SF. Therefore, it becomes essential to explore other types of control methods that rely on output feedback and can deliver sufficient stability margins.

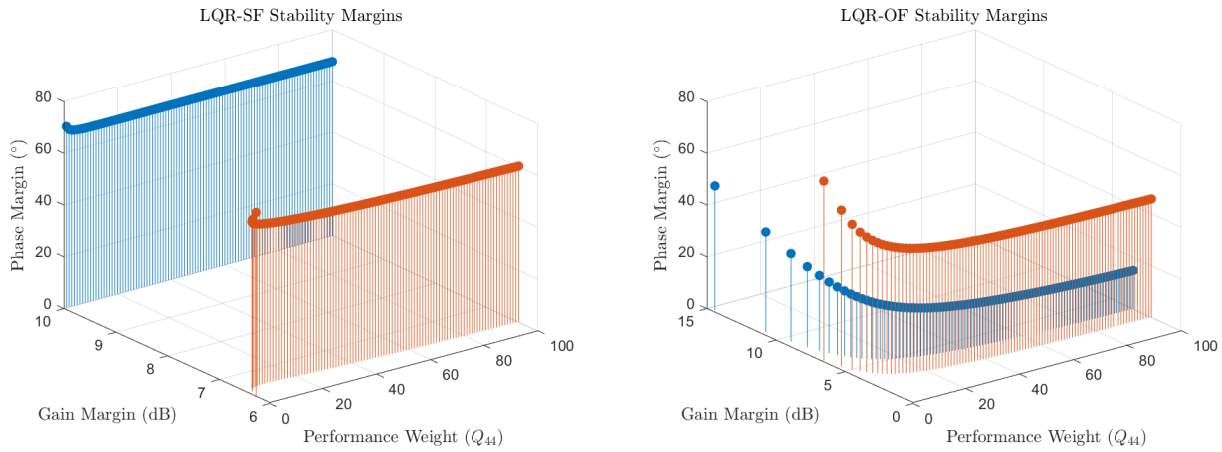

(a) LQR State-Feedback **(b)** LQR Output-Feedback

Figure 6.6: Stem plot depicting stability margins at the plant input (blue) and output (red) with increasing Q_{44} weighting parameter for the LQR-SF and LQR-OF cases

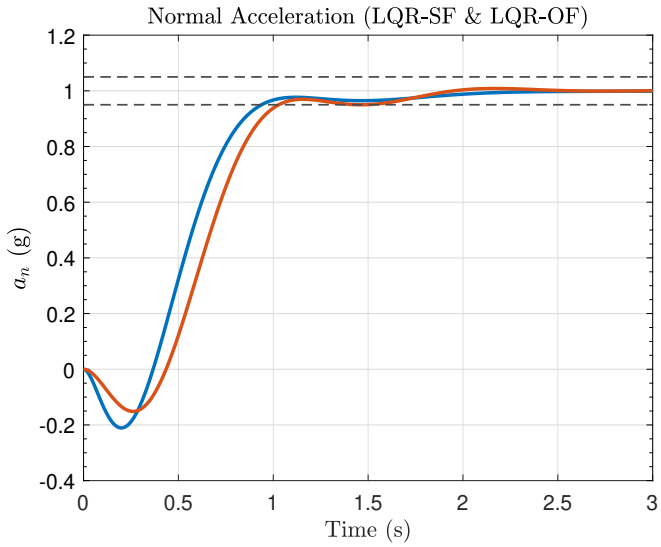

Figure 6.7: LQR-SF (blue) and LQR-OF (red) controlled closed-loop responses to a unit step normal acceleration command

Table 6.1: Comparison of the key characteristics of LQR-SF and LQR-OF control methods

Time and Frequency Domain Characteristics	LQR State-Feedback	LQR Output-Feedback
Settling Time (s)	0.93	1.02
Overshoot (%)	0	0
Undershoot (%)	21.10	15.10
Gain Margin at Plant Input (dB)	∞	9.97
Phase Margin at Plant Input $(^\circ)$	67.50	35.31
Gain Margin at Plant Output (dB)	6.57	5.16
Phase Margin at Plant Output $(^\circ)$	62.12	57.11
Closed-Loop Poles	-12.51, -2.32, -3.13 $\pm$ 4.56i	-2.17 $\pm$5.57, -2.52 $\pm$1.06
Integrator Gains	K_{int} = -2.77	K_{int} = -0.83
Feedback Gains	$K_{feedback}$ = [-8.42, -3.63, -0.61]	$K_{feedback}$ = [0.18, -1.22]

6.3.2. LQG Control

In Chapter 4, the development of the LQG controller is discussed, which is achieved by integrating the LQR state-feedback control law with a Kalman filter that is used to estimate states from measurable outputs. Despite utilizing state-feedback control law, this configuration has been shown to reduce the excellent stability margins found in systems controlled by full state-feedback LQR controllers. Figure 6.8 illustrates the stability margins for both the LQR-SF and LQG cases. There is a noticeable decline in stability margins at the plant input for the LQG case, while the margins at the plant output are relatively similar for both cases. This indicates an imbalance in stability margins, and the desired thresholds of $6dB$ gain margin and $45°$ phase margin are not met for the LQG-controlled system. Consequently, there is a need to restore the stability margins at the plant input, which is where the loop transfer recovery method becomes relevant.

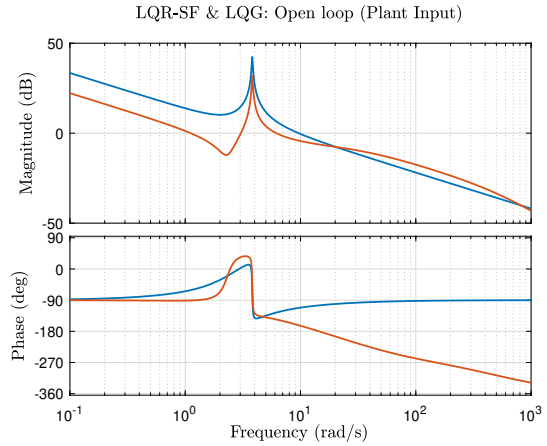

(a) Bode diagrams of the open-loop transfer function at the plant input

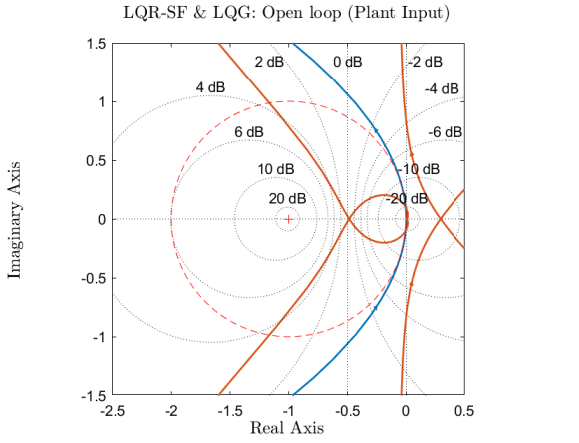

(b) Nyquist diagrams of the open-loop transfer function at the plant input

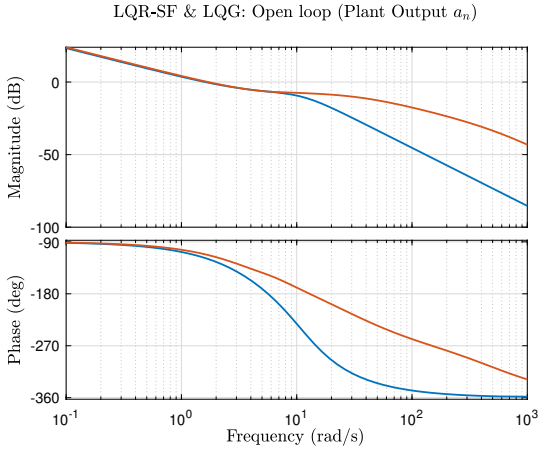

(c) Bode diagrams of the open-loop transfer function at the plant output

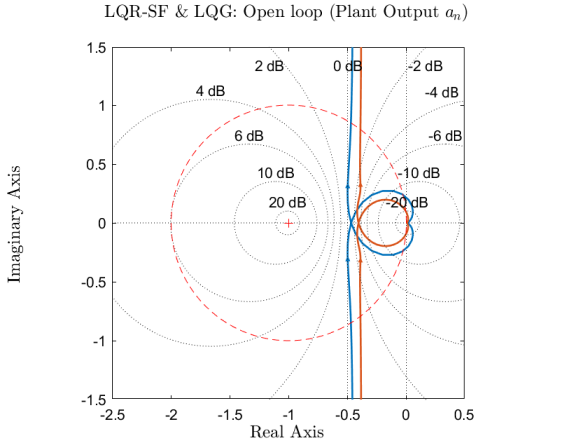

(d) Nyquist diagrams of the open-loop transfer function at the plant output

Figure 6.8: Bode and Nyquist plots comparing the stability margins for the LQR-SF (blue) and LQG (red)

6.3.3. iLTR Control

This study explores two LTR approaches: the classical LTR method known as '*input*-LTR', described by J. Doyle and Stein, 1981, and a method developed by Lavretsky, 2012, termed 'LTR-*input/output*' in this study. The scalar parameter in iLTR, labeled ρ, is varied from $5.17 \cdot 10^{-4}$ to $1.03 \cdot 10^{-1}$ and is used to illustrate the improvement of stability margins at the plant input compared to the LQG case, as shown in Figure 6.9. The recovery is evident in these figures, particularly in the Bode plots of Figure 6.9a, where the input transfer function magnitudes for iLTR shift upward, aligning more closely with the LQR magnitude plot as the recovery parameter ρ is increased. This trend is also seen in the phase plots of iLTR at higher frequencies. The Nyquist plot in Figure 6.9b further highlights the effectiveness of iLTR, as it shows the shift from the LQG to the LQR case.

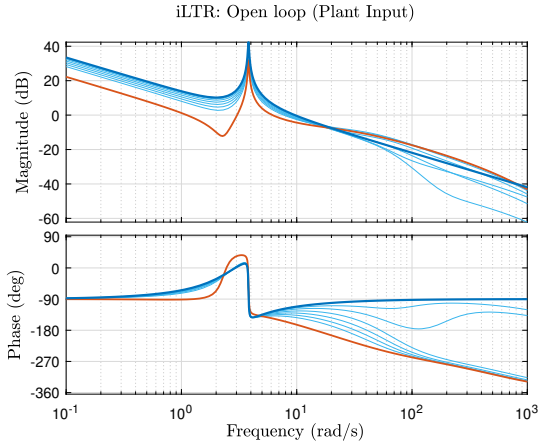

(a) Bode diagrams of the open-loop transfer function at the plant input

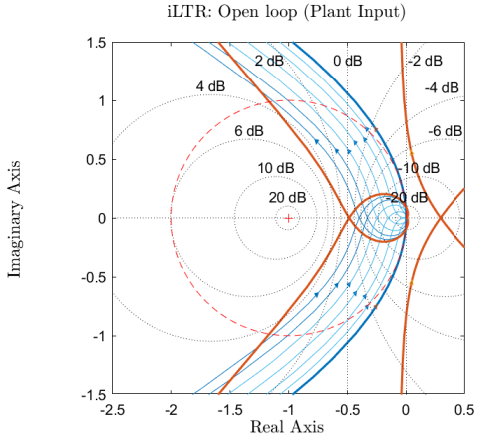

(b) Nyquist diagrams of the open-loop transfer function at the plant input

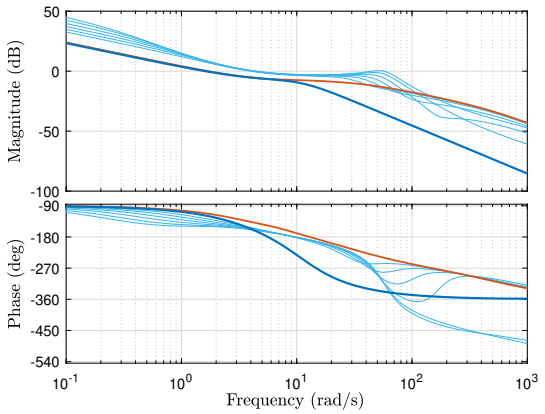

(c) Bode diagrams of the open-loop transfer function at the plant output

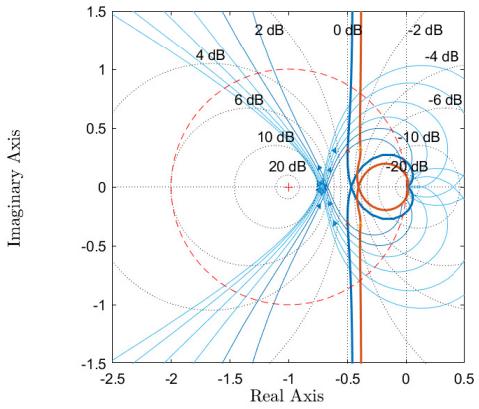

(d) Nyquist diagrams of the open-loop transfer function at the plant output

Figure 6.9: Bode and Nyquist plots illustrating the recovery process for the iLTR method as the recovery parameter ρ increases, compared with the LQR (dark blue) and the LQG (red) case

However, this improvement in stability margins is not visible at the plant output. As the ρ value is increased to recover stability at the plant input, the margins at the plant output diminish. This is a known drawback of LTR theory, which is unable to restore stability margins simultaneously at both the plant input and output. Therefore, the challenge lies in achieving a balance in the stability margins at both points to fulfill standard stability criteria. In this case, the ideal ρ parameter was determined to be $\rho = 1.03 \cdot 10^{-4}$ by aiming for such a balance, yet the resulting margins given in Table 6.2 did not meet the necessary stability requirements. The controller matrices for this iLTR case is given in Equation 6.5.

$$A_k = \begin{bmatrix} 0 & 0 & 0 & 0 \\ 0 & -579.4 & -15.46 & -73.45 \\ 0 & -1.528 & -20.54 & -2.275 \\ 36.02 & 92.75 & 133.4 & -23.15 \end{bmatrix}, \qquad B_k = \begin{bmatrix} 1 & 0 & 0 \\ 0 & 48.9 & -6.966 \\ 0 & -1.154 & -20.04 \\ 0 & 1.415 & 86.41 \end{bmatrix}$$
$$C_k = \begin{bmatrix} 2.77 & 8.425 & 3.634 & -0.6176 \end{bmatrix}, \qquad D_k = \begin{bmatrix} 0 & 0 & 0 \end{bmatrix} \tag{6.5}$$

In Figure 6.10, the adjustments in sensitivity functions are shown as the value of the recovery parameter in the iLTR method is increased. Specifically, when examining the output sensitivity function in Figure 6.10a, there is a notable increase in peak values compared to those observed in both LQR and LQG controlled systems. This

Table 6.2: Stability margins at both the plant input and the normal acceleration output a_n for different values of ρ in the iLTR case with the optimal iLTR case highlighted

ρ	**Plant Input**		**Plant Output**	
	Gain Margin (dB)	**Phase Margin** $(^\circ)$	**Gain Margin** (dB)	**Phase Margin** $(^\circ)$
$\mathbf{1.03 \cdot 10^{-4}}$	**6.74**	**36.01**	**4.06**	**34.01**
$5.16 \cdot 10^{-4}$	7.94	40.61	3.49	27.41
$1.86 \cdot 10^{-3}$	9.60	45.21	3.24	24.33
$5.59 \cdot 10^{-3}$	12.08	50.02	3.05	22.32
$1.46 \cdot 10^{-2}$	16.29	55.03	2.88	20.88
$3.79 \cdot 10^{-2}$	∞	60.01	2.75	19.84
$1.03 \cdot 10^{-1}$	∞	63.86	2.67	19.21

trend indicates a potential downside of the iLTR method when applied to the plant input: it tends to deteriorate the robustness at the plant output. On the other hand, the input sensitivity function, shown in Figure 6.10b, presents a different picture. Here, the beneficial effects of the recovery process are evident. As the recovery parameter is increased, the input sensitivity function shows clear signs of improvement, underscoring the effectiveness of this approach in enhancing the system's performance at the input side.

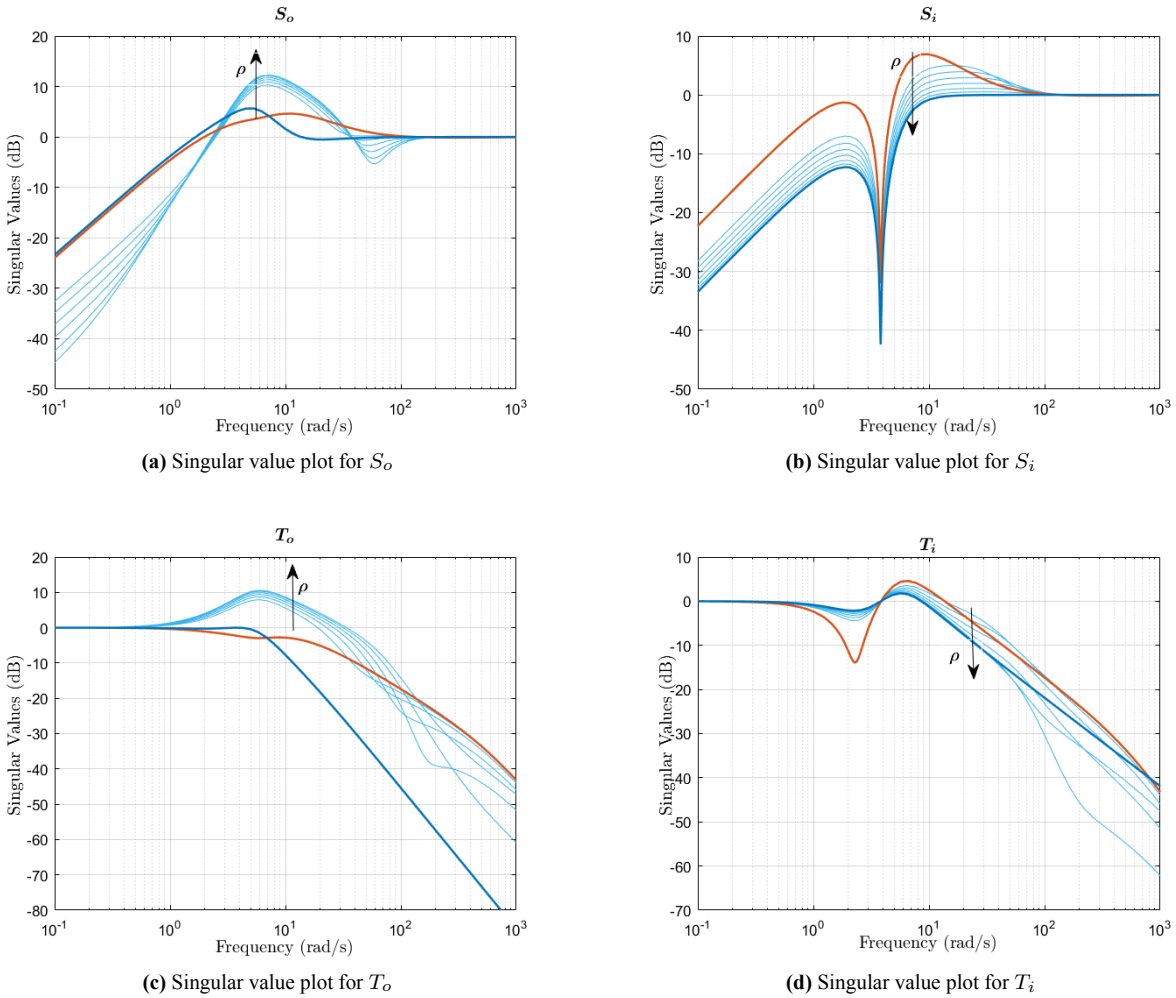

(a) Singular value plot for S_o

(b) Singular value plot for S_i

(c) Singular value plot for T_o

(d) Singular value plot for T_i

Figure 6.10: Sensitivity functions for iLTR controlled system with increasing value of the recovery parameter ρ, compared with the LQR (dark blue) and the LQG (red) case

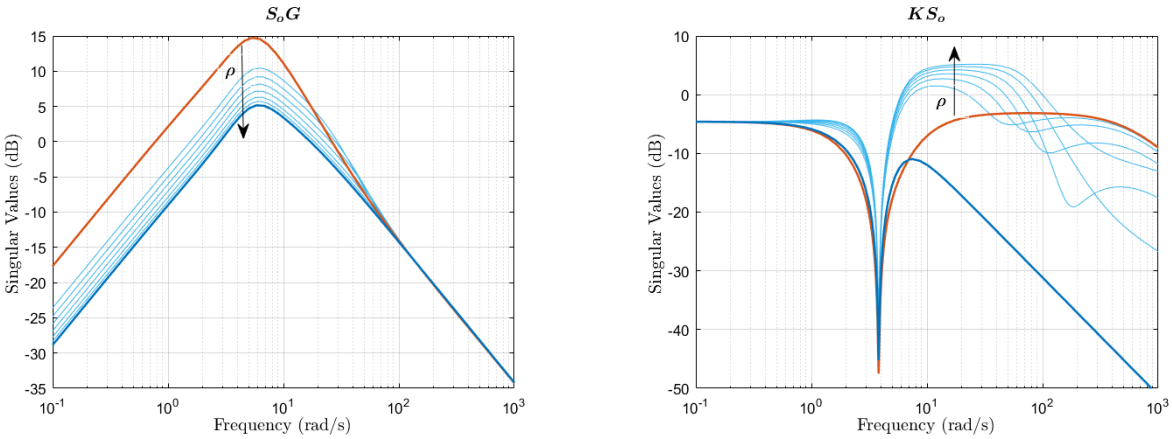

(e) Singular value plot for S_oG

(f) Singular value plot for KS_o

Figure 6.10: Sensitivity functions for iLTR controlled system with increasing value of the recovery parameter ρ, compared with the LQR (dark blue) and the LQG (red) case

6.3.4. LTRio Control

The LTRio method, discussed in detail in Section 5.3, demonstrates that as the scalar recovery parameter ν decreases, the system's behavior asymptotically aligns with that of a positive real system. The implementation of this approach is different from the iLTR method, as it entails the modification and scaling of both the process noise and measurement noise covariance matrices in proportion to the recovery parameter ν. Throughout this analysis, ν is varied from 1.05 to 4.10×10^{-3}, with specific values chosen to illustrate how the classical stability margins change with a decreasing recovery parameter. The impact of reducing ν is prominently seen at the plant input, by the Bode plot in Figure 6.11a, where both the magnitude and phase plots move upwards, approaching the Bode plots of the LQR-controlled system. Correspondingly, the Nyquist plot in Figure 6.11b exhibits a shift towards the LQR Nyquist plot with the decrement of ν.

In Figure 6.12a, the output sensitivity function shows an interesting trend: as the recovery parameter is decreased, the peaks in this function become higher[1]. This suggests that the improvements made at the plant input (via recovery) negatively affect the robustness properties at the plant output.

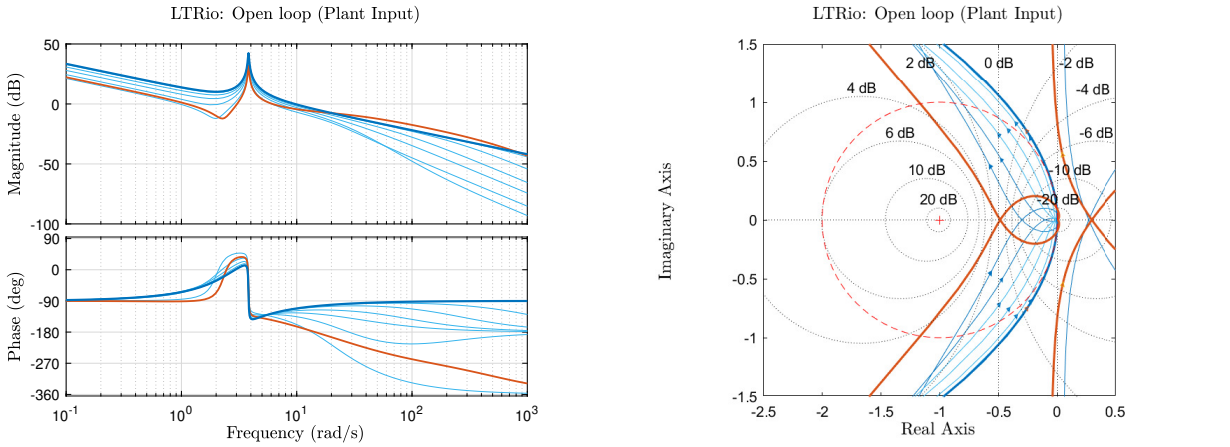

(a) Bode diagrams of the open-loop transfer function at the plant input

(b) Nyquist diagrams of the open-loop transfer function at the plant input

Figure 6.11: Bode and Nyquist plots illustrating the recovery process for the LTRio method as the recovery parameter ν decreases, compared with the LQR (dark blue) and the LQG (red) case

[1] It should be noted that the arrows in Figure 6.12 indicate the direction of increasing values of ν

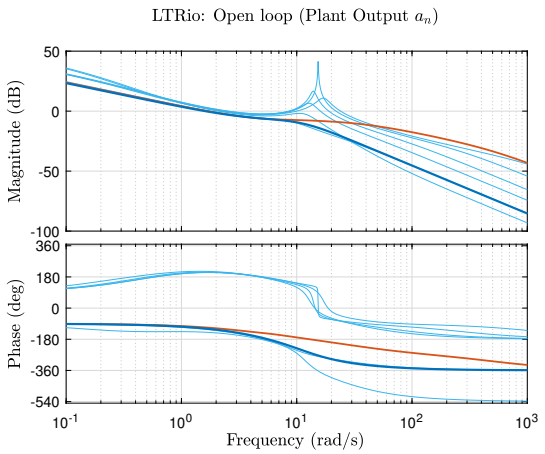

(c) Bode diagrams of the open-loop transfer function at the plant output

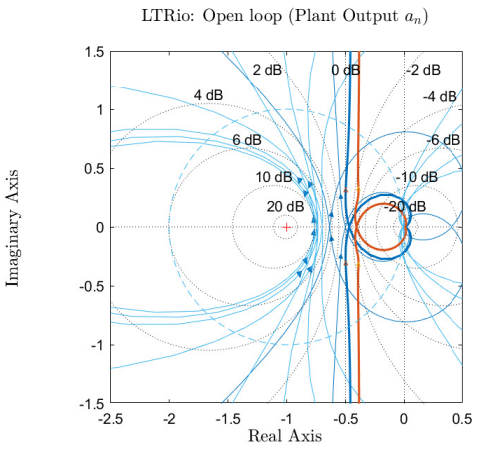

(d) Nyquist diagrams of the open-loop transfer function at the plant output

Figure 6.11: Bode and Nyquist plots illustrating the recovery process for the LTRio method as the recovery parameter ν decreases, compared with the LQR (dark blue) and the LQG (red) case

A key distinction from the iLTR-controlled system is how these peaks behave. In the LTRio case, the peak of the output sensitivity function starts at the same level as that of the LQR-controlled system and then progressively rises. Conversely, in the iLTR scenario, the peak begins at a level around 4dB higher than that of the LQR peak and increases further as the recovery parameter is increased. This comparison indicates that while the LTRio method might offer a possibility of achieving a balance in stability and robustness at the plant input and output, the iLTR method appears to consistently lead to poor robustness properties at the plant output, irrespective of the recovery at the plant input. Considering the input sensitivity function (S_i) in Figure 6.12b, both the iLTR and LTRio cases show a decrease in the peak, moving towards the benchmark set by the LQR function. This similarity indicates a consistent improvement in system performance at the input side in both methods.

The stability margins corresponding to the chosen values of the recovery parameter, denoted by ν, are presented in Table 6.3. The optimal value of the recovery parameter was found to be 1.05 which gives a balanced situation in terms of the plant input and output stability margins. The LTRio controller state-space system in this case is given in Equation 6.6.

$$A_k = \begin{bmatrix} 0 & 0 & 0 & 0 \\ 0 & -1.994 & 0.6872 & -0.3495 \\ 0 & -12.46 & -7.751 & -3.66 \\ 36.02 & 90.13 & 55.66 & -23.48 \end{bmatrix}, \qquad B_k = \begin{bmatrix} 1 & 0 & 0 \\ 0 & 0.2243 & -0.2583 \\ 0 & -0.2316 & -7.065 \\ 0 & 1.635 & 8.736 \end{bmatrix}$$
$$C_k = \begin{bmatrix} 2.77 & 8.425 & 3.634 & -0.6176 \end{bmatrix}, \qquad D_k = \begin{bmatrix} 0 & 0 & 0 \end{bmatrix} \tag{6.6}$$

In the LTRio case, the stability margins at the input were recovered without a substantial compromise in the margins at the normal acceleration output. Figure 6.13 provides a comparison between the iLTR and LTRio controlled systems, focusing on the changes in their phase margins with varying recovery parameter. In the case of the iLTR-controlled system, it is evident that there is no value of ρ where the phase margins at both the input and output simultaneously exceed the minimum requirement of $45°$. This limitation highlights a key challenge in achieving optimal phase margins using the iLTR method. On the other hand, the LTRio-controlled system shows a more promising outcome. There exists a specific range of ν where the phase margins at both the plant input and output can indeed be adjusted to be above the $45°$ desired value. However, it is crucial to note that while adjusting for phase margins, the gain margin should not be overlooked. The gain margin needs to meet its own requirement of being at least $6dB$. This additional constraint means that even within the favorable settings identified for the LTRio system, careful calibration is necessary to ensure that both phase and gain margins meet their respective thresholds.This suggests that with careful tuning, the LTRio method can potentially meet the desired stability margins criteria at both critical points of the plant. A balanced scenario was achieved where the margins at both breakpoints meet the conventional standards of $6dB$ gain margin and a $45°$ phase margin.

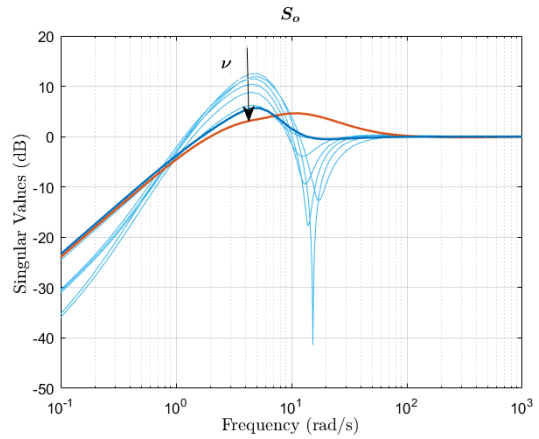

(a) Singular value plot for S_o

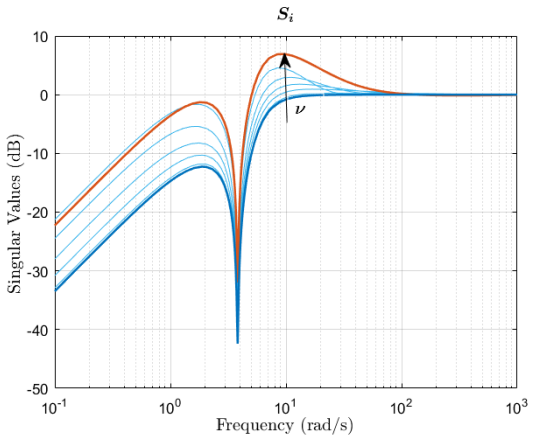

(b) Singular value plot for S_i

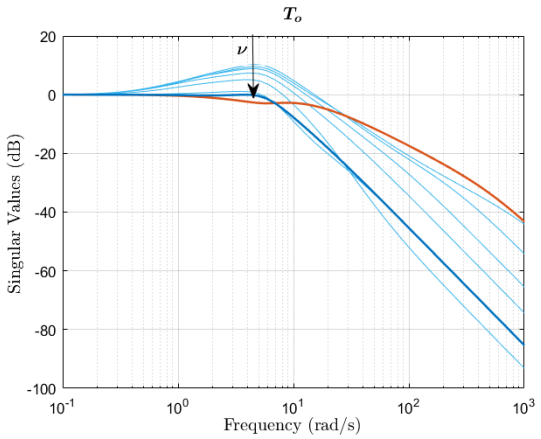

(c) Singular value plot for T_o

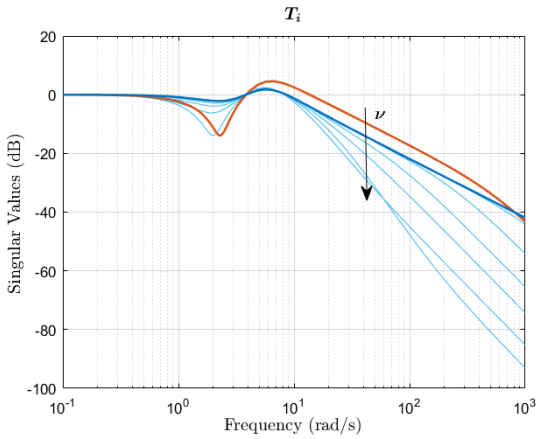

(d) Singular value plot for T_i

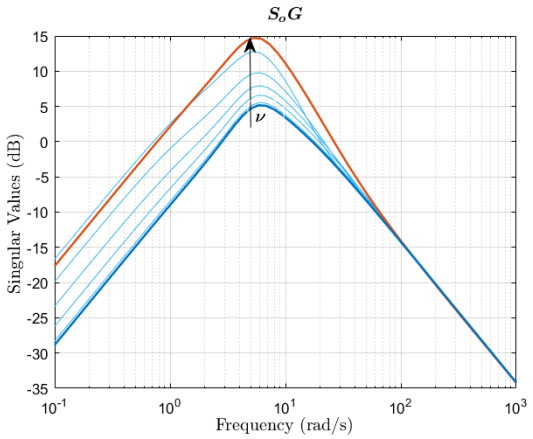

(e) Singular value plot for S_oG

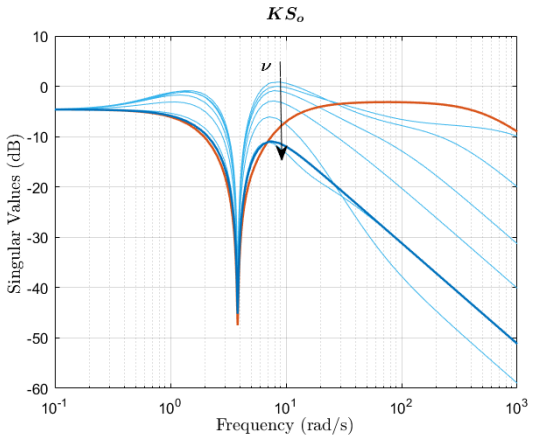

(f) Singular value plot for KS_o

Figure 6.12: Sensitivity functions for LTRio controlled system with increasing value of the recovery parameter ν, compared with the LQR (dark blue) and the LQG (red) case

Table 6.3: Stability margins at both the plant input and the normal acceleration output a_n for different values of ν in the LTRio case with the optimal LTRio case highlighted

ν	Plant Input		Plant Output	
	Gain Margin (dB)	**Phase Margin** $(^\circ)$	**Gain Margin** (dB)	**Phase Margin** $(^\circ)$
$\mathbf{1.05 \cdot 10^{0}}$	**10.38**	**45.00**	**6.00**	**55.97**
$2.81 \cdot 10^{-1}$	19.73	50.03	3.94	35.76
$1.36 \cdot 10^{-1}$	∞	55.19	3.12	28.49
$6.82 \cdot 10^{-2}$	∞	60.23	2.68	24.79
$2.01 \cdot 10^{-2}$	∞	65.33	2.34	22.01
$4.11 \cdot 10^{-3}$	∞	67.13	2.55	23.07

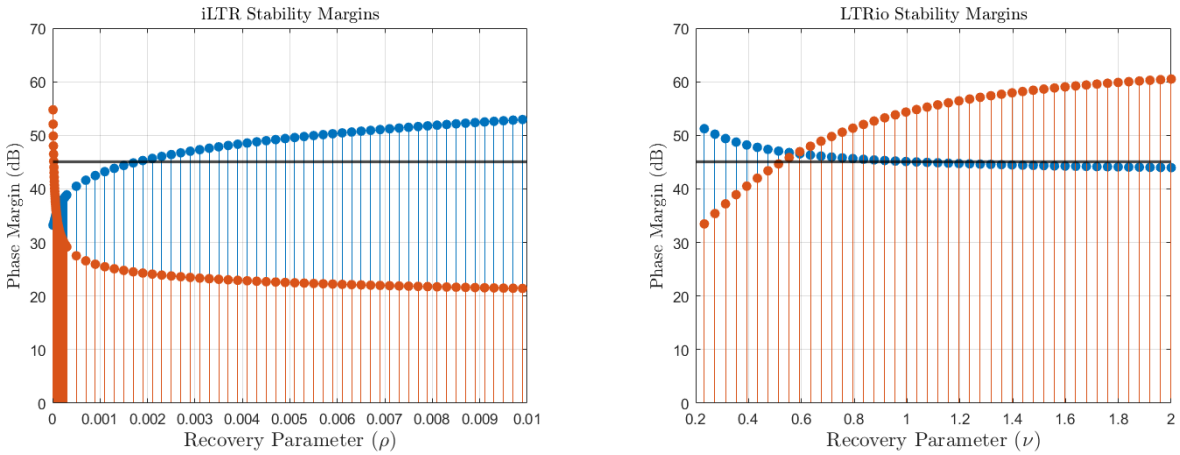

(a) iLTR Phase Margins

(b) LTRio Phase Margins

Figure 6.13: Stem plot depicting phase margins at the plant input (blue) and output (red) with increasing recovery parameters for the iLTR and LTRio case

6.4. Comparison of Linear Quadratic Control Techniques

The open-loop transfer functions at the plant input for both the LQG and iLTR cases are very similar, as seen in Figure 6.14a and Figure 6.14b. This similarity is also reflected in their stability margins, given in Table 6.4. Notably, the LTRio method provides enhanced attenuation of high-frequency noise, which is observable in the Bode plot (Figure 6.14a). In Figure 6.14b, the plot for the LTRio method is positioned between the Nyquist plots of LQR-SF and, LQG system and thus exhibits higher stability margins when compared to LQG and iLTR. In the Nyquist plot for the LQR-OF case, it is noted that the system's gain margin at the plant input is almost identical to the gain margin of the LTRio-controlled system. This is seen where both plots intersect the x-axis. Furthermore, the phase margin in the LQR-OF case appears to be very close to the phase margins of both the LQG and iLTR-controlled systems. This is observable at the points where the plots intersect the unit circle at the origin, although these intersections are not shown in the figures.

When examining the open-loop transfer functions at the plant output, it is clear that the optimal iLTR case displays the smallest stability margins. On the other hand, the LTRio case shows a strong similarity to the LQR-OF open-loop transfer functions, leading to similar stability margins. Among all the controllers, the LQG-controlled system demonstrates the highest stability margins. Overall, the LTRio-controlled system stands out as the sole output-feedback structure capable of achieving stability margins that meet the requirements.

Table 6.5 presents the minimum singular values of the return difference and stability robustness functions shown in Figure 6.15, along with the maximum singular values of the output sensitivity, and complementary sensitivity functions. The objective is to achieve higher values for $\underline{\sigma}(I + L)$ and $\underline{\sigma}(I + L^{-1})$, while aiming for lower values for $\bar{\sigma}(S_o)$ and $\bar{\sigma}(T_o)$. According to Table 6.5, the LQR-SF design emerges as the most proficient in frequency-domain characteristics. In contrast, while the LQG design shows undesirable characteristics at the plant input with low values

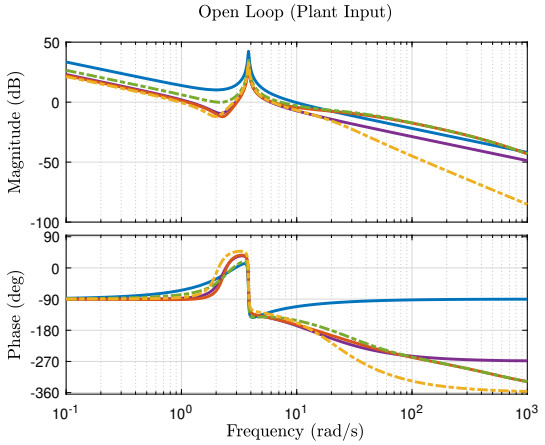

(a) Bode diagrams of the open-loop transfer function at the plant input

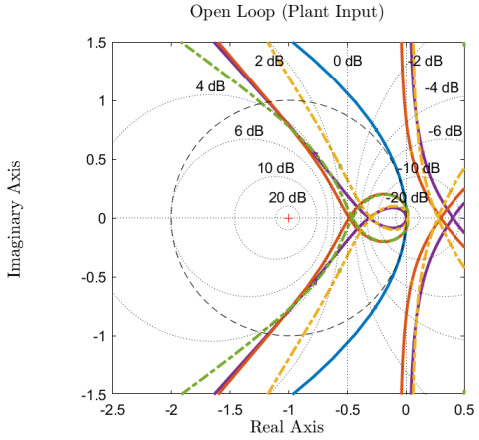

(b) Nyquist diagrams of the open-loop transfer function at the plant input

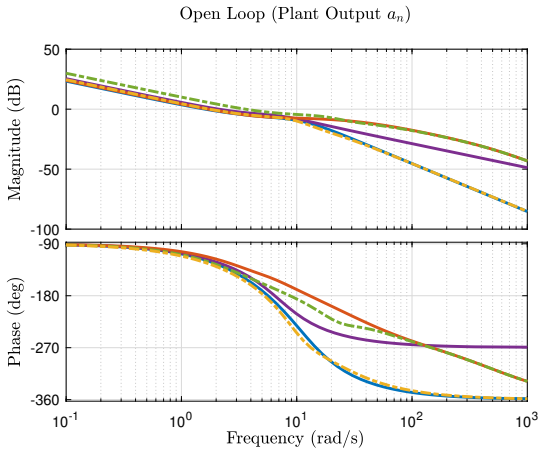

(c) Bode diagrams of the open-loop transfer function at the plant output

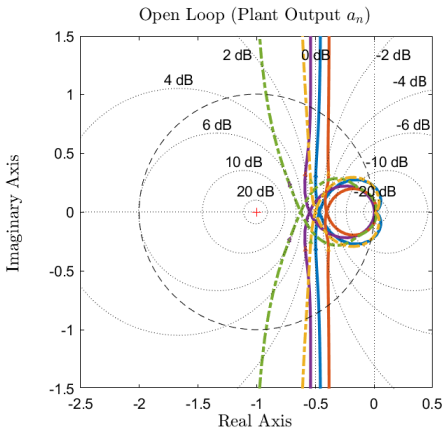

(d) Nyquist diagrams of the open-loop transfer function at the plant output

Figure 6.14: Bode and Nyquist plots of the open loop transfer functions at the plant input and output for LQR-SF (blue), LQR-OF (purple), LQG (red), iLTR (green - -) and LTRio (yellow - -) controlled systems

of $\underline{\sigma}(I + L)$ and $\underline{\sigma}(I + L^{-1})$, it performs well at the plant output. The iLTR method provides marginally improved values at the input relative to the LQG controlled system, but is less effective at the plant output. The LTRio method, however, demonstrates well-balanced performance both at the plant input and output.

Table 6.4: Comparison of stability margins at both the plant input and the normal acceleration output a_n for the LQR-SF, LQR-OF, LQG, iLTR and LTRio-controlled systems

Controller	ρ/ν	**Plant Input**		**Plant Output**	
		Gain Margin (dB)	**Phase Margin** $(^\circ)$	**Gain Margin** (dB)	**Phase Margin** $(^\circ)$
LQR-SF	-	∞	67.5	6.57	62
LQR-OF	-	9.97	35.3	5.16	57
LQG	-	6.26	34.2	7.82	67.1
i-LTR	$1.03 \cdot 10^{-4}$	6.74	36.01	4.06	34.01
LTRio	$1.05 \cdot 10^{0}$	10.38	45.00	6.00	55.97

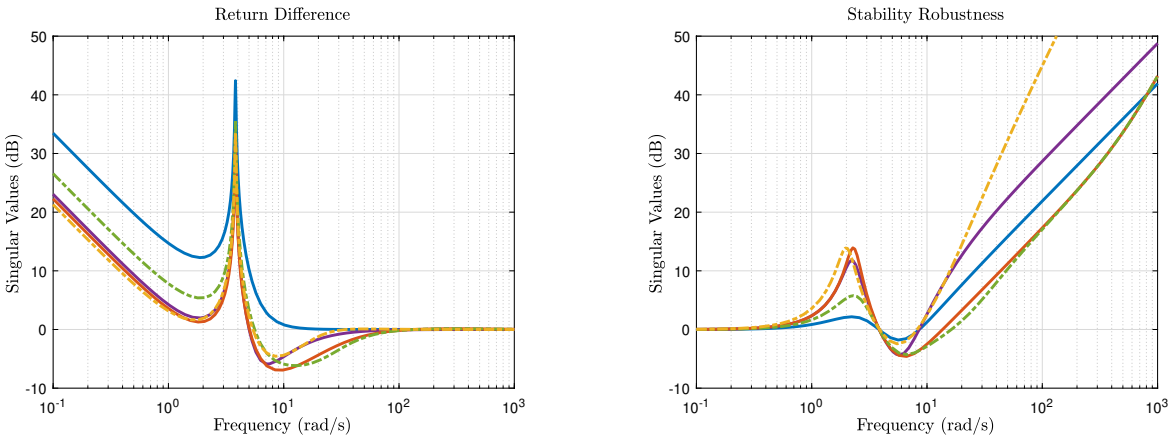

(a) Return difference at the plant input

(b) Stability robustness at the plant input

Figure 6.15: Comparison of the return difference and stability robustness functions for the LQR-SF (blue), LQR-OF (purple), LQG (red), iLTR (green - -) and LTRio (yellow - -) controlled systems

Table 6.5: Singular values of the input return difference and stability robustness, and output sensitivity and complimentary sensitivity functions for the LQR-SF, LQR-OF, LQG, iLTR and LTRio-controlled systems

Controller	ρ/ν	**Plant Input**		**Plant Output**	
		$\underline{\sigma}(\mathbf{I}+\mathbf{L})$	$\underline{\sigma}(\mathbf{I}+\mathbf{L}^{-1})$	$\bar{\sigma}(\mathbf{S_o})$	$\bar{\sigma}(\mathbf{T_o})$
LQR-SF	-	1.00	0.81	1.93	0.99
LQR-OF	-	0.50	0.60	1.93	0.99
LQG	-	0.45	0.59	1.70	0.99
i-LTR	$1.03 \cdot 10^{-4}$	0.49	0.61	2.90	2.08
LTRio	$1.05 \cdot 10^{0}$	0.59	0.76	2.03	1.13

The iLTR controlled system's subpar stability margins are apparent as high peaks in the normal acceleration output sensitivity function (S_o) and the input sensitivity function (S_i), as shown in Figures 6.16a and 6.16b, respectively. In contrast, the excellent stability at the plant input for the LQR-SF case is evident in its input sensitivity function (S_i), where no significant peak is observed in the singular value plot in Figure 6.16b. The notable roll-off at high frequencies in both the complementary input sensitivity function (T_i) and the complementary output sensitivity function (T_o) highlights the controllers' capability to diminish high-frequency disturbances. Among all the methods, the LTRio approach demonstrates a steeper roll-off, indicating superior noise attenuation capability. For the function S_oG, which should be minimized to attenuate input disturbance signals at the plant output, the LQR-SF controlled systems exhibit the highest effectiveness. The performance in LQR-OF, LQG, iLTR, and LTRio controlled systems is relatively similar in this regard. Considering the function KS_o, the LQG and iLTR control methods show less effectiveness in minimizing the impact of high-frequency measurement noise at the plant input. In comparison, the LQR-SF, LQR-OF and LTRio methods demonstrate a steeper roll-off thus indicating better abilities in attenuating high-frequency noise.

Classical stability margins might provide an overly optimistic assessment of system stability, as they do not account for simultaneous gain and phase variations. To evaluate system stability under more conservative scenarios, it is beneficial to consider the effects of such variations by obtaining the disk margins for the various controller techniques used in this study. From the information in Table 6.6, it is evident that, with the exception of the LQR-SF-controlled system, the LTRio-controlled system presents balanced stability margins that are also close to the required margins. Figure 6.17a displays the Nichols plot for both the LQR-SF and LTRio cases, alongside their respective exclusion regions for comparison. Additionally, Figure 6.17b depicts the disk margins for the LQR-SF, LQG, and LTRio cases. This illustration clearly demonstrates the LTRio method's effectiveness in recovering stability margins for the LQG scenario.

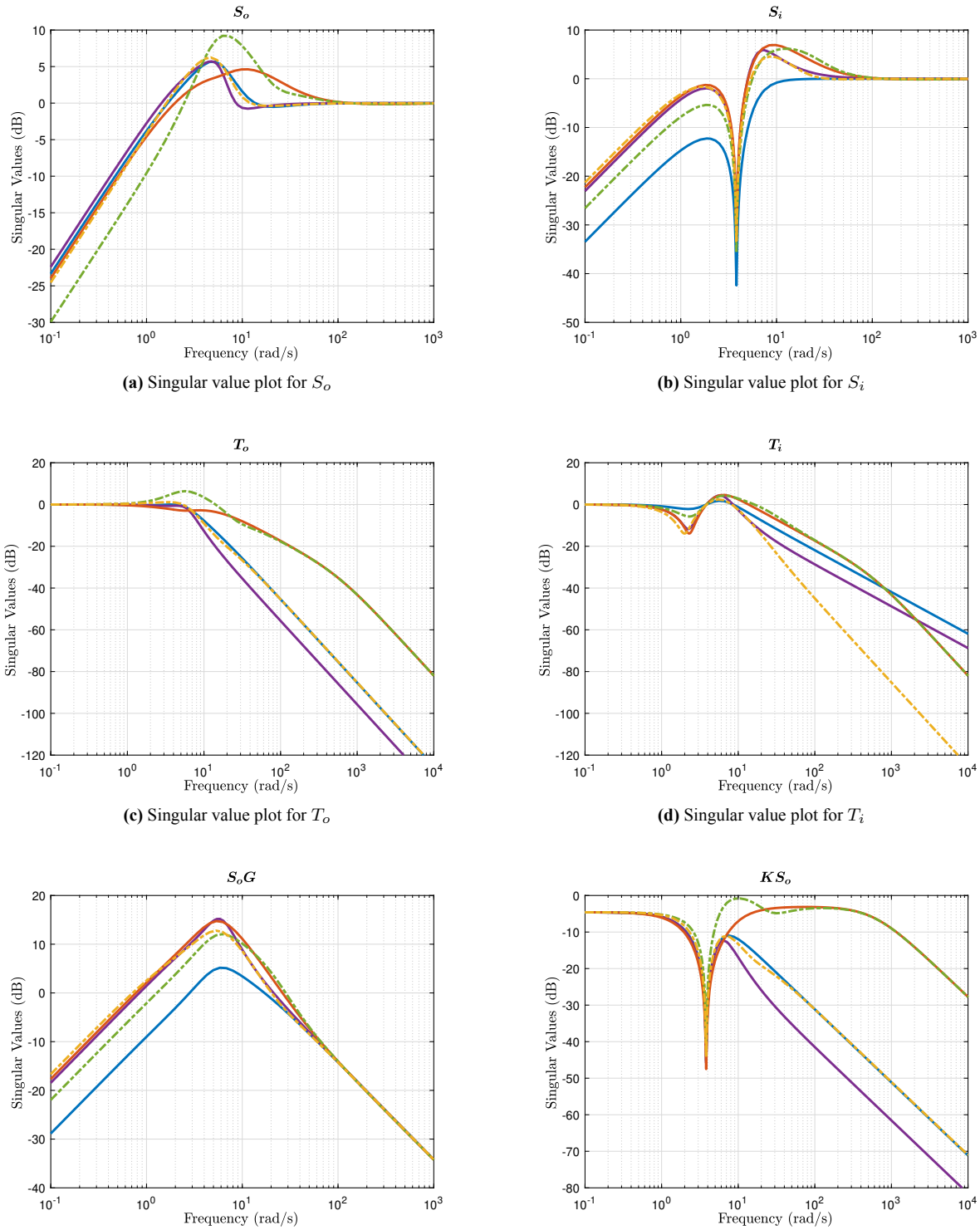

(a) Singular value plot for S_o

(b) Singular value plot for S_i

(c) Singular value plot for T_o

(d) Singular value plot for T_i

(e) Singular value plot for S_oG

(f) Singular value plot for KS_o

Figure 6.16: Comparison of the sensitivity functions for the LQR-SF (blue), LQR-OF (purple), LQG (red), iLTR (green - -) and LTRio (yellow - -) controlled systems

Table 6.7 shows that both the LQG and iLTR controllers have poles at very high frequencies. The actuators surfaces that implement the control commands have inherent limits on how fast they can operate. If a controller's design expects an actuator to respond at these high frequencies, it is likely that the actuator will not be able to meet

Table 6.6: Comparison of disk margins at the plant input and output for the LQR-SF, LQR-OF, LQG, iLTR and LTRio-controlled systems

Controller	Input Disk Margins		Output Disk Margins	
	Gain Margin	Phase Margin	Gain Margin	Phase Margin
	(dB)	$(^\circ)$	(dB)	$(^\circ)$
LQR-SF	12.24	62.52	6.29	38.27
LQR-OF	5.41	33.59	6.33	38.52
LQG	4.86	30.49	7.64	44.93
iLTR	5.48	33.99	3.58	22.99
LTRio	6.99	41.83	5.74	35.37

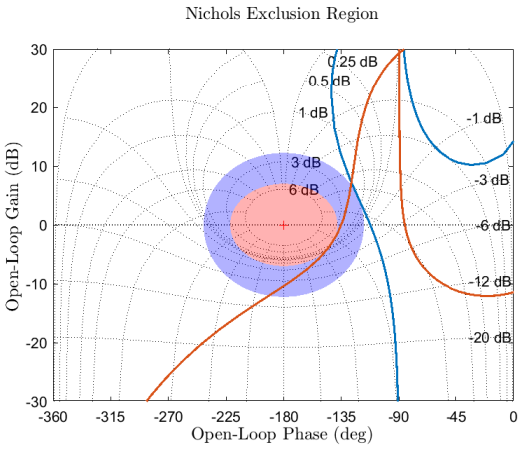

(a) Nichols exclusion region comparing LQR-SF (blue) with LTRio (red)

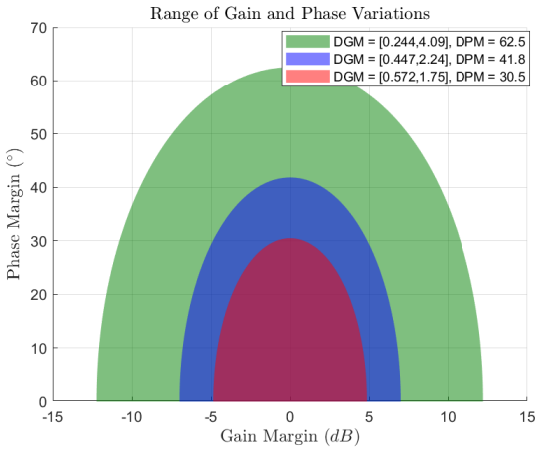

(b) Disk margin plot comparing LQR-SF (green), LQG (red) and LTRio (blue)

Figure 6.17: Nichols plot and disk margins illustrating the gain and phase variation in LQR-SF, LQG and LTRio controlled systemss

these demands due to its physical limitations. Such poles in a controller tend to amplify any high-frequency noise present in the sensor signal, which can degrade system performance. Moreover, for digital control systems, the sampling rate (dictated by the Nyquist rate) must be at least twice the highest frequency in the control system to accurately represent the dynamics. If the system cannot be sampled at a high enough rate to capture the dynamics associated with HF poles, they cannot be realized. Figure 6.18 shows that the LQG and iLTR controllers exhibit

Table 6.7: Pole locations of LQG, iLTR and LTRio controllers

Controller	Pole Location
LQG	-564.50
	-31.66
	-12.03
iLTR	-566.84
	-28.12 $\pm$ 0.15i
LTRio	-15.11 $\pm$ 12.99i
	-3.02

less attenuation of high-frequency noise compared to the LTRio controller. This observation supports the concept that poles at high frequencies can lead to the amplification of sensor noise. The LTRio controller's superior noise attenuation at high frequencies indicates a potential advantage in applications where sensor noise is a significant concern.

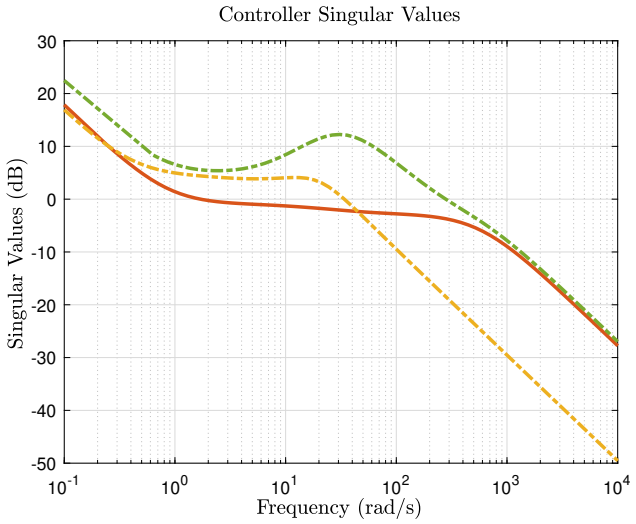

Figure 6.18: Singular values of the LQG (red), iLTR (green - -) and LTRio (yellow - -) controllers

6.5. Robustness in the Presence of Uncertainties

The H_∞ norm gives a measure of the worst-case amplification of the system. It tells us the maximum amount by which any input can be amplified in the output, considering all frequencies. In robust control, one common objective is to design a controller that minimizes the H_∞ norm of the closed-loop system. This essentially means minimizing the worst-case amplification, which in turn enhances the robustness of the system against disturbances and uncertainties. This section delves into the use of robustness and worst-case analyses to assess how varying amounts of uncertainty within the closed-loop system affect its overall stability and the magnitude of its peak gain. Various types of uncertainties, such as additive and multiplicative-input uncertainties are introduced into the system and the robustness of these systems is then analyzed using the structured singular value μ, as outlined in Section 6.2. Furthermore, real-parametric uncertainties are incorporated into the models to evaluate the extent to which the control methods can tolerate inaccuracies in the system modelling.

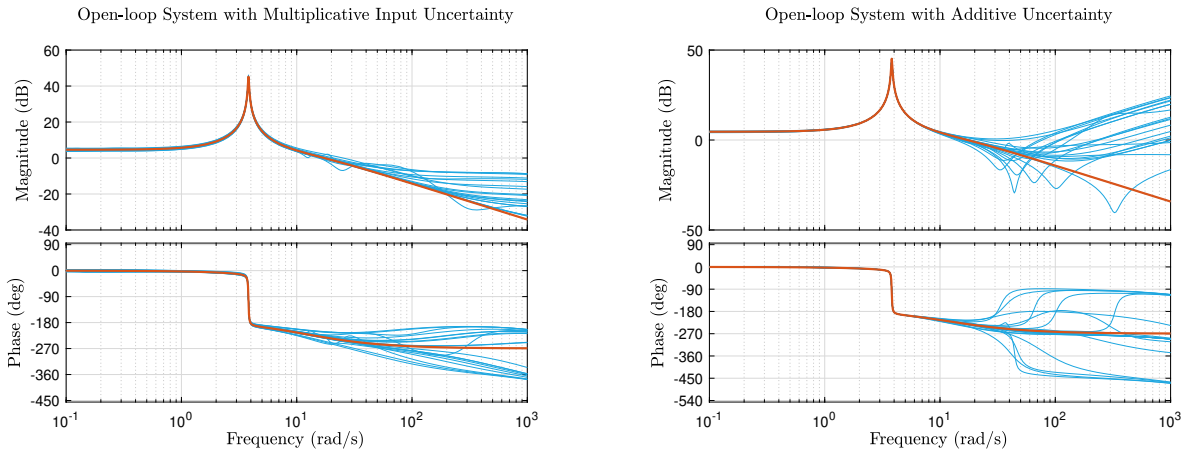

(a) Uncertain system with multiplicative-input uncertainty

(b) Uncertain system with additive uncertainty

Figure 6.19: Uncertain open-loop system dynamics for normal acceleration a_n output when faced with different types of uncertainties with the nominal plant dynamics shown in red

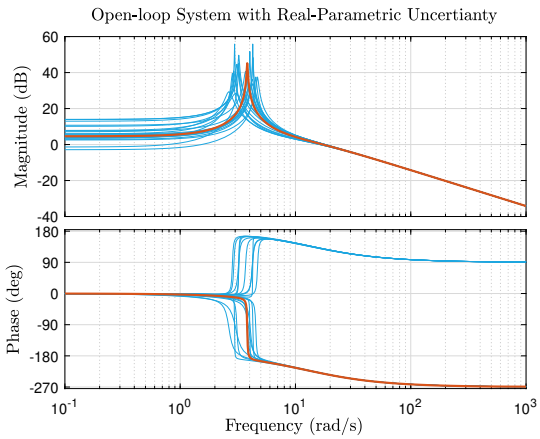

(c) Uncertain system with real-parametric uncertainty

Figure 6.19: Uncertain open-loop system dynamics for normal acceleration a_n output when faced with different types of uncertainties with the nominal plant dynamics shown in red

To simulate frequency-dependent uncertainty, `MATLAB` was used to create an uncertain linear-time invariant dynamic entity utilizing the `ultidyn` function, which was then combined with an appropriate shaping filter. This was based on the premise that the system might have unmodelled dynamics at higher frequencies. Consequently, the system's dynamics are precisely modelled (with a 10% level of uncertainty) at lower frequencies, but this accuracy diminishes after exceeding a frequency of 50 rad/s, indicating a large amount of uncertainty at higher frequencies. This specifically modelled uncertainty is then incorporated into the systems in both multiplicative and additive forms.

In the case of real-parametric uncertainty, some of the parameters within the short period approximation, as given in Equation 2.6, are subjected to variations of up to 40%. The objective is to determine the maximum percentage alteration in the values of these variables that would lead to instability in the system. To analyse the effects of multiplicative-input and additive forms of high-frequency uncertainty on the closed-loop system, μ-analysis is carried out to find out the maximum uncertainty (normalized) that can be tolerated by the uncertain system before it becomes unstable. The uncertain open-loop plant dynamics for the normal acceleration output are shown in Figure 6.19.

6.5.1. Multiplicative-Input Uncertainty

Analysis of the complementary input sensitivity function T_i provides valuable insights into how the closed loop system manages high-frequency noise at the plant input. Observations from Figure 6.20 show that the LQG controller demonstrates effective attenuation of this high-frequency noise. However, when compared to the iLTR and LTRio controllers, its ability to suppress such disturbances is somewhat limited.

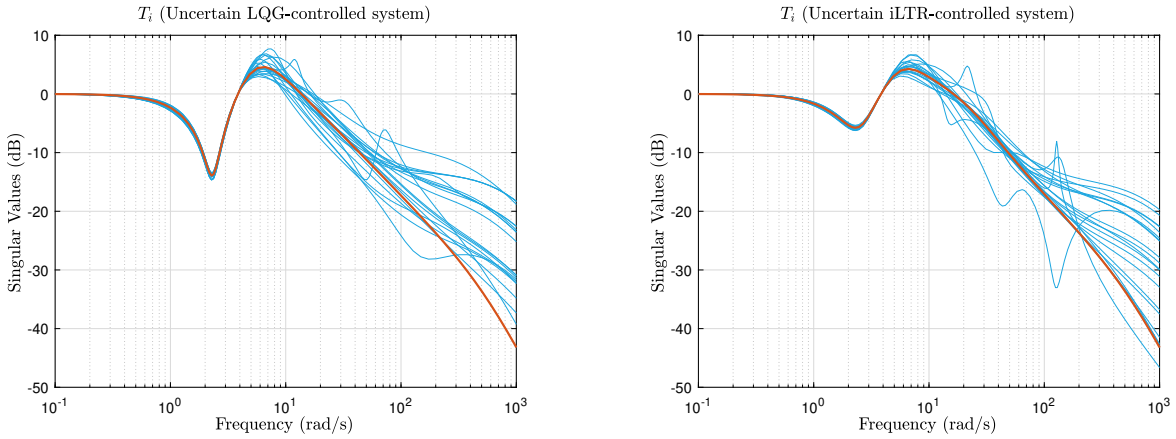

(a) T_i for the LQG-controlled system

(b) T_i for the iLTR-controlled system

Figure 6.20: T_i for the LQG, iLTR and LTRio-controlled systems in the presence of multiplicative-input uncertainties with the nominal case shown in red

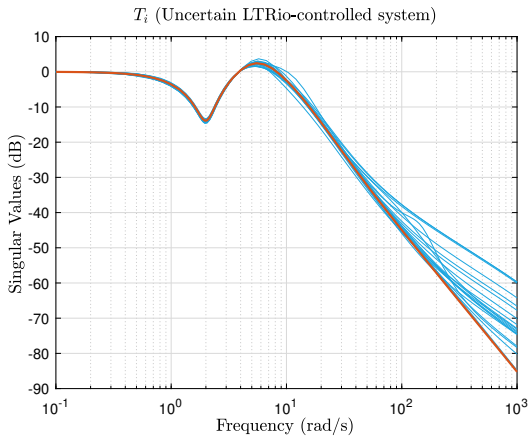

(c) T_i for the LTRio-controlled system

Figure 6.20: T_i for the LQG, iLTR and LTRio-controlled systems in the presence of multiplicative-input uncertainties with the nominal case shown in red

On the other hand, the LTRio controller exhibits a notably superior performance in handling high-frequency noise, outperforming both the LQG and iLTR controllers. This enhanced capability of the LTRio controller is reflected in the robust stability margin analysis (G. Balas et al., 2007). It is a metric in control system design, essentially representing the maximum level of normalized uncertainty that the closed-loop system can tolerate before losing stability. It is closely related to the structured singular value μ, with the robust stability margin being the inverse of μ. This margin is not constant but varies across different frequencies. In this analysis, the focus is on the frequency range of 0.1 to 1000 rad/s. The minimum value of the robust stability margin within this frequency range is considered the defining parameter for system robustness.

As seen in Figure 6.21a, the robust stability margins indicate that the iLTR controlled system has the lowest tolerance, capable of withstanding up to 287.3% of the modelled uncertainty. In contrast, the system controlled by LTRio demonstrates a significantly higher robust stability margin of 4.83, enabling the closed-loop to tolerate up to 483.0% of the modelled uncertainty. These figures are notably high for all the three control methods, indicating a strong capability for tolerating multiplicative-input uncertainty, especially at high frequencies.

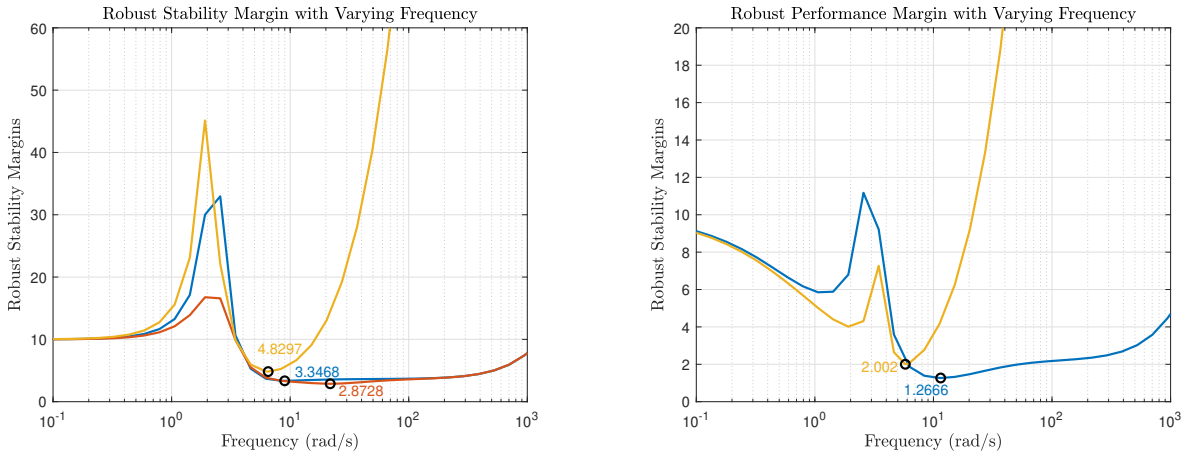

(a) Robust stability margins

(b) Robust performance margins

Figure 6.21: Robust stability margins, robust performance margins and the performance degradation curve of the LQG (blue), iLTR (red) and LTRio (yellow) controlled systems in the presence of multiplicative-input uncertainty

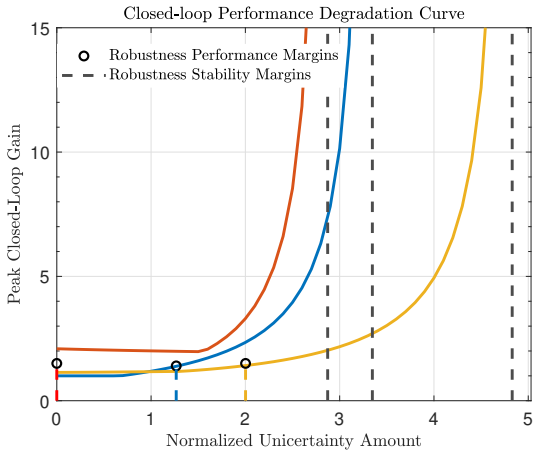

(c) Closed-loop performance degradation curve

Figure 6.21: Robust stability margins, robust performance margins and the performance degradation curve of the LQG (blue), iLTR (red) and LTRio (yellow) controlled systems in the presence of multiplicative-input uncertainty

The robust performance margin, defined for a specified gain γ, represents the maximum level of uncertainty a system can tolerate while maintaining a peak gain below γ which in this study, is set at 1.5. Therefore, the robust performance of the closed-loop system is assessed based on how much uncertainty it can withstand before its peak gain surpasses 1.5. Figure 6.21c provides an example of a trade-off curve, illustrating the balance between performance and robustness in this scenario. A value of $x = 1$ denotes the uncertainty ranges defined in the uncertain model, while $x = 2$ indicates a system with double the amount of uncertainty. Conversely, $x = 0$ represents the nominal system in the absence of uncertainty. Performance is depicted on the y-axis, represented by the peak gain of the closed-loop transfer function from the reference to the normal acceleration output.

In Figure 6.21c, the nominal gain for both the LQG and LTRio controlled systems is approximately 1, whereas it is around 1.5 for the iLTR controlled system. This suggests that the iLTR controller, even in its nominal state, without the presence of multiplicative-input uncertainties, shows suboptimal performance in the closed-loop system. As the normalized uncertainty in the system increases, there is a corresponding rise in the peak gain across the uncertainty range, forming what is known as the performance degradation curve. This curve invariably shows an upward trend with increasing uncertainty levels.

6.5.2. Additive Uncertainty

When considering additive uncertainties in the closed-loop system, the focus shifts to the analysis of the transfer function from output measurement noise to the plant input, denoted as (KS_o). The objective is to minimize the peak in these plots, aiming to reduce large control signals that may arise in response to noise and disturbances at the output. From Figure 6.22, it is observed that there are significant peaks in the (KS_o) function for the iLTR-controlled system, indicating a pronounced effect of additive uncertainty on the closed-loop system in this case. For the LQG-controlled system, the attenuation of high-frequency noise also appears inadequate. In contrast, the LTRio-controlled system shows a much steeper roll-off in its plot of around -20dB/dec, indicating superior performance compared to the LQG and iLTR controlled systems in managing additive uncertainties.

The distinct characteristics of the LQG and iLTR controlled systems, in comparison to the notably superior output noise attenuation properties of the LTRio-controlled system, are further validated by examining their robust stability and performance margins. Figure 6.23a clearly demonstrates that the LTRio controlled system can accommodate a substantially larger proportion of the modelled uncertainty, up to 144.5%, compared to the LQG and iLTR controlled systems, which can manage only about 13-15% of the modelled uncertainty. It is seen from Figure 6.23b that the LQG controlled system shows robust performance against only up to 9% of the modelled uncertainty, while the LTRio controlled system can handle approximately 125% of the modelled uncertainty before it shows decreased performance. Therefore, in scenarios involving additive uncertainties, the LQG and iLTR controlled systems struggle to maintain stability, whereas the LTRio controlled system remains stable even under significant uncertainties. Furthermore, the KS_o singular value plot of the LTRio system (Figure 6.22c) mimics that of the LQR controlled system as seen in Figure 6.16f, indicating that the LQR controlled system should also remain stable under additive uncertainties.

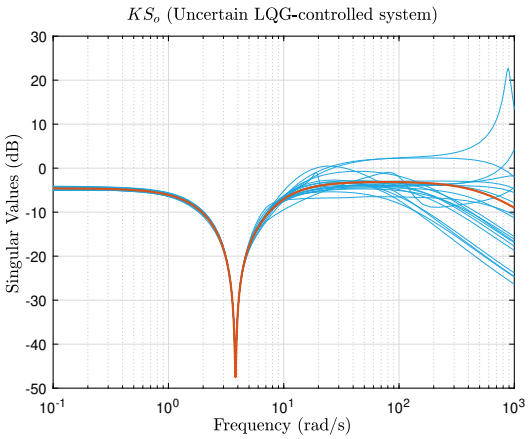

(a) KS_o for the LQG-controlled system

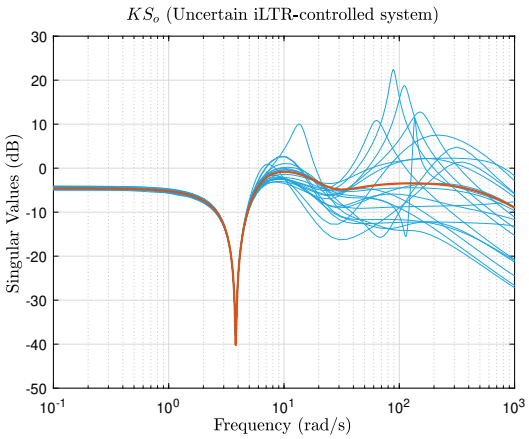

(b) KS_o for the iLTR-controlled system

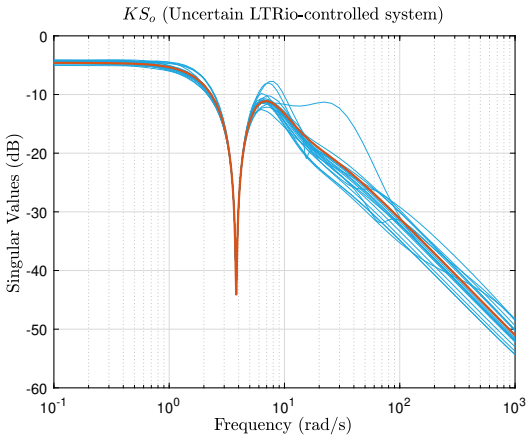

(c) KS_o for the LTRio-controlled system

Figure 6.22: KS_o for the LQG, iLTR and LTRio-controlled systems in the presence of additive uncertainty with the nominal case shown in red

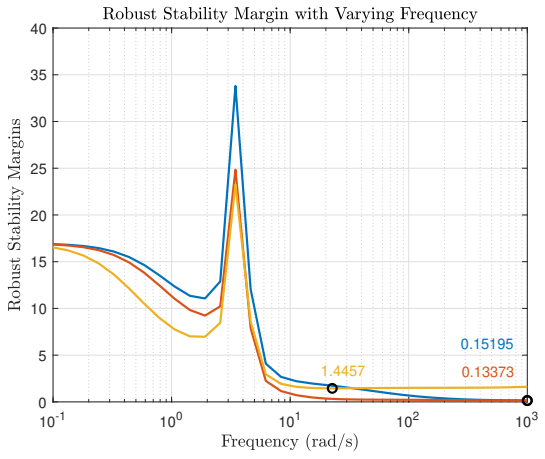

(a) Robust stability margins

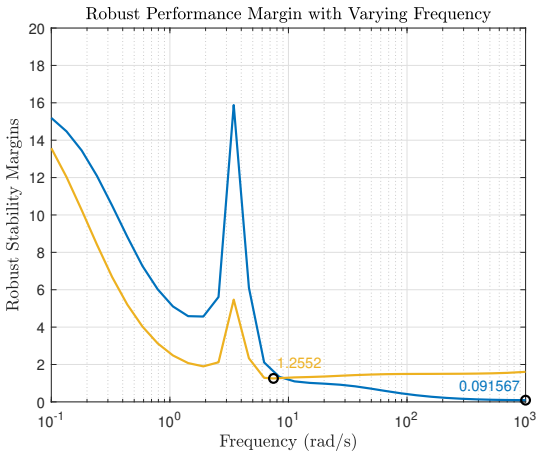

(b) Robust performance margins

Figure 6.23: Robust stability margins, robust performance margins and the performance degradation curve of the LQG (blue), iLTR (red) and LTRio (yellow) controlled systems in the presence of additive uncertainty

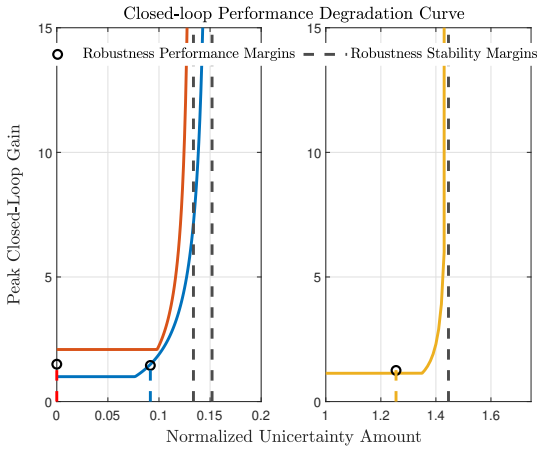

(c) Closed-loop performance degradation curve

Figure 6.23: Robust stability margins, robust performance margins and the performance degradation curve of the LQG (blue), iLTR (red) and LTRio (yellow) controlled systems in the presence of additive uncertainty

6.5.3. Real-Parametric Uncertainty

To evaluate the impact of parametric uncertainty on the closed-loop system, the parameters M_α and M_{δ_e} were varied within a range of $\pm 40\%$ in the short-period approximation, as specified in Equation 2.6 and the corresponding changes in the peak gain of the closed-loop system were observed. The results of this analysis are depicted in Figure 6.24, which shows the performance degradation curve for the system under this type of uncertainty. It is observed that the LQG-controlled system is the first to reach instability with increasing parameter variation. However, prior to reaching the instability threshold, the LQG system demonstrates superior performance compared to the iLTR and LTR systems, which is indicated by the lower gain values for the LQG system relative to the others for any given percentage change in system parameters before the point of instability. Table 6.8 provides information on how different levels of normalized uncertainty (for unstructured uncertainties) and increasing percentage change in the short-period parameters (for structured uncertainties) affect the stability of systems controlled by LQG, iLTR, and LTRio.

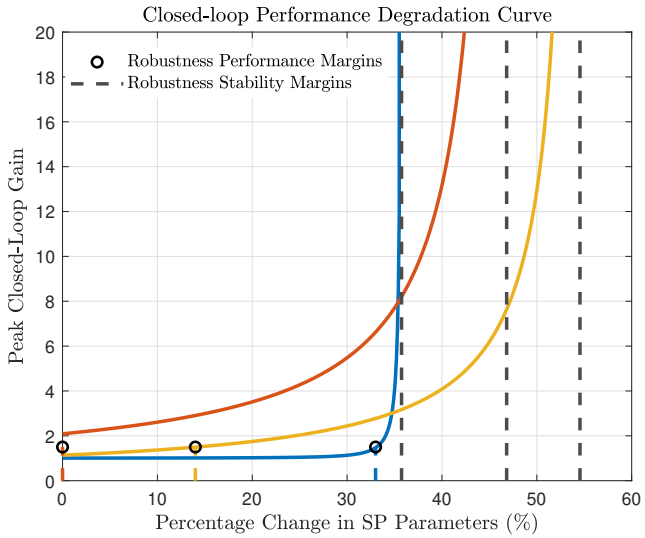

Figure 6.24: Closed-loop system degradation curve of the LQG (blue), iLTR (red) and LTRio (yellow) controlled systems in the presence of real-parametric uncertainties)

The sensitivity of the closed-loop system to uncertainties in the SP parameters is quantified by determining how inaccuracies in the system parameters affect the system's stability margin. For instance, a sensitivity of $x\%$ indicates that a deviation of dx in a parameter would lead to an approximate change of $0.01 \times x \times dx$ in the stability margin. In Table 6.8, it can be seen that the stability margins of the LQG and iLTR controlled systems are more sensitive to variations in the M_{δ_e} parameter compared to the M_α parameter. In contrast, LTRio-controlled systems exhibit a

relatively greater sensitivity to changes in the M_α parameter over the M_{δ_e} parameter. This suggests that the LTRio controller, with its lower sensitivity to parameter variations, especially in the M_{δ_e} parameter, offers a more robust solution against parametric uncertainties.

Table 6.8: Robust stability margins and robust performance margins for LQG, iLTR and LTRio controlled systems in the presence of different types of uncertainties

	Mulriplicative-Input		Additive		Real-Parametric			
Conroller Type	**Robust Stability Margin** (%)	**Robust Performance Margin** (%)	**Robust Stability Margin** (%)	**Robust Performance Margin** (%)	**Max Percentage Change in SP Parameters** (%)		**Sensitivity**	
					$\mathbf{M}_\alpha$	$\mathbf{M}_{\delta_e}$	$\mathbf{M}_\alpha$	$\mathbf{M}_{\delta_e}$
LQG	334.68	126.66	15.19	9.15	-35.74	-35.75	33	67
iLTR	287.28	0	13.37	0	-46.82	-46.82	32	41
LTRio	482.97	200.20	144.57	125.52	-54.55	-54.55	12	1

6.6. Uncertainty Effect in Time-Domain

In this section, the time-domain characteristics of the normal acceleration response of the closed-loop system is analyzed. The emphasis is on multiplicative-input and real-parametric uncertainties, excluding additive uncertainties, as these manifest as white noise in the normal acceleration output, thus having less affect on the time-domain response. Observations indicate that both LQG and iLTR controllers have limited tolerance to high-frequency additive uncertainties, with maximum thresholds of 15% and 13% respectively, as demonstrated in Table 6.8. Such low uncertainties result in minimal changes in time-domain characteristics, such as settling time and overshoot. This can be confirmed by observing the normal acceleration responses of all three controllers in the presence of additive uncertainties in Figure 6.25. The time-domain characteristics are not significantly affected by additive uncertainties in the case of LQG and iLTR controlled systems. Conversely, the LTRio approach shows more significant time-domain variations when faced with large amount of relatively lower-frequency additive uncertainties, as observed in Figrue 6.25c.

Figure 6.26 displays normal acceleration time responses under different levels of multiplicative-input uncertainties. Notably, the LTRio-controlled system encounters its worst-case at a lower frequency compared to the LQG and iLTR systems, as observed from Figure 6.26. Moreover, the iLTR system shows a lower tolerance to uncertainty levels than both LQG and LTRio systems. It is observed from Figure 6.27 that real-parametric uncertainties appear as low-frequency uncertainties in the closed-loop system. The worst-case for all the three systems appear at different frequencies and the iLTR and LTRio-controlled systems are able to handle a larger variation of the SP parameters than the LQG-controlled system. In summary, from Figures 6.25, 6.26 and 6.27, it is evident that unstructured uncertainties like multiplicative-input and additive uncertainties manifest as medium to high frequency disturbances, whereas real-parametric uncertainties typically appear as low-frequency disturbances in the time responses of closed-loop systems.

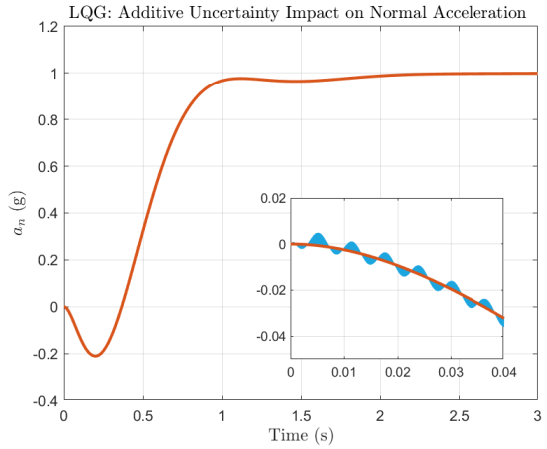

(a) LQG-controlled system

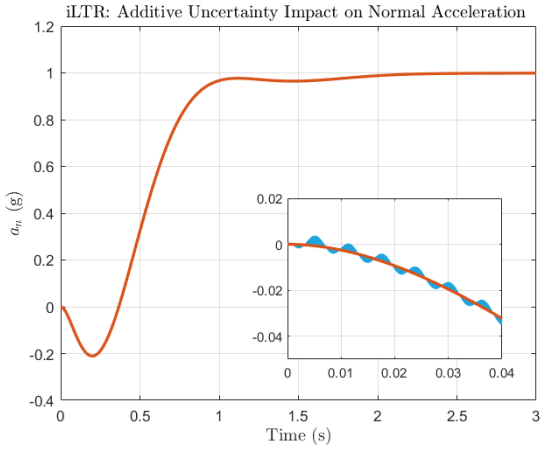

(b) iLTR-controlled system

Figure 6.25: Normal acceleration response under additive uncertainties for the LQG, iLTR and LTRio controlled systems along with the nominal case shown in red

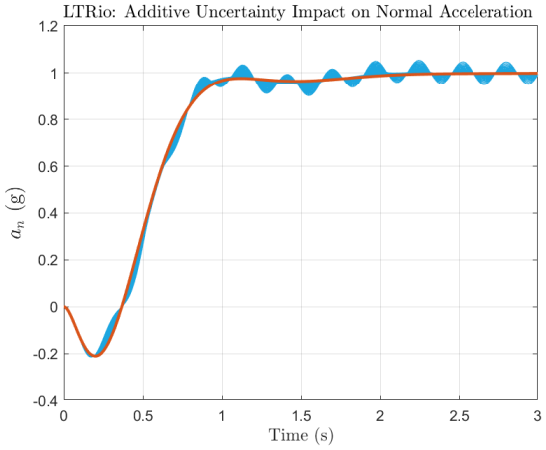

(c) LTRio-controlled system

Figure 6.25: Normal acceleration response under additive uncertainties for the LQG, iLTR and LTRio controlled systems along with the nominal case shown in red

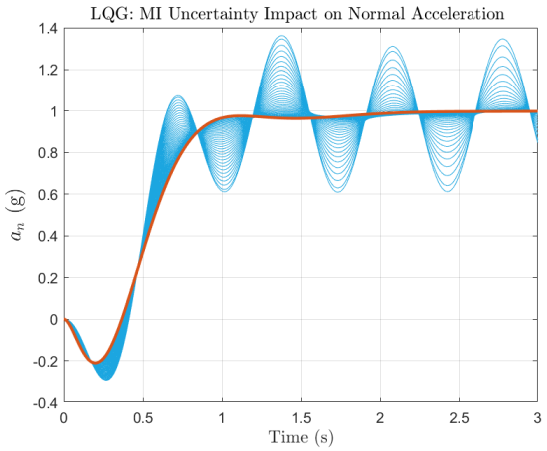

(a) LQG-controlled system

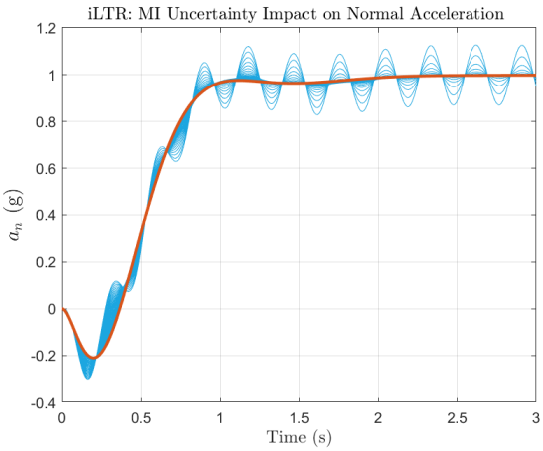

(b) iLTR-controlled system

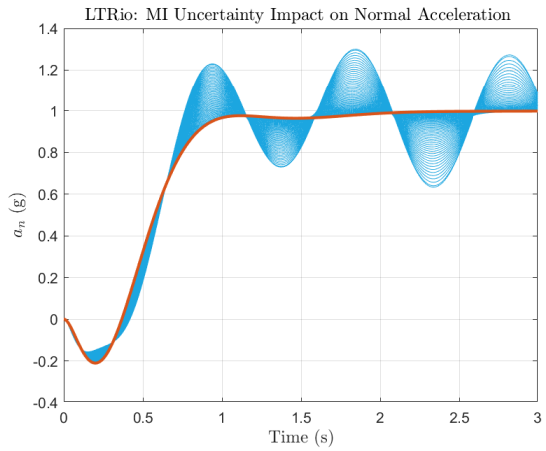

(c) LTRio-controlled system

Figure 6.26: Normal acceleration response under multiplicative-input uncertainties for the LQG, iLTR and LTRio controlled systems along with the nominal case shown in red

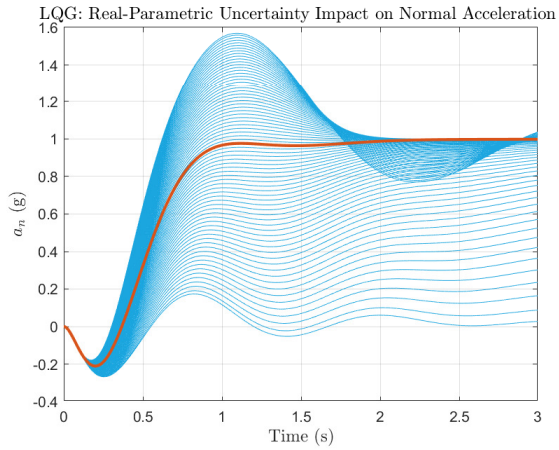

(a) LQG-controlled system

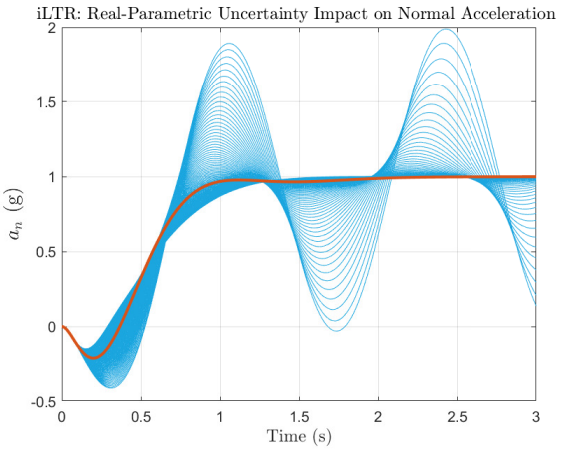

(b) iLTR-controlled system

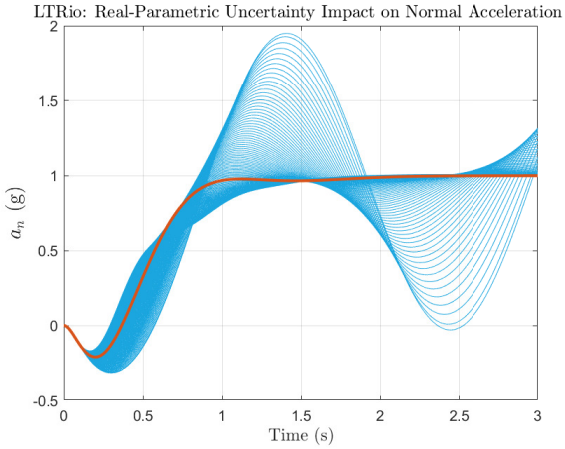

(c) LTRio-controlled system

Figure 6.27: Normal acceleration response under real-parametric uncertainties for the LQG, iLTR and LTRio controlled systems along with the nominal case shown in red

The Bubble plots in Figure 6.28 show the bahaviour of the time-domain characteristics in the time response of normal acceleration output for the dynamic-output feedback controllers, namely LQG (blue), iLTR (red) and LTRio (yellow), examined in this study. As normalized multiplicative-input uncertainty increases, there is a corresponding incremental increase in both the settling time, indicated by the size of the bubbles in Figure 6.28, and the overshoot, on the y-axis, for all types of dynamic output-feedback controllers.

Specifically in LQG-controlled systems, there is a notably faster increase in overshoot as uncertainty increases, as illustrated in Figure 6.28a. Additionally, the robust performance is maintained (as indicated by black outline of the bubbles) by LQG controlled systems upto the uncertainty range of 0 to 1. In contrast, LTRio-controlled systems show an increase in settling time with growing uncertainty, but their overshoot remains consistently below 20%. Also, they exhibit robust performance upto normalized uncertainty of 2. For uncertainties in the 1.5-2 normalized magnitude range, the LQG-controlled systems exhibit a shorter settling time compared to LTRio systems, possibly due to differences in the peaks of their output sensitivity functions, which can affect time-domain characteristics. In iLTR-controlled systems, settling times are shorter when uncertainty is below 2.5, but they sharply rise beyond this point. In all cases, settling times exceed 3 seconds, as indicated by a $*$ inside the bubbles, under high levels of uncertainty.

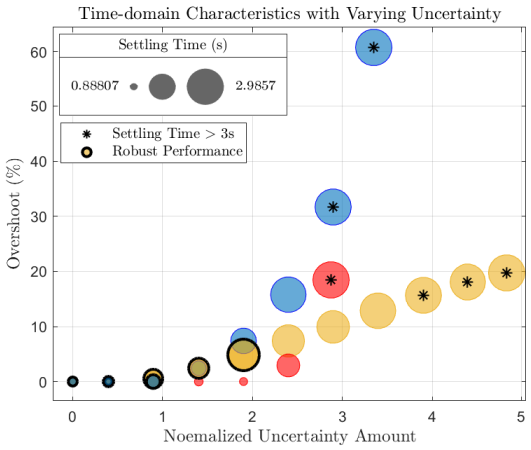

(a) Closed-loop systems with multiplicative-input uncertainty

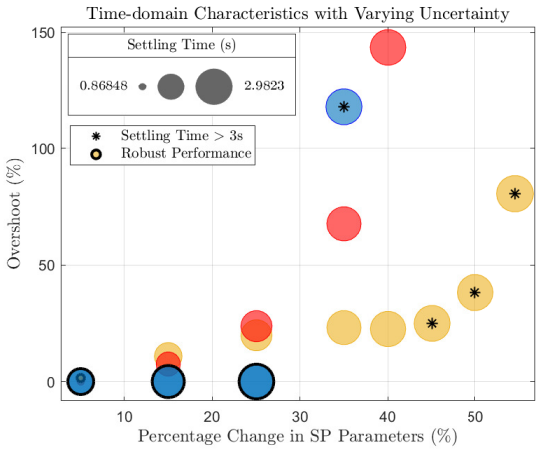

(b) Closed-loop systems with real-parametric uncertainty

Figure 6.28: Bubble plot showing the variation of normal acceleration a_n response settling time (s) and overshoot (%) with increasing uncertainty in LQG (blue), iLTR (red) and LTRio (yellow) controlled systems

In case of real-parametric uncertainties, LQG-controlled systems exhibit long settling times even with minor changes in SP parameters. The increase in overshoot with rising uncertainty is steep for both LQG and iLTR systems, potentially reaching up to 150% as seen from Figure 6.28b. The LTRio-controlled system, while having rapidly increasing settling times, maintains a relatively lower overshoot compared to other controllers. In scenarios with substantial uncertainty in SP parameters, the settling time can exceed the 3-second threshold. Overall, while the settling time for LTRio systems increases with greater uncertainty, their ability to maintain stability under higher uncertainty levels is evident in their relatively lower overshoot.

Part IV

Conclusion

7

Conclusion & Recommendations

This research primarily conducts a comparative analysis of various linear quadratic control methods, emphasizing their stability and robustness under uncertain conditions. The central objective is to assess the performance of different Loop Transfer Recovery (LTR) methods, particularly focusing on the classical LTR technique described by J. Doyle and Stein, 1981 and a more recent approach developed by Lavretsky, 2012. The foundation for modelling these control systems is laid out in Part I of the thesis, which introduces the simulation model of the Citation aircraft. Given the study's focus on evaluating the stability and robustness of linear quadratic controllers, the scope of this thesis is limited to the implementation and analysis of controllers under specific flight conditions—namely, low velocity and high altitude. The aim of this study is to highlight the effectiveness of the Loop Transfer Recovery method, which necessitates presenting the limitations inherent in the LQG control method, specifically in terms of stability and robustness. These limitations become particularly apparent at flight points characterized by lower damping and reduced control authority.

Furthermore, Part III of the thesis outlines the robustness analysis tools widely recognized in the field, detailing those which are used in this study. Before delving into the limitations of LQG controllers in the context of stability margins and robustness, Part II of the thesis presents the implementation of various LQ control techniques. Furthermore, the two LTR techniques investigated in this study are described, along with their processes for restoring stability margins, complete with theoretical justifications. Part III of the thesis is dedicated to analyzing and comparing the stability and robustness of these control techniques, focusing on their stability margins and tolerance to uncertainty before instability occurs. This section also explores the practical aspects of LQR, LQG, and LTR control methods, particularly highlighting how stability margins at the plant input shift during the LTR methods' recovery process.

7.1. Reflecting on the Research Questions

Chapter 1 of the thesis outlines the primary research objective and divides it into a series of research questions. The following provide concise, point-by-point answers to each of these questions.

1. Chapter 2 of the thesis is dedicated to outlining the structure of the plant used in this research. A notable characteristic of the plant is that its normal acceleration output possesses a right-half-plane (RHP) zero at a value of 4.342, which categorizes the plant as a non-minimum phase system.
2. Chapter 3 discusses the tuning method and implementation of both state and output feedback LQR methods. It was observed that the stability margins at the plant input and output were more than adequate, surpassing the required stability criteria. The chapter further distinguishes between the state-feedback and output-feedback approaches within the LQR framework. It was found that the LQR output feedback structure is somewhat simpler than its state-feedback counterpart. The process of implementing both LQR approaches using the `systune` function in `MATLAB` is explored. This discussion emphasizes how `systune` provides a direct and efficient means for calculating the LQR feedback gains, hence making the implementation process simpler.
3. Chapter 4 of the thesis presents an in-depth study of the LQG problem, focusing particularly on the stability margins. The analysis showed that incorporating Kalman filter dynamics into the LQR controllers degrades their inherent property of guaranteed stability at the plant input. This effect was Furthermore, by carefully adjusting the covariance matrices of the Kalman filter within the LQG controller, it was established that the state and output estimates provided by the Kalman filter closely aligned with the actual output measurements.
4. Given that the LQG-controlled system exhibited reduced stability margins at the plant input compared to the LQR scenario, the implementation of an LTR (Loop Transfer Recovery) method was considered essential to

recover these margins. Among the two LTR techniques studied, namely iLTR and LTRio, the iLTR method effectively enhanced stability and robustness at the plant input but significantly compromised these aspects at the plant output. On the other hand, the LTRio method proved to be more efficient in restoring margins at the input while simultaneously preserving stability at the output, thereby achieving the desired satisfactory stability margins.

5. In most scenarios, the LTRio-controlled system demonstrated superior robustness compared to other linear quadratic control methods, with the exception of the LQR state feedback method. Relative to the output feedback LQR, the LTRio method successfully achieved the desired stability margins at both plant input and output. Although the LQR output feedback exhibits more than satisfactory stability margins at the output, it falls short at the input. In comparison with other dynamic output feedback controllers like LQG and iLTR, the LTRio method showcased significantly better robustness against uncertainties.

7.2. Outlook

In industrial applications, the robust stability margins provided by the full-state feedback LQR-controlled systems at the plant input are highly appealing. However, it is important to note that this control strategy does not inherently ensure similar stability margins at the plant output. In this study, it was found that the stability margins at the plant output were satisfactory, surpassing the standard requirements, thereby making the LQR state feedback design highly effective. Yet, it is crucial to recognize that the full-state feedback LQR method typically overcompensates for stability at the plant input. This overcompensation may not always be necessary or desired in practical applications. Generally, the goal in designing control systems is to achieve a balance in stability margins and robustness at both the plant input and output. While LQR's ability to ensure stability at the plant input is advantageous, it can lead to an imbalance between the input and output stability margins. This imbalance can become even more pronounced when a state-estimator is added to form an LQG (Linear Quadratic Gaussian) system. In such scenarios, this could lead to either a significant reduction in stability margins at the plant input or inadequate margins at the output.

To address these challenges, the LTR (Loop Transfer Recovery) method emerges as a promising solution. It offers a structured and straightforward approach to adjust the LQG stability margins at either the plant input or output to mirror those characteristic of LQR controllers. This process is similar to the 'waterbed effect' observed in physics. Much like pressing down on one side of a waterbed causes a rise on the other side, improving stability margins at one point (either the input or output of the plant) in a control system often leads to decreased margins at the other point. One of the key limitations of the LTR process is that it is not possible to simultaneously enhance the stability margins at both the plant input and output to match the ideal LQR scenario. In other words, while LTR can effectively adjust the stability margins at one point, this adjustment usually comes at the cost of reduced margins at the other, maintaining a delicate balance in the system's overall stability profile.

7.3. Future Perspectives

The introduction of Loop Transfer Recovery theory, as initially presented in (J. Doyle and Stein, 1979; J. Doyle and Stein, 1981), marked a significant milestone in control theory. During the 1980s and 1990s, numerous other LTR theories were developed, each contributing unique perspectives and methodologies. A valuable direction for future research could involve a detailed research of some of the prominent LTR theories from that era, particularly analyzing their applicability and effectiveness in modern flight control systems. This research could present new insights and potentially lead to innovative applications in the field of aerospace engineering. In addition to this historical view, there is a possibility of integrating LQR (Linear Quadratic Regulator), LQG (Linear Quadratic Gaussian), and LTR theories with modern computational tools. For instance, the `MATLAB` function `systune` offers a platform for developing unstructured controllers that are potentially simpler and less computationally demanding. Using the theories studied in this research, along with `systune`, could yield efficient control systems that balance simplicity with robust performance.

Furthermore, enhancing these control algorithms by incorporating a reference model adds another layer of sophistication. This approach could include specific requirements such as a desired damping ratio and natural frequency into the tuning process, further developing the control system to meet performance criteria. Lastly, applying the LTR methods discussed in this study to different aircraft models would be a big step forward. This application across a variety of platforms can validate the versatility and effectiveness of LTR methods in diverse settings. Such investigations could lead to broader applications in aerospace and even other industries, demonstrating the broad applications of these control theories in various engineering domains. This approach would not only deepen our understanding of LTR theories but also pave the way for innovative applications in advanced control systems.

References

Anderson, Brian DO and John B Moore (2007). *Optimal control: linear quadratic methods*. Courier Corporation.

Athans, M. (1971). "On the LQG Problem". In: *IEEE Transactions on Automatic Control* 16.6, pp. 528–528. DOI: 10.1109/TAC.1971.1099845. URL: https://ieeexplore.ieee.org/document/1099845.

Athans, M. et al. (1977). "The Stochastic Control of the F-8C Aircraft Using a Multiple Model Adaptive Control (MMAC) Method–Part I: Equilibrium Flight". In: *IEEE Transactions on Automatic Control* 22.5, pp. 768–780. DOI: 10.1109/TAC.1977.1101599. URL: https://ieeexplore.ieee.org/document/1101599.

Balas, Gary et al. (2007). "Robust control toolbox user's guide". In: *The Math Works, Inc., Tech. Rep*.

Doyle, J. (1978). "Guaranteed Margins for LQG Regulators". In: *IEEE Transactions on Automatic Control* 23.4, pp. 756–757. DOI: 10.1109/TAC.1978.1101812. URL: https://ieeexplore.ieee.org/document/1101812.

— (1982). "Analysis of Feedback Systems with Structured Uncertainty". In: *IEEE Proceedings Control Theory and Applications*. URL: https://digital-library.theiet.org/content/journals/10.1049/ip-d.1982.0053.

— (1985). "Structured Uncertainty in Control System Design". In: *1985 24th IEEE Conference on Decision and Control*, pp. 260–265. DOI: 10.1109/CDC.1985.268842. URL: https://ieeexplore.ieee.org/document/4048283.

Doyle, J. and G. Stein (1979). "Robustness with Observers". In: *IEEE Transactions on Automatic Control* 24.4, pp. 607–611. DOI: 10.1109/TAC.1979.1102095. URL: https://ieeexplore.ieee.org/document/1102095.

— (1981). "Multivariable Feedback Design: Concepts for a Classical/Modern Synthesis". In: *IEEE Transactions on Automatic Control* 26.1, pp. 4–16. DOI: 10.1109/TAC.1981.1102555. URL: https://ieeexplore.ieee.org/abstract/document/1102555.

Grondman, Fabian et al. (Jan. 2018). "Design and flight testing of incremental nonlinear dynamic inversion based control laws for a passenger aircraft". In: American Institute of Aeronautics and Astronautics Inc, AIAA. ISBN: 9781624105265. DOI: 10.2514/6.2018-0385.

Kalman, Rudolf (1964). "When is a Linear Control System Optimal?" In: URL: https://asmedigitalcollection.asme.org/fluidsengineering/article/86/1/51/392203/When-Is-a-Linear-Control-System-Optimal.

Kashani, R. and S. Kiriczi (1992). "Robust Stability Analysis of LQG-Controlled Active Suspension with Model Uncertainty Using Structured Singular Value μ Method". In: *Vehicle System Dynamics* 21.1, pp. 361–384. DOI: 10.1080/00423119208969016. eprint: https://doi.org/10.1080/00423119208969016. URL: https://doi.org/10.1080/00423119208969016.

Kazerooni, H and PK Houpt (1986). "On the loop transfer recovery". In: *International Journal of Control* 43.3, pp. 981–996.

Khalil, H.K. (2002). *Nonlinear Systems*. Pearson Education. Prentice Hall. ISBN: 9780130673893. URL: https://books.google.nl/books?id=t_d1QgAACAAJ.

Kokotovic, P.V. (1985). "Recent Trends in Feedback Design: An Overview". In: *Automatica* 21.3, pp. 225–236. ISSN: 0005-1098. DOI: https://doi.org/10.1016/0005-1098(85)90056-1. URL: https://www.sciencedirect.com/science/article/pii/0005109885900561.

Konatala, Ramesh, E Van Kampen, and Gertjan Looye (2021). "Reinforcement Learning based Online Adaptive Flight Control for the Cessna Citation II(PH-LAB) Aircraft". In: DOI: 10.2514/6.2021-0883. URL: http://arc.aiaa.org.

Kwakernaak, H. (1969). “Optimal Low-Sensitivity Linear Feedback Systems”. In: *Automatica* 5.3, pp. 279–285. ISSN: 0005-1098. DOI: https://doi.org/10.1016/0005-1098(69)90070-3. URL: https://www.sciencedirect.com/science/article/pii/0005109869900703.

Lavretsky, Eugene (2012). “Adaptive Output Feedback Design Using Asymptotic Properties of LQG/LTR Controllers”. In: *IEEE Transactions on Automatic Control* 57.6, pp. 1587–1591. DOI: 10.1109/TAC.2011.2174692. URL: https://ieeexplore.ieee.org/document/6069834.

Lavretsky, Eugene and Kevin Wise (2013). *Robust and Adaptive Control With Aerospace Applications*. Advanced Textbooks in Control and Signal Processing. Dordrecht: Springer. ISBN: 978-1-4471-4395-6. URL: https://link.springer.com/book/10.1007/978-1-4471-4396-3.

Levine, William S (2018). *The Control Handbook (three volume set)*. CRC press.

Lhachemi, Hugo, David Saussie, and Guchuan Zhu (Jan. 2014). “A Robust and Self-Scheduled Longitudinal Flight Control System: a Multi-Model and Structured H-infinity Approach”. In: DOI: 10.2514/6.2014-0601.

Middleton, R.H. (1991). “Trade-offs in linear control system design”. In: *Automatica* 27.2, pp. 281–292. ISSN: 0005-1098. DOI: https://doi.org/10.1016/0005-1098(91)90077-F. URL: https://www.sciencedirect.com/science/article/pii/000510989190077F.

Moerder, D. and A. Calise (1985). “Convergence of a numerical algorithm for calculating optimal output feedback gains”. In: *IEEE Transactions on Automatic Control* 30.9, pp. 900–903. DOI: 10.1109/TAC.1985.1104073.

Nason, Malcolm (Aug. 2013). *CESSNA 550 CITATION PH-LAB DELFT UNIVERSITY OF TECHNOLOGY*. https://www.flickr.com/photos/shanair/9516698776.

Niemann, Hans Henrik and Jakob Stoustrup (1995). “An Introduction to the Special Issue on Loop Transfer Recovery”. In: *International Journal of Robust and Nonlinear Control*. URL: https://onlinelibrary.wiley.com/doi/10.1002/rnc.4590050702.

Packard, A., J. Doyle, and G. J. Balas (1993). “Linear, Multivariable Robust Control With a μ Perspective”. In: *Journal of Dynamic Systems Measurement and Control-transactions of The Asme* 115, pp. 426–438. URL: https://asmedigitalcollection.asme.org/dynamicsystems/article/115/2B/426/417451/Linear-Multivariable-Robust-Control-With-a?casa_token=Io-BpphNDjAAAAAA:KVORXInRyU_FHaNtgpWqlAaik_4gBsFY3Xxf_jSEunQxJ9UN8sR7ocN3uJECAW5JW6p3sN0i.

Petersen, Ian R. and Roberto Tempo (2014). “Robust Control of Uncertain Systems: Classical Results and Recent Developments”. In: *Automatica* 50.5, pp. 1315–1335. ISSN: 0005-1098. DOI: https://doi.org/10.1016/j.automatica.2014.02.042. URL: https://www.sciencedirect.com/science/article/pii/S0005109814000806.

Rosenbrock, H. and P. McMorran (1971). “Good, Bad, or Optimal?” In: *IEEE Transactions on Automatic Control* 16.6, pp. 552–554. DOI: 10.1109/TAC.1971.1099822. URL: https://ieeexplore.ieee.org/document/1099822.

Safonov, Michael (1981). “Stability Margins of Diagonally Perturbed Multivariable Feedback Systems”. In: *1981 20th IEEE Conference on Decision and Control including the Symposium on Adaptive Processes*, pp. 1472–1478. DOI: 10.1109/CDC.1981.269503. URL: https://ieeexplore.ieee.org/abstract/document/4047182.

— (2012). “Origins of Robust Control: Early History and Future Speculations”. In: *IFAC Proceedings Volumes* 45.13. 7th IFAC Symposium on Robust Control Design, pp. 1–8. ISSN: 1474-6670. DOI: https://doi.org/10.3182/20120620-3-DK-2025.00179. URL: https://www.sciencedirect.com/science/article/pii/S1474667015376540.

Safonov, Michael and Michael Athans (1977). “Gain and Phase Margin for Multiloop LQG Regulators”. In: *IEEE Transactions on Automatic Control* 22.2, pp. 173–179. URL: https://ieeexplore.ieee.org/document/1101470.

Skogestad, Sigurd and Ian Postlethwaite (2005). *Multivariable Feedback Control: Analysis and Design*. Hoboken, US-NJ: John Wiley.

Stevens, Brian L., Frank L. Lewis, and Eric N. Johnson (2016). *Aircraft Control and Simulation*. Dynamics, Controls Design and Autonomous Systems. New Jersey: John Wiley & Sons Inc. ISBN: 978-1-118-87099-0. URL:

https://www.wiley.com/en-us/Aircraft+Control+and+Simulation%5C%3A+Dynamics%5C%2C+Controls+Design%5C%2C+and+Autonomous+Systems%5C%2C+3rd+Edition-p-9781118870976.

van der Linden, C.A.A.M. (1998). *DASMAT-Delft University Aircraft Simulation Model and Analysis Tool: A Matlab/Simulink Environment for Flight Dynamics and Control Analysis*. Delft University Press. ISBN: 90-407-1582-3. URL: http://resolver.tudelft.nl/uuid:25767235-c751-437e-8f57-0433be609cc1.

Veld, R C Van 't, E Van Kampen, and Q P Chu (2018). "Stability and Robustness Analysis and Improvements for Incremental Nonlinear Dynamic Inversion Control". In: DOI: 10.2514/6.2018-1127. URL: http://arc.aiaa.org.

Weinmann, A. (1991). *Uncertain Models and Robust Control*. New York: Springer Vienna. ISBN: 978-3-7091-6711-3. URL: https://link.springer.com/book/10.1007/978-3-7091-6711-3.

Wise, Kevin A and Eugene Lavretsky (2013). "Flight control design using observer-based loop transfer recovery". In: *AIAA Guidance, Navigation, and Control (GNC) Conference*, p. 5105.

Zhou, Kemin, John Doyle, and Keith Glover (1996). *Robust and Optimal Control*. USA: Prentice-Hall, Inc. ISBN: 0134565673. URL: https://ieeexplore.ieee.org/document/572756.

A LQR feedback Control

A.1. LQR Output Feedback Optimal Gain Selection

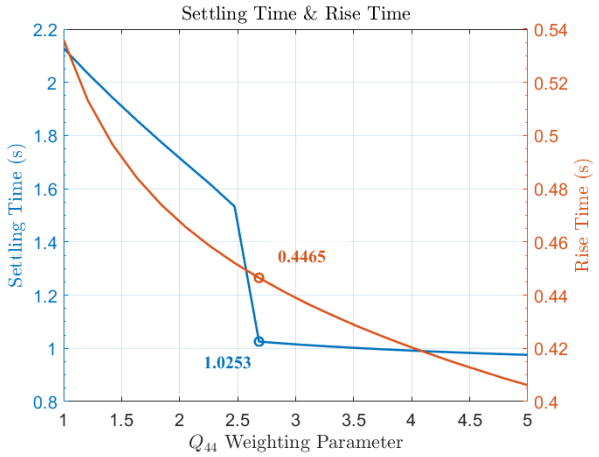

(a) Settling Time (blue) and Rise Time (red)

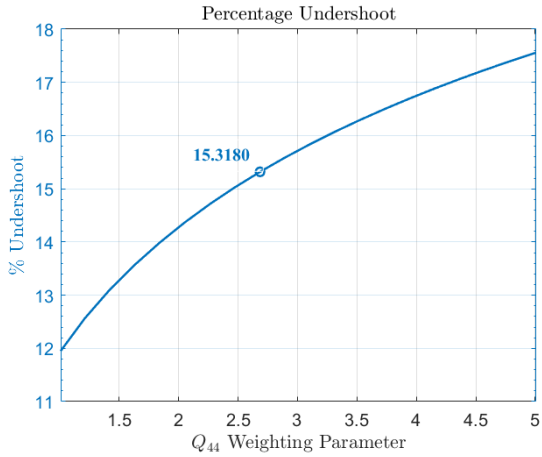

(b) Percentage undershoot

Figure A.1: Time-domain performance metrics with increasing Q_{44} weighting parameter for output-feedback LQR design

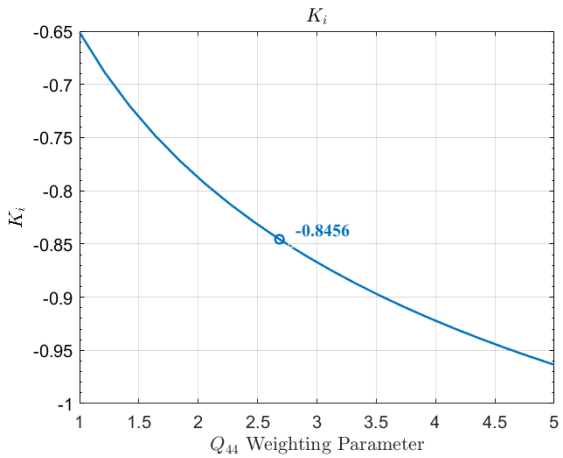

(a) K_i

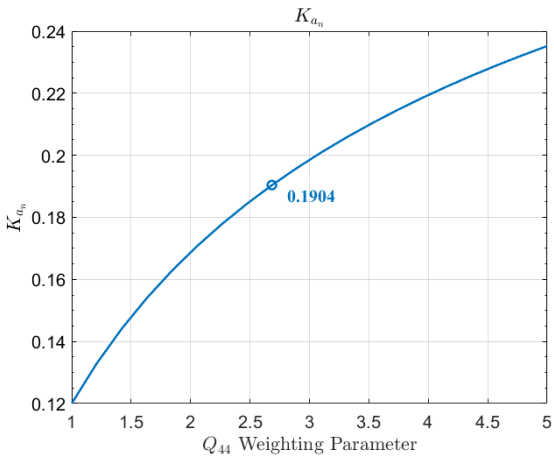

(b) K_{a_n}

Figure A.2: Increasing absolute values of output-feedback LQR controller feedback gains with increasing Q_{44} weighting parameter

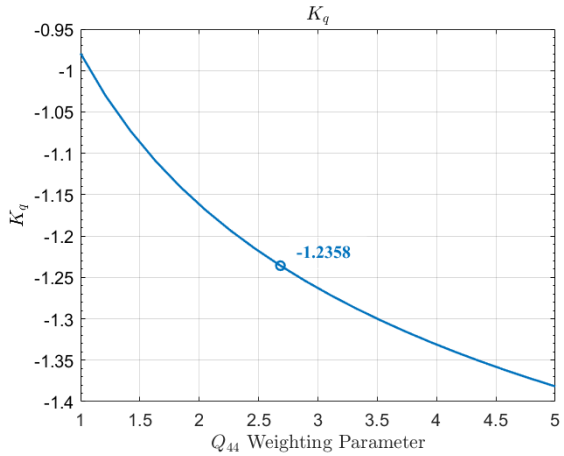

(c) K_q

Figure A.2: Increasing absolute values of output-feedback LQR controller feedback gains with increasing Q_{44} weighting parameter

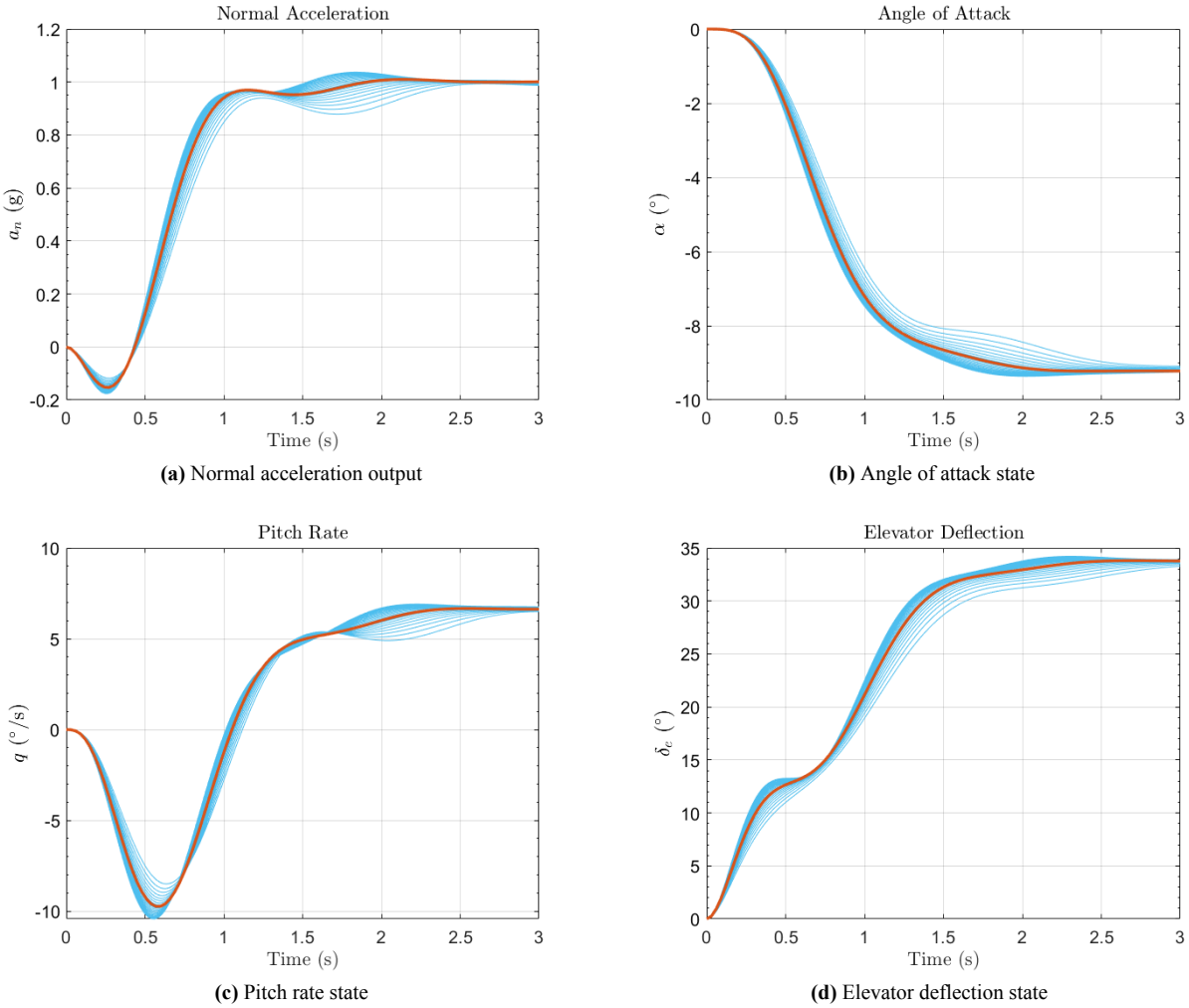

(a) Normal acceleration output

(b) Angle of attack state

(c) Pitch rate state

(d) Elevator deflection state

Figure A.3: Time responses of system states (α, q, $delta_e$) and output (a_n, q) to a unit normal acceleration command for varying Q_{44} weighting parameter (blue) and the optimum Q_{44} value (red) for output-feedback LQR design

A.2. LQR Design using systune

```
%% Standard form
P_lft = ss(A, [B_w B_u], [C_z; C_y], [D_zw D_zu; D_yw D_yu]);
% systune options
options_stn              = systuneOptions();
options_stn.Display      = 'Final';
options_stn.MaxIter      = 1000;
options_stn.RandomStart  = 10;
options_stn.UseParallel  = false;
options_stn.SoftTarget   = 0;
options_stn.SoftTol      = 1e-4;
options_stn.SoftScale    = 1;
options_stn.MinDecay     = 1e-7;
options_stn.MaxRadius    = 1e8;

% Tunable gain
K0 = tunableGain('K0', nu, ny);
% Tunable closed loop
CL0 = lft(P_lft, -K0, nu, ny);

% Defining tuning goal LQG
CL0.InputName      = 'w';
CL0.OutputName     = 'z';
NoiseCovariance    = 1;
PerformanceWeight  = blkdiag(Q, R);
LQGoal             = TuningGoal.LQG(CL0.InputName, CL0.OutputName, NoiseCovariance,
    PerformanceWeight);
LQGoal.Name        = 'LQGoal';

% Soft and Hard goals
SoftGoals = LQGoal;
HardGoals = [];

[CL, fSoft, gHard, info_stn] = systune(CL0, SoftGoals, HardGoals, options_stn);
```

B

LQG feedback Control

B.1. LQG-Controlled System Pole-Zero Map

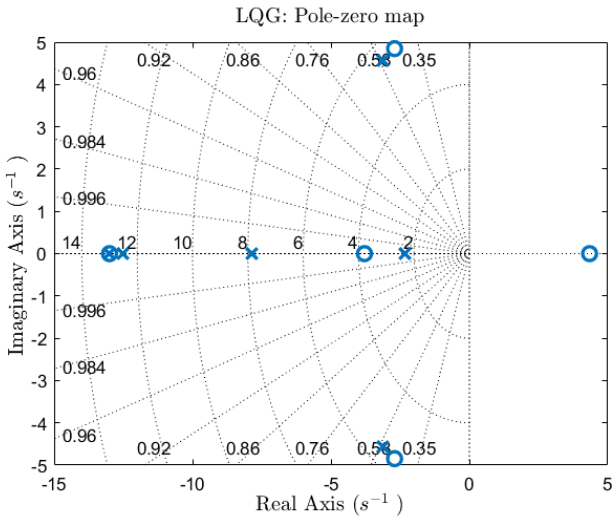

Figure B.1: Pole-zero map of LQG-controlled closed-loop system showing the union of the LQR and LQE poles

B.2. LQG Design Using `systune`

```
% Relevant Matrices
A     = Aaug;
B_w   = [sqrt(W) zeros(nx,ny); zeros(1,nx) -1 0];
B_u   = B_aug;
C_z   = [sqrt(Q); zeros(1,nx+1)];
C_y   = [zeros(1,nx) 1;C_aug];
D_zw  = zeros(nz,nw);
D_zu  = [zeros(4,1); eye(R)];
D_yw  = [zeros(nx,nx) [zeros(1,ny); -sqrt(V)]];
D_yu  = D_aug;

%% Standard form
P_lft = ss(A, [B_w B_u], [C_z; C_y], [D_zw D_zu; D_yw D_yu]);
% systune options
options_stn               = systuneOptions();
options_stn.Display       = 'Final';
options_stn.MaxIter       = 1000;
options_stn.RandomStart = 10;
```

```
options_stn.UseParallel = false;
options_stn.SoftTarget  = 0;
options_stn.SoftTol     = 1e-4;
options_stn.SoftScale   = 1;
options_stn.MinDecay    = 1e-7;
options_stn.MaxRadius   = 1e8;

% Tunable LQR and Kalman filter gains
Kc0         = realp('Kc0', zeros(1, 4)); % contains state-feedback gains and
    integrator gain
Kc0.Free    = ones(1,4);

Kf0         = realp('Kf0', zeros(3, 2));
Kf0.Value   = zeros(3, 2);
Kf0.Free    = [ones(2,2); zeros(1, 2)]; % Elements corresponding to the actuator are
    zero

% Tunable controller
Ac  = G_y.A-G_y.B*Kc0(1,1:3)-Kf0*G_y.C;
Bcy = [-G_y.B*Kc0(1,4) -Kf0];
Cc  = -Kc0(1,1:3);
Dcy = [-Kc0(1,4) 0 0];
K0  = ss(Ac,Bcy,Cc,Dcy);

% Tunable closed-loop
CL0 = lft(P_lft, K0, nu, ny+1); % Outputs include the additional integral of error
    state

% Defining tuning goal LQG
CL0.InputName      = 'w';
CL0.OutputName     = 'z';

% Tuning goal specifications
NoiseCovariance    = blkdiag(W, V); % Weight for the disturbance/noise signals
PerformanceWeight = blkdiag(Q, R); % Weight for the performance signals

LQGoal             = TuningGoal.LQG(CL0.InputName, CL0.OutputName, NoiseCovariance,
    PerformanceWeight);
LQGoal.Name        = 'LQGoal'; % Tuning goal name

% Set soft and hard goals
SoftGoals          = LQGoal;
HardGoals          = [];

% Solving tuning goal
[CL,fSoft,gHard,info_stn] = systune(CL0,SoftGoals,HardGoals,options_stn)

% LQR and LQE gains
gains  = getBlockValue(CL);
K_lqr  = gains.Kc0;
K_lqe  = gains.Kf0;
```